European Journal of Medicinal Chemistry 260 (2023) 115730

Contents lists available at ScienceDirect

European Journal of Medicinal Chemistry

journal homepage: www.elsevier.com/locate/ejmech

Research paper

Discovery of potent pyrrolo-pyrimidine and purine HDAC inhibitors for the treatment of advanced prostate cancer

Davide Moi, Davide Bonanni, Silvia Belluti, Pasquale Linciano [1], Andrea Citarella, Silvia Franchini, Claudia Sorbi, Carol Imbriano, Luca Pinzi [**], Giulio Rastelli [*]

Department of Life Sciences, University of Modena and Reggio Emilia, Via Giuseppe Campi 103, 41125, Modena, Italy

ARTICLE INFO

Handling Editor: Dr. Z Liu

Keywords:
HDAC inhibitors
HDAC6
Drug design
Trifluoromethyloxadiazole (TFMO)
Prostate cancer

ABSTRACT

The development of drugs for the treatment of advanced prostate cancer (PCA) remains a challenging task. In this study we have designed, synthesized and tested twenty-nine novel HDAC inhibitors based on three different zinc binding groups (trifluoromethyloxadiazole, hydroxamic acid, and 2-mercaptoacetamide). These warheads were conveniently tethered to variously substituted phenyl linkers and decorated with differently substituted pyrrolo-pyrimidine and purine cap groups. Remarkably, most of the compounds showed nanomolar inhibitory activity against HDAC6. To provide structural insights into the Structure-Activity Relationships (SAR) of the investigated compounds, docking of representative inhibitors and molecular dynamics of HDAC6-inhibitor complexes were performed. Compounds of the trifluoromethyloxadiazole and hydroxamic acid series exhibited promising anti-proliferative activities, HDAC6 targeting in PCA cells, and *in vitro* tumor selectivity. Representative compounds of the two series were tested for solubility, cell permeability and metabolic stability, demonstrating favorable *in vitro* drug-like properties. The more interesting compounds were subjected to migration assays, which revealed that compound **13** and, to a lesser extent, compound **15** inhibited the invasive behaviour of androgen-sensitive and –insensitive advanced prostate cancer cells. Compound **13** was profiled against all HDACs and found to inhibit all members of class II HDACs (except for HDAC10) and to be selective with respect to class I and class IV HDACs. Overall, compound **13** combines potent inhibitory activity and class II selectivity with favorable drug-like properties, an excellent anti-proliferative activity and marked anti-migration properties on PCA cells, making it an excellent lead candidate for further optimization.

1. Introduction

Prostate cancer (PCA) represents one of the most commonly diagnosed male malignancies and the fifth leading cause of cancer death worldwide [1]. Aberrant activation of the androgen receptor (AR) pathway is the most important mechanism fuelling PCA progression. Consequently, androgen deprivation therapy (ADT), either *via* surgical or chemical castration, has become the standard treatment for PCA and metastatic hormone-sensitive prostatic carcinoma (mHSPC), also known as castration-sensitive cancer (mCSPC) [2,3]. Nonetheless, many ADT-treated patients still progress to a poor prognosis stage of castration-resistant prostate cancer (CRPC), so-called because the androgen axis is still active even in the absence of androgens [4,5], which is frequently metastatic (mCRPC). Therefore, the identification of new and more effective therapeutics against metastatic PCA is urgently needed. In this regard, the Food and Drug Administration (FDA) approved in 2012 the AR antagonist Enzalutamide [6] for use in patients with chemotherapy-naïve mCRPC, which was extended in 2014 to mCRPC either before or after cytotoxic chemotherapy. The androgen biosynthesis inhibitor Abiraterone acetate followed a similar FDA history, and is currently recommended for both mCRPC and mCSPC [7]. More recently, the AR inhibitors Darolutamide and Apalutamide have also been approved [8]. However, the therapeutic benefits of these drugs are limited mainly due to the establishment of drug resistance mechanisms, including AR overexpression, AR mutations, and by enhanced androgen synthesis in cancer cells [9]. Mechanisms of resistance to AR-directed therapies (*e.g.*, Abiraterone or Enzalutamide) can give rise to neuroendocrine prostate cancer (NEPC), which is highly metastatic

* Corresponding author.
** Corresponding author.
E-mail addresses: luca.pinzi@unimore.it (L. Pinzi), giulio.rastelli@unimore.it (G. Rastelli).
[1] Present address: Department of Drug Sciences, University of Pavia. Viale Taramelli 12, 27100 Pavia, Italy.

https://doi.org/10.1016/j.ejmech.2023.115730
Received 1 June 2023; Received in revised form 1 August 2023; Accepted 14 August 2023
Available online 16 August 2023

and has a worse outcome compared to mCRPC [10]. Given its role in PCA progression and drug-resistance, the AR pathway has been extensively studied for the discovery of new therapeutic targets. For example, it has been demonstrated that AR maintenance is driven by the activity of Heat Shock Proteins (HSPs) and that AR expression and transactivating ability are modulated by the activity of histone acetyltransferases (HATs) and histone deacetylases (HDACs) [11]. In particular, HDACs play a key role in regulating gene expression, through acetylation/deacetylation of lysine residues in histones and non-histone proteins [12]. The HDAC superfamily comprises 18 different histone deacetylases isoforms grouped into four main classes. These include: (i) class I (HDAC1, 2, 3, 8); (ii) class II divided into subgroup IIa (HDAC4, 5, 7, 9) and IIb (HDAC6, 10); (iii) class III (sirtuins 1−7), and; (iv) class IV (HDAC11) [13,14]. All HDACs are zinc-dependent deacetylases, except for class III, whose members require nicotinamide adenine dinucleotide (NAD) as a cofactor [15]. Class I HDACs are characterized by a highly conserved deacetylase domain and are predominantly located in the cell nucleus. Conversely, members of Class II HDACs are able to shuttle between the cytoplasm and nucleus in response to various regulatory signals [16]. The contribution of class IIa HDACs to cancer development is complex and different roles can be depicted in different tumor models [17,18]. Class IIa HDACs present a unique adapter domain in the N-terminus that specifically interacts with the 14-3-3 chaperone and the members of the myocyte enhancer factor-2 (MEF2) transcription factors family that fine tune differentiation, cell growth and survival [19,20]. In PCA cells, endogenous HDAC4 localisation and function depends upon androgen stimulation. In particular, HDAC4 is recruited in the nucleus of hormone-refractory cells, where it may inhibit their differentiation and contribute to the growth of prostate cancer aggressive phenotype [21]. Moroever, the transactivation repression mediated by the AR corepressor-19 kDa (ARR19) is exerted through the recruitment of HDAC4 [22]. In addition, HDAC4 has also been reported to modulate HOXB13 transcription, thus affecting cell growth in AR-negative PCA [23]. Based on these evidences, research efforts have been devoted to the development of HDAC4 inhibitors, albeit none of them being already tested in clinical trials. Besides, HDAC7 controls proliferation and angiogenesis, and emerging evidences indicate an association between this histone deacetylase and cancer progression [24]. Class IIb HDACs are mainly located in the cell cytoplasm, with the microtubule-associated deacetylase HDAC6 isoform being the most studied in a variety of diseases, particularly in cancer [25,26]. HDAC6 regulates microtubule dynamics through deacetylation of Lys40 in the α-tubulin subunit [27], which is crucial for cell migration and proliferation of cancer cells [28]. The role of HDAC6 in PCA is deeply connected to the regulation of AR hypersensitivity mainly through the modulation of Hsp90 acetylation levels [11]. In particular, recent studies have shown that modulation of HDAC6 induces hyperacetylation, and thus inhibition, of Hsp90. In turn, this triggers proteasomal-assisted degradation of Hsp90 clients, such as HDAC6 and AR. Selective HDAC6-inhibition by 4-hydroxybenzoic acid derivatives has a demonstrated therapeutic activity on PCA aggressiveness [11,29]. While no selective HDAC6 inhibitors are currently undergoing clinical evaluation for PCA treatment, significant interest has arisen for their use in combination therapies [30–32]. For example, the HDAC6 inhibitor ACY-1215 has proven to be effective in cell models of CRPC, in particular when administered in combination with the MEK inhibitor selumetinib (AZD6244) [30]. Moreover, Zeta55, a new dual inhibitor of AR expression and HDAC6 activity, potently inhibits the proliferation of PCA both *in vitro* and *in vivo*, suggesting a key role of HDAC6 in the modulation of AR pathway, and hence in the response to AR inhibitors [33]. Therefore, the development of HDAC6 inhibitors represents an appealing approach for advanced PCA treatment [34]. Since class I and class II HDACs are overexpressed in PCA, nonselective HDAC inhibitors (HDACis), such as the hydroxamate class agent Vorinostat (SAHA) and Trichostatin A (TSA) have been widely investigated. The evaluation of HDACis in clinical trials has mostly been limited to hematological malignancies, while poor clinical outcomes are observed in solid tumors when administered as monotherapy. The FDA-approved *pan*-HDACis Vorinostat and Belinostat, as well as the Class I HDAC inhibitor Romidepsin, have side effects that limit their use in patients. These side effects were ascribed to the lack of selectivity against HDAC isoforms [18,35–37]. In general, acute toxicity appears to be primarily due to inhibition of HDACs1-3. For example, the inhibition of HDAC1 and 3 upregulates pro-inflammatory cytokines [38] and induces Epithelial-Mesenchymal Transition (EMT) [39], which can result in increased proliferation and aggressiveness of cancer cells. Therefore, current research efforts are focused on developing effective HDACis with higher target selectivity and lower toxicity. In this respect, the development of HDACis selective for class II HDACs endowed with tolerable side effects [40] represents an attractive therapeutic strategy against metastatic PCA, especially considering the involvement of some of their members in cellular processes associated with tumor development and progression.

To date, a number of small-molecule HDACis have been reported, all of them presenting recurrent pharmacophoric features [41,42]. The general pharmacophoric model of HDACis is composed by three main units (Fig. 1, **panel A**): (i) a zinc binding group (ZBG), which is essential for the coordination of the catalytic Zn^{2+} ion in the active site; (ii) a cap group located in the outer surface of the binding pocket and important for driving isoform selectivity, and; (iii) a linker of the appropriate length to connect these two portions. The general binding mode of the *pan*-HDAC inhibitor Vorinostat in complex with HDAC6 is reported in Fig. 1, **panel B**.

Based on these general features, we designed a series of novel HDAC inhibitors obtained through the combination of: (i) differently substituted pyrrolo-pyrimidine or purine chemical moieties as cap groups; (ii) variously substituted phenyl or pyridine rings acting as linkers, and; (iii) trifluoromethyloxadiazole (TFMO), hydroxamic acid (HA) or 2-mercaptoacetamide (MCA) moieties as ZBGs, as depicted in Fig. 1, **panel C**. We explored the pyrrolo-pyrimidine or purine scaffolds as a cap group since it has been reported that sterically bulky moieties are generally unfavorable for the binding to class I HDACs, whose binding site is narrower than that of other isoforms [44]. In addition, the pyrrolo-pyrimidine and purine moieties hold great promises in anticancer drug discovery [45–50]. For example, Suh *et al.* [51] investigated the anti-proliferative effects of compounds bearing a pyrrolo-pyrimidine scaffold on PCA cell lines with different androgen responsiveness, reporting promising activities. Moreover, a library of purine derivatives has recently been synthesized and tested against HCT-116 and SW480 human colon cancer cell lines, corroborating the importance of this scaffold in anticancer drug discovery [46]. The use of pyrrolo-pyrimidine as a cap group for HDACis with a benzamide ZBG was recently reported by Nepali *et al.* [52], providing compounds with interesting anti-proliferative activity against triple-negative breast cancer cells MDA-MB-231 and MDA-MB-468 and liver cancer cells HepG2. Phenyl or pyridine rings decorated with small substituents were used as linkers, their selection being guided by the evidence that non-sterically hindered aromatic moieties, unlike linear alkyl ones, are able to confer selectivity for class II over class I histone deacetylases, particularly for HDAC6 [53].

As for the exploration of the zinc binding group, our attention focused on the TFMO, HA and MCA groups, which have been previously explored for the design of HDACis [54,55]. In particular, the TFMO group has been identified as a non-chelating zinc moiety preferentially binding to class IIa HDACs [56] through weak electrostatic interactions with the Zn^{2+} ion. Such ZBG has also been used for the design of HDAC6 inhibitors showing selectivity over class I HDACs (*e.g.*, patent ID: WO2017222952). Indeed, this zinc-binding group represents a chemical moiety of high interest for different purposes in drug discovery. In previous studies, we identified HDAC6 inhibitors with multi-target activity bearing TFMO as a ZBG, highlighting the potential of this moiety also in polypharmacological contexts [57,58]. Besides, HAs are strong

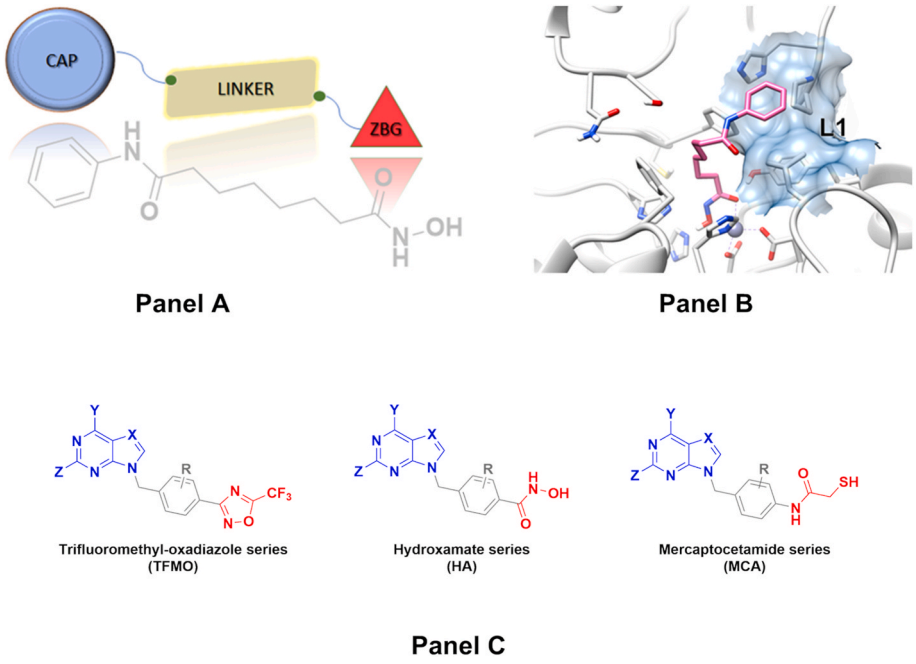

Fig. 1. **Panel A** reports the general architecture of a HDAC inhibitor mapped on SAHA (Vorinostat). **Panel B** reports the binding of SAHA in the L1 sub-pocket of HDAC6 (PDB code: 5EEI) [43]. **Panel C** reports the general chemical structures of the three new series of ligands described in this study. The cap, linker and ZBG portions are coloured in blue, green and red, respectively, as represented in the general framework of **panel A**.

Zn^{2+} chelators frequently present in potent HDAC inhibitors [59]. Previous studies have indicated that HAs bearing *p*-substituted aromatic linkers generally show HDAC6 selectivity [15,60]. The observed selectivity is due to the establishment of favorable π-π stacking interactions with the side chain of aromatic residues lining the catalytic channel of HDAC6. Although HAs provided very active HDAC inhibitors, mutagenicity issues potentially arising from Lossen rearrangement of HAs have fueled research efforts towards the identification of alternative ZBGs [61–63]. One of these is 2-mercaptoacetamide (MCA), which has recently demonstrated to provide selective HDAC6 inhibitors [54]. Therefore, selected compounds embedding the MCA zinc binding group were also synthesized. Overall, the combination of warheads, linkers and caps pursued in this work was never explored before, resulting in compounds with significant chemical diversity with respect to previously reported HDAC inhibitors.

In summary, in this work we have designed and synthesized twenty-nine novel compounds obtained through the combination of variously decorated pyrrolo-pyrimidine and purine cap groups, differently substituted phenyl or pyridine linkers, and three different ZBGs. All compounds were initially tested for *in vitro* inhibition of recombinant HDAC6 (class IIb), which we considered as a priority target for our investigations. Then, several representative compounds of each series were profiled also on HDAC1 (class I) and HDAC4 (class IIa) in order to investigate the selectivity profile against representative members of class I and class IIa HDACs. Docking followed by molecular dynamics (MD) simulations were performed on representative ligands of the three series to provide structural insights into the Structure-Activity Relationships (SARs) and inhibitor binding modes. The compounds were tested *in vitro* for their anti-proliferative activity on PCA cell lines. Then, their tumor selectivity was assessed through comparison with results obtained on RWPE1 healthy prostate cells. Western blot analysis of the expression levels of acetylated tubulin (AcTub) and acetylated histone H3 (AcH3) ruled out that the observed anti-proliferative effect was ascribable to the inhibition of class I HDACs. Target-selectivity analysis was performed on two PCA cell lines derived from metastatic sites that differ in their dependence on androgens for growth, *i.e.* LNCaP and PC3, commonly used as models of CSPC and CRPC, respectively. Two representative compounds, *i.e.* one of the TFMO and one of the HA series, were tested for solubility, bidirectional cell permeability and metabolic stability. Moreover, the effects on Class IIa activity were also evaluated on LNCaP cells using a luciferase-based assay. Lastly, the most interesting compounds were evaluated for anti-migratory properties on both LNCaP and PC3 cells. The results led to the identification of previously unreported inhibitors with promising biological activities. In particular, compounds of the TFMO and HA series provided interesting anti-proliferative cellular activities. Although compounds of the HA series resulted in very potent and selective HDAC6 inhibitors *in vitro*, their cellular activity was to some extents limited by a lower cellular permeability compared to TFMO analogues. Once profiled against all HDACs, compound **13** of the TFMO series was found to inhibit both HDAC6 (class IIb) and all members of class IIa HDACs with similar potencies, and to be highly selective with respect to classes I and IV HDACs. Overall, **13** combined potent HDAC6 and class IIa multi-target inhibitory activity, selectivity with respect to class I and class IV HDACs, favorable drug-like properties, excellent anti-proliferative activity and marked anti-migration properties on advanced PCA cells.

2. Results and discussion

2.1. Chemistry

The synthetic approach adopted to obtain compounds of the TFMO series (**10–22** in Scheme 1) firstly involves the reaction between benzyl bromide and potassium acetate, in order to protect the benzylic position. The cyano group was then converted into *N*′-hydroxyimidamide by reaction with hydroxylamine. The trifluoromethyloxadiazole ring was obtained by using trifluoroacetic anhydride (TFAA). After removal of the acetyl group under basic conditions, the benzyl alcohols were then converted into the corresponding benzyl chlorides, which reacted with the commercially available pyrrolo-pyrimidines and purines to afford the desired compounds in good yields.

Compounds of the HA series (**37–48** and **51** in Scheme 2) were obtained in two steps starting from the commercially available pyrrolo-pyrimidines or purines and the methyl 4-(bromomethyl)-benzoates,

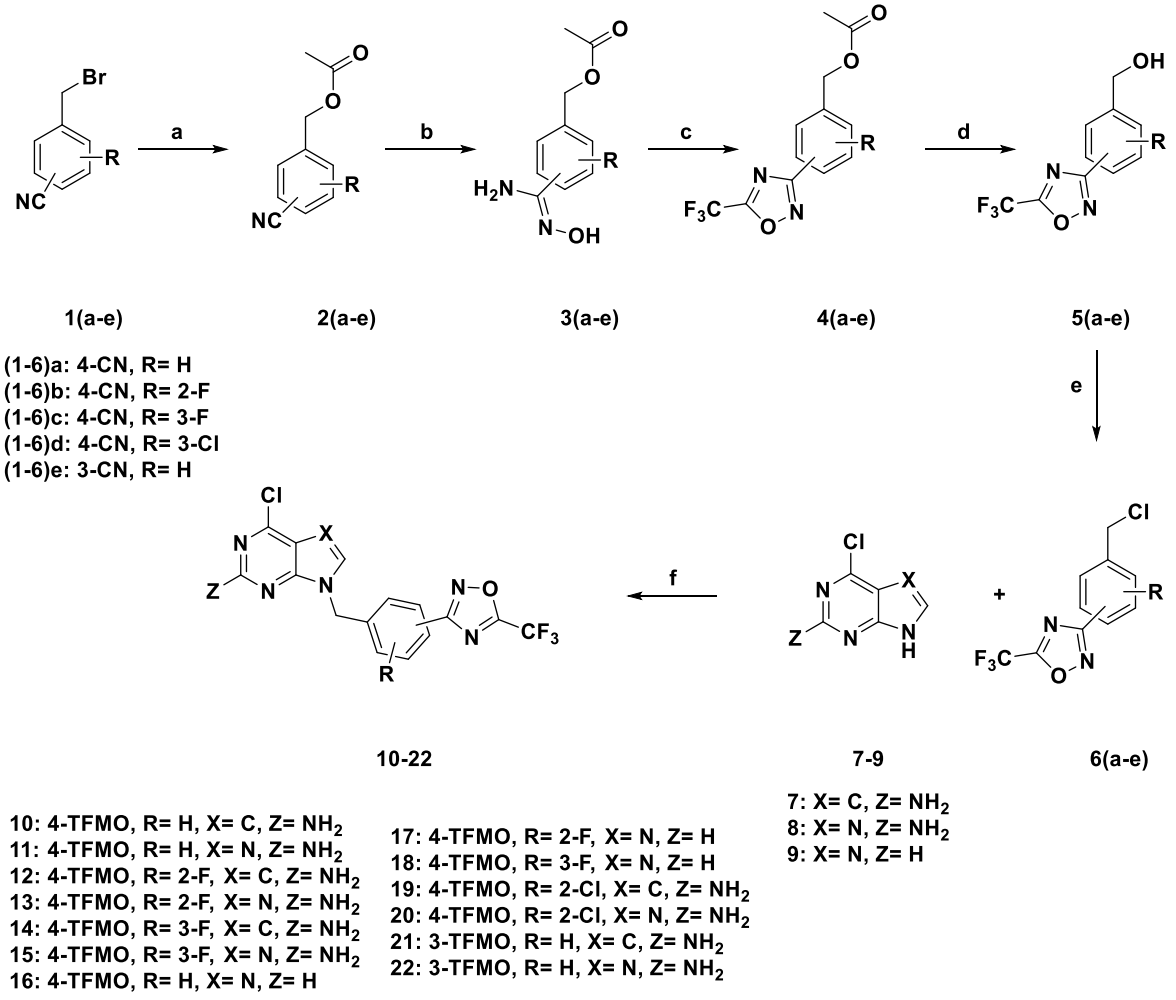

Scheme 1. Reagents and conditions for the preparation of TFMO compounds 10–22: a) AcOK, DMF, RT, overnight, 83–86% yield; b) $NH_2OH{\cdot}HCl$, TEA, EtOH, RT, overnight, 58–81% yield; c) TFAA, dry DCM, 0 °C to RT, 3 h, 58–94% yield; d) NaOH 1 N, THF/MeOH 3:1 (v/v), RT, 1 h, 75–98% yield; e) $SOCl_2$, 75 °C 3 h, 78–98% yield; f) K_2CO_3, DMF, RT, 8 h, 5–52% yield.

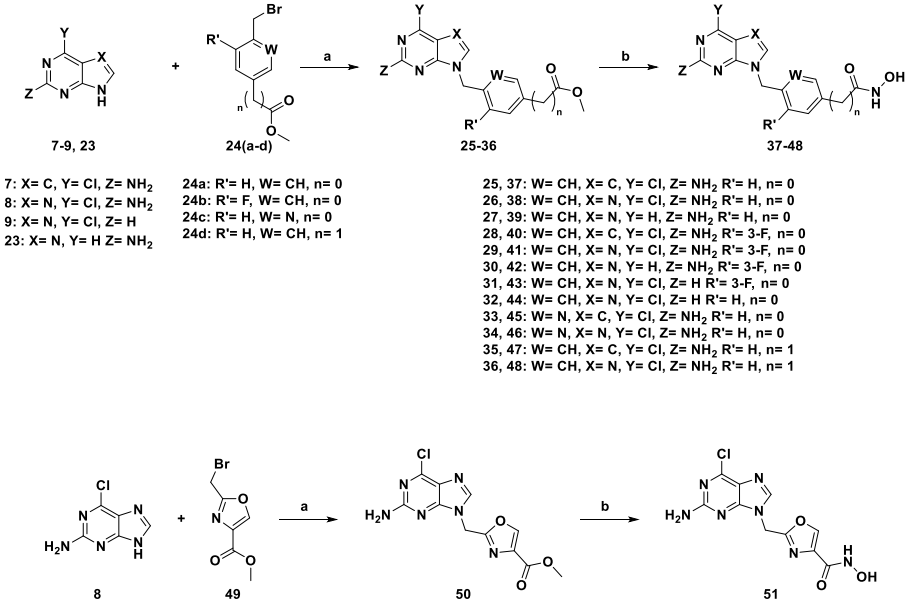

Scheme 2. Reagents and conditions for the preparation of HA compounds 37–48, 51: a) K_2CO_3, DMF, RT, overnight, 13–54% yield; b) NH_2OH 50 wt % in H_2O, NaOH 1 N, THF/MeOH 1:1 (v/v), RT, 3 h, 26–77% yield.

methyl 6-(bromomethyl)nicotinate, methyl 2-(4-(bromomethyl)phenyl) acetate **24** or methyl 2-(bromomethyl)oxazole-4-carboxylate **49**. The intermediates **25–36** and **50** were then converted into the corresponding hydroxamic acids after treatment with aqueous hydroxylamine in 1 N sodium hydroxide solution to afford the final compounds in good yields.

The synthetic pathway for the synthesis of compounds **59** and **60** of the MCA series (Scheme 3) started with the S_N2 reaction between 1-(bromomethyl)-4-nitrobenzene and the commercially available 4-chloro-7*H*-pyrrolo [2,3-*d*]pyrimidin-2-amine or 6-chloro-9*H*-purin-2-amine. The nitro group was reduced using iron powder and NH_4Cl. Then, the coupling reaction between the amines **55** and **56** and the 2-(tritylthio)acetic acid in the presence of *N*-(3-dimethylaminopropyl)-*N*′-ethylcarbodiimide hydrochloride (EDCI) and hydroxybenzotriazole (HOBt) as coupling agents gave the corresponding S-protected mercaptoacetamides. Finally, the trityl group was removed under acid conditions to afford the final compounds in good yields.

Finally, the thioacetamide **65** was obtained starting from Boc-protected *N*-(4-(bromomethyl)benzyl)-amine and the 6-chloro-9*H*-purin-2-amine. The Boc group was removed under acid conditions and the corresponding benzylamine reacted with the 2-(tritylthio)acetic acid in the presence of EDCI/HOBt coupling agents for amide bond formation. The final compound **65** was obtained in good yield after cleavage of the trityl protecting group (Scheme 4).

2.2. In vitro HDAC inhibitory activity and SAR

All synthesized compounds were firstly tested *in vitro* to assess their ability to inhibit the purified recombinant HDAC6. Then, a number of compounds were also tested for inhibition of HDAC1 and HDAC4, chosen as representatives of class I and IIa HDACs, in order to have a first check for selectivity. The inhibitory activities, expressed as IC_{50}, are reported in Tables 1–3, while the corresponding dose-response curves are reported in the Supplementary Information section (Figures S1 – S3).

The compounds belonging to the TFMO series (Table 1) displayed IC_{50} values against HDAC6 in the micromolar to nanomolar range. Interestingly, compounds bearing the purine ring (X = N: **11**, **13**, **15**–**18**, **20**) showed higher HDAC6 inhibitory activity compared to their pyrrolo-pyrimidine (X = CH: **10**, **12**, **14**, **21**) analogues. Indeed, compound **11**, with an IC_{50} of 290 nM, was eight-fold more potent than the corresponding pyrrolo-pyrimidine derivative **10** (IC_{50} = 2200 nM). The same trend was observed also for other purines with different phenyl linker decorations, as for **13** (HDAC6 IC_{50} = 85 nM) *vs* **12** (HDAC6 IC_{50} = 1900 nM). The fluorine atom substitution on the phenyl linker had a minor effect on HDAC6 inhibitory activity. In fact, the 2-fluorophenyl derivatives **12**, **13** and **17** and the 3-fluorophenyl ones (**14**, **15** and **18**) were almost as active as the corresponding unsubstituted analogues **10**, **11** and **16**. Conversely, in the purine series, the introduction of a chlorine atom at position 3 (**20**) led to a 3-fold improvement of HDAC6 inhibitory activity (IC_{50} = 93 nM) compared to the unsubstituted compound **11** (IC_{50} = 290 nM). Unexpectedly, the same substitution in the pyrrolo-pyrimidine analogue yielded the completely inactive compound **19**. The importance of the 2-amino group was investigated by synthesizing compounds **16**–**18** in which the amine group was removed. Removal of the amine did not significantly affect the HDAC6 inhibitory activity (see compounds **16** *vs* **11**, **17** *vs* **13**, and **18** *vs* **15**). Noteworthy, compounds **21** and **22**, bearing the TFMO ZBG in *meta* position, resulted in almost 3- to 17-fold drop in the activity compared to the *para*-substituted compounds **10** and **11**, respectively. This result demonstrates that the *para* substitution is optimal for binding to the HDAC6 catalytic site [64].

Eight of the thirteen TFMO derivatives were also tested against HDAC1, a member of class I HDACs, resulting in almost 100-fold selectivity in favor of HDAC6 (Table 1). When tested for inhibition of HDAC4, five TFMO compounds resulted to be from 2- to 5- times more active with respect to HDAC6. These results demonstrate that TFMO compounds inhibit members of both class IIa and IIb HDACs with similar potency, but are selective against the class I HDAC1 enzyme.

The compounds **37–48,** belonging to the HA series (Table 2), turned out to be around 2 orders of magnitude more potent on HDAC6 than the corresponding TFMO derivatives, their IC_{50} values being in the nanomolar range (Table 2).

Unlike the TFMO series, the substitution of the N7 nitrogen with a carbon atom was better tolerated in the HA series. Indeed, the pyrrolo-pyrimidine **40** and **47** showed HDAC6 IC_{50} values (3 and 27 nM, respectively) comparable to those of the purine analogues **41** and **48** (4 and 14 nM, respectively), while the pyrrolo-pyrimidine **37** was around 5 fold more active than the corresponding purine derivative **38** (5 and 23 nM, respectively). These results suggest that the HA derivatives present structure-activity relationships on HDAC6 different than those described for the TFMO compounds. Remarkably, representative HA compounds (*i.e.*, **37**, **38**, **40**, **45** and **46**) tested against HDAC1 and HDAC4 showed 100- to 1000-fold lower activity compared to HDAC6, demonstrating that compounds of the HA series are highly selective for the class IIb HDAC6 enzyme (Table 2).

The effects of the 2-amino and 4-chlorine groups in the cap moiety were also investigated on HDAC6. In particular, compounds **39** and **42**,

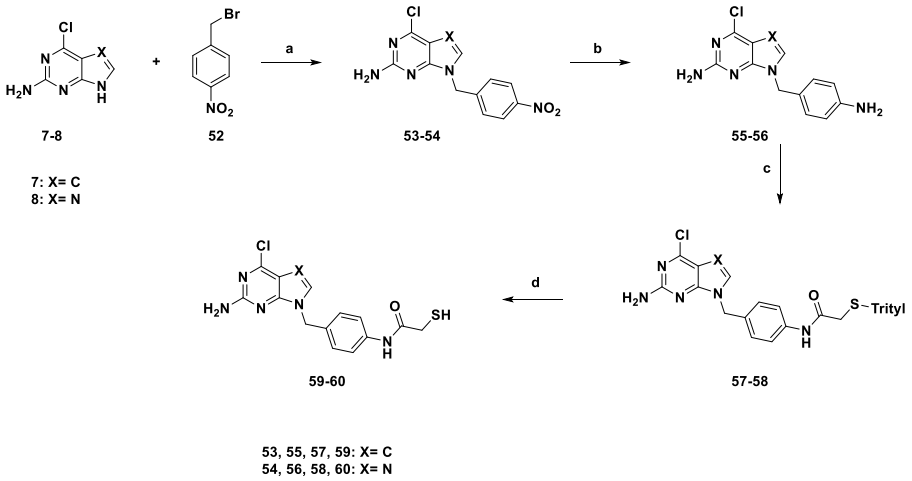

Scheme 3. Reagents and conditions for the preparation of MCA compounds 59 and 60: a) K_2CO_3, DMF, RT, overnight, 43-40% yield; b) Fe, NH_4Cl, EtOH/H_2O 1:1 (v/v), 85 °C, 4 h, 41–83% yield; c) 2-[(Triphenylmethyl)thio]acetic acid, EDCI, HOBt, DMF, RT, overnight, 34–38% yield; d), Et_3SiH, TFA, DCM, 0 °C to RT, 2 h, 88–93% yield.

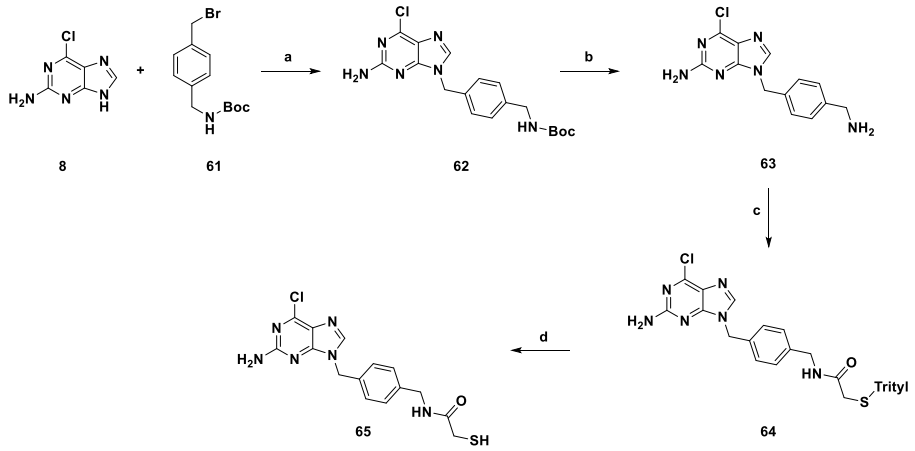

Scheme 4. Reagents and conditions for the preparation of the MCA compound 65: a) K_2CO_3, DMF, RT, overnight, 52% yield; b) TFA, DCM, RT, 6 h, 87% yield; c) 2-[(Triphenylmethyl)thio]acetic acid, EDCI, HOBt, DMF, RT, overnight, 62% yield; d), Et_3SiH, TFA, DCM, 0 °C to RT, 2 h, 82% yield.

Table 1
In vitro inhibitory activity (IC_{50}, nM) of compounds **10**–**22** (TFMO series) on HDAC1, HDAC4 and HDAC6 enzymes. n.t.: not tested; n.a.: not active. Titration curves of the compounds on HDAC1, HDAC4 and HDAC6 are reported in Figs. S1–S3.

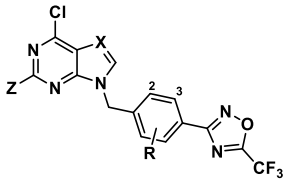

Compound	R	X	Z	IC_{50} (nM)		
				HDAC1	HDAC4	HDAC6
10	H	CH	NH_2	>100,000	n.t.	2200
11	H	N	NH_2	73,300	97	290
12	2-F	CH	NH_2	45,400	n.t.	1900
13	2-F	N	NH_2	38,800	24	85
14	3-F	CH	NH_2	>100,000	n.t.	1530
15	3-F	N	NH_2	29,300	67	320
16	H	N	H	n.t.	n.t.	280
17	2-F	N	H	3200	56	120
18	3-F	N	H	n.t.	n.t.	330
19	3-Cl	CH	NH_2	n.t.	n.t.	n.a.
20	3-Cl	N	NH_2	8560	20	93

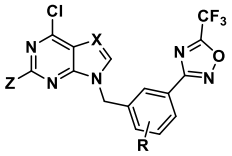

Compound	R	X	Z	IC_{50} (nM)		
				HDAC1	HDAC4	HDAC6
21	H	CH	NH_2	n.t.	n.t.	38,100
22	H	N	NH_2	n.t.	n.t.	730
TMP269				n.t.	13	52,100
Tubastatin A				n.t.	n.t.	7
Trichostatin A				7.2	n.t.	1.9
Vorinostat				n.t.	n.t.	14

which lack the chlorine atom on the purine ring had IC_{50} of 14 nM and 1 nM, while compounds **43** and **44** lacking the 2-amino group were almost equipotent. The 2-amino and 4-chlorine groups were more important in compounds with an unsubstituted phenyl linker. The introduction of a fluorine atom on the phenyl linker was well tolerated (Table 2). In addition, replacement of the phenyl ring with a pyridine resulted in the active HDAC6 inhibitors **45** and **46** (IC_{50} values of 20 and 5 nM). However, the introduction of a methylene spacer between the hydroxamate ZBG and the phenyl ring, as in **47** resulted in a slightly lower HDAC6 inhibitory activity compared to **37**, while compounds **48** and **38** were almost equipotent (Table 2). We made a single attempt to replace the phenyl ring with a five-membered heterocycle, selecting the oxazole ring as it is one of the more active hydroxamate heterocycle reported in Senger's work [65]. The oxazole compound **51** displayed an IC_{50} value of 71 nM, thus resulting significantly less active than the corresponding phenyl derivative **37** (HDAC6 IC_{50} of 5 nM). Therefore,

Table 2
In vitro inhibitory activity (IC_{50}, nM) of compounds **37**–**48** and **51** (HA series) on HDAC6, HDAC1 and HDAC4 enzymes. Assays were performed in singlicate. n.t.: not tested.

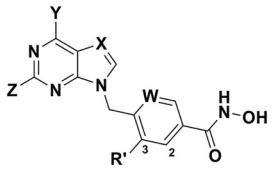

Compound	W	X	Y	Z	R'	IC_{50} (nM)		
						HDAC1	HDAC4	HDAC6
37	CH	CH	Cl	NH_2	H	390	1400	5
38	CH	N	Cl	NH_2	H	980	7700	23
39	CH	N	H	NH_2	H	n.t.	n.t.	14
40	CH	CH	Cl	NH_2	3-F	1000	570	3
41	CH	N	Cl	NH_2	3-F	n.t.	n.t.	4
42	CH	N	H	NH_2	3-F	n.t.	n.t.	1
43	CH	N	Cl	H	3-F	n.t.	n.t.	7
44	CH	N	Cl	H	H	n.t.	n.t.	4
45	N	CH	Cl	NH_2	H	990	1100	20
46	N	N	Cl	NH_2	H	1300	n.t.	5

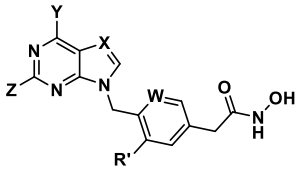

Compound	**W**	**X**	**Y**	**Z**	**R'**	**IC_{50} (nM)**		
						HDAC1	**HDAC4**	**HDAC6**
47	CH	CH	Cl	NH_2	H	n.t.	n.t.	27
48	CH	N	Cl	NH_2	H	n.t.	n.t.	14

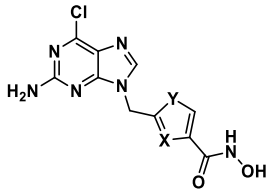

Compound	**X**	**Y**	**IC_{50} (nM)**		
			HDAC1	**HDAC4**	**HDAC6**
51	N	O	n.t.	n.t.	71

we decided not to explore further heterocycle replacements of the phenyl ring at this stage.

Compounds **59**, **60** and **65**, belonging to the MCA series, were tested to explore the effects of the 2-mercaptoacetamide ZBG in the selected scaffolds (Table 3).

Interestingly, the pyrrolo-pyrimidine derivative **59** was the most potent HDAC6 inhibitor of the MCA series (IC_{50} = 7 nM), the corresponding purine derivative **60** being slightly less active (IC_{50} = 19 nM). As previously observed for the HA series, the introduction of a methylene spacer between the MCA ZBG and the aromatic portion of the linker (compound **65**) led to a decrease of the HDAC6 inhibitory activity. Remarkably, compounds of the MCA series were ~400 times and >10.000 times more active on HDAC6 compared to HDAC1 and HDAC4, respectively, demonstrating excellent selectivity for type IIb HDAC6 (Table 2).

2.3. Molecular Modelling

To provide structural insights into the binding properties of the investigated compounds in HDAC6, which we considered our priority target, molecular docking followed by 100 ns molecular dynamics simulations were performed on a set of representative members of each series (*i.e.*, TFMO, HA, and MCA). Indeed, MD is very often used in order to better evaluate the dynamics behaviour of docking complexes [66]. Docking of representative compounds of the TFMO series was also performed on HDAC1 and HDAC4, for comparison (see below). As mentioned above, the binding to HDAC6 requires the coordination of the catalytic Zn^{2+} ion placed at the bottom of a narrow crevice with the length of approximately 10 Å. The cap group of the ligands is located at the rim of the crevice in the upper part of the binding site and is mainly solvent-exposed. Additionally, the upper part of the HDAC6 binding site presents two sub-pockets, *i.e.* the L1 sub-pocket lined by the L1 loop (Asp497-Pro501), and the L2 sub-pocket defined by the L2 loop (Glu677−Met682) (Fig. S4). Interestingly, the L1 sub-pocket is absent in class I HDACs due to a shift of the L1 loop inward the cavity. Therefore, selective inhibition of HDAC6 can be achieved through bulky cap groups that accommodate in the L1 sub-pocket [67,68].

The TFMO derivatives **10**, **11** and **16** were firstly analyzed. In particular, the TFMO group accommodated into HDAC6 by establishing interactions with the catalytic Zn^{2+} ion, similarly to those experimentally observed for ligands bearing the same ZBG (see the **Methods** section for details) [49,50]. According to the performed *in silico* analyses, the TFMO group established electrostatic interactions with the catalytic Zn^{2+} ion *via* the fluorine atoms of the trifluoromethyl moiety and the oxygen atom of the oxadiazole ring. The phenyl linker was predicted to be co-planar with the TFMO ring establishing favorable π-π staking

Table 3
In vitro inhibitory activity (IC_{50}, nM) of compounds **59**, **60**, and **65** (MCA series) on HDAC1, HDAC4 and HDAC6 enzymes. Assays were performed in singlicate. n.t.: not tested.

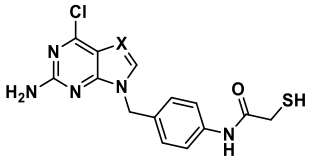

Compound	X	IC_{50} (nM)		
		HDAC1	HDAC4	HDAC6
59	CH	2800	92,000	7
60	N	8900	>100,000	19

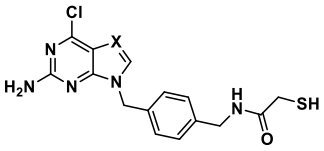

Compound	**X**	**IC_{50} (nM)**		
		HDAC1	**HDAC4**	**HDAC6**
65	N	39,000	>100,000	320

interactions with the Phe620 and Phe680 side chains, thus contributing to favorable binding to HDAC6 [69]. The wide entrance and solvent-exposed environment of the outer enzyme surface allowed significant flexibility to the cap group of the ligands, as detected by the root-mean-square deviations (RMSDs) observed in the MD trajectories (Fig. S5). Interestingly, the MD simulations predicted that compounds of this series adopted predominantly two different orientations, depending on the presence (*i.e.*, **11** - X = N) or absence (*i.e.*, **10** - X = CH) of the nitrogen atom at position 7 of the cap group. In particular, the cap group of the pyrrolo-pyrimidine compound **10** remained anchored to the L2 loop for over half of the MD simulation time, the cap group being directed towards Phe680 (Fig. 2A).

Conversely, the purine cap of compound **11** was more frequently directed towards the L1 loop (Fig. 2B). The switch between occupation of the L1 or the L2 pockets occurred through rotation along the benzylic methylene bond. Interestingly, a water molecule bridging the N7 atom of purine **11** and the side chains of Asp497 and His500 was detected for about 20% of the MD trajectory. Such a water-mediated interaction, which is established only by compounds bearing a purine-based cap group, may account for the consistently higher inhibitory activity of the purine compounds **11**, **13**, **15** and **20**, with respect to the corresponding pyrrolo-pyrimidine analogues **10**, **12**, **14** and **19**. Noteworthy, the binding orientation observed for **16** overlapped well with that of **11**, demonstrating that removal of the 2-amino substituent did not affect the position of the cap moiety (Fig. S6). In agreement with this, removal of the 2-amino group in compounds **16**, **17** and **18** had a marginal effect on the inhibitory activity, compared to the corresponding 2-amino derivatives **11**, **13** and **15**.

Furthermore, docking analyses were also performed for the representative compound **11** in HDAC1 and HDAC4 crystallographic structures, belonging to HDAC class I and IIa, respectively. Of note, the interaction between the TFMO group and the HDAC4 Zn^{2+} ion (Fig. S7, panel A) was similar to that observed in HDAC6, although the binding sites of the two proteins differ significantly. On the contrary, the size of the HDAC1 binding site hinders the interactions of TFMO with the metal ion by producing a less efficient interaction, in agreement with the *in vitro* results (Fig. S7, panel B) [70]. Docking of the fluoro-substituted TFMO derivatives in HDAC1 and HDAC4 produced almost identical

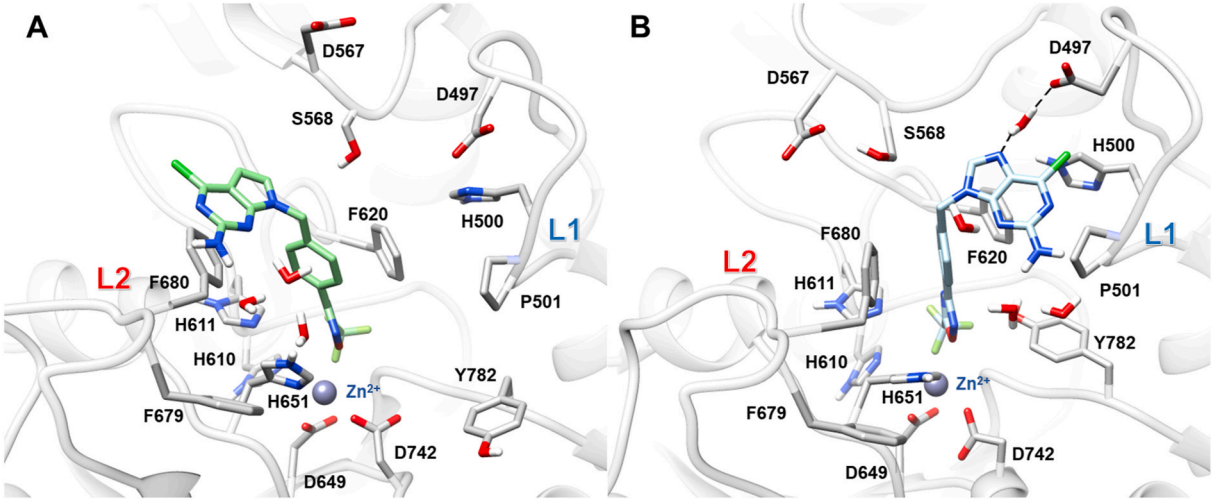

Fig. 2. Representative binding modes of compounds **10** (**panel A**) and **11** (**panel B**) in complex with HDAC6, resulting from the MD simulations. The hydrogen bonds are shown as black dashed lines. Only relevant water molecules are shown.

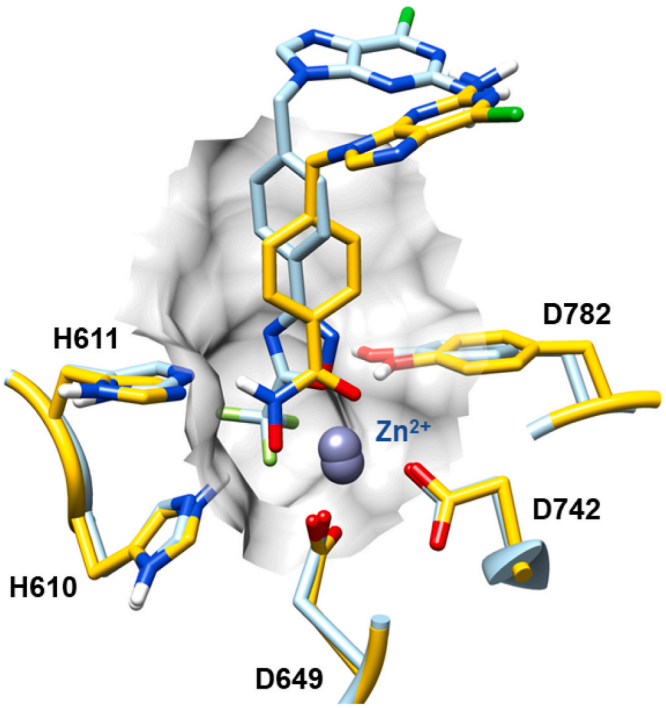

Fig. 3. Superimposition of the representative binding modes of compounds **11** (light blue sticks) and **38** (yellow sticks) in complex with HDAC6, resulting from the MD simulations.

complexes (data not shown).

Compounds **37**, **38** and **44** were chosen as representative members of the HA series. Compared to the corresponding compounds of the TFMO series, the phenyl rings of the HA derivatives accommodated approximately 1.5 Å deeper inside into the HDAC6 catalytic cleft (Fig. 3). This is likely due to the smaller size of the hydroxamate ZBG and its stronger coordination ability to the zinc ion. In turn, this affected the position of the rest of the molecule by pulling the linker and the cap closer to the bottom of the cavity. Overall, compounds **37** and **38** showed a similar binding mode (Fig. 4), the hydroxamate group establishing a bidentate coordination with the zinc ion and the cap group being oriented toward the L1 sub-pocket. In the MD simulations, the cap group of **37** (X = CH) occupied the L1 sub-pocket for most of the MD simulation time (see RMSD plot of compound **37** in Fig. S5), while the cap of compound **38** (X = N) swapped between the L1 and L2 sub-pockets, the latter orientation displaying the purine ring close to Ser568 and Phe569 (Fig. S8). The observed fluctuation of the cap group of **38** is likely due to a network of water-mediated interactions established by the nitrogen atom at position 7 of the purine. Since the inhibitory activity of **38** was similar to that of **37**, the higher mobility of the former compound does not seem to play a role on activity. Likewise, the 2-amino group of **37** and **38** was mainly involved in water-mediated interactions in the L1 sub-pocket, while the MD analyses performed on **44** showed that the cap group was shifted towards the L2 sub-pocket (Fig. S9). Such different poses of the compounds highlight a water-mediated hydrogen bond performed by the 2-amino group in the L1 loop.

Finally, compounds **59** and **60** of the MCA series were analyzed. In the HDAC6 complexes, the negatively charged thiolate of the mercaptoacetamide group coordinated the catalytic Zn^{2+} ion with a tetrahedral geometry and it accepted a hydrogen bond from the positively charged side chain of His610 [54]. The carbonyl oxygen of the MCA was placed outside the coordination sphere of the metal ion and it hydrogen bonded with the phenolic hydroxyl of Tyr782. The coordination geometry of the MCA derivatives was consistent with that observed in other crystallographic complexes of HDACis bearing the MCA ZBG [54,71]. In the MD simulations, the cap group of **59** (X = CH) showed higher fluctuations compared to compound **60** (Fig. S5). As shown in Fig. 5A, the cap group of **59** accommodated in the L1 sub-pocket, positioning the purine ring next to Leu749 and the 2-amino group towards Pro501, similarly to what observed for the HA derivatives **37** and **38**, while the cap of compound **60** (X = N) remained close to L2 throughout the simulation. In particular, compound **60** established interactions with residues of the L2 sub-pocket (Fig. 5B). The purine ring was positioned between Phe679 and Phe680, and the N7 nitrogen extended near L2, establishing water-mediated interactions with the imidazole ring of His651.

In summary, the shape of the HDAC6 binding site allowed the cap group of the reported compounds to explore more than one orientation, albeit recurring patterns could be identified across ligands of the TFMO, HA or MCA series. The MD results highlighted two distinct cap orientations for the TFMO and HA derivatives, due to the different length of the two ZBGs and the different interactions established with the Zn^{2+} ion. This finding may explain why the SAR of TFMO compounds is influenced by the presence of the nitrogen at position 7 of the purine ring. Two distinct cap orientations were observed in the MCA derivatives, although the inhibitory activities of the corresponding pyrrolo-pyrimidine and purine derivatives were very similar. Docking of selected TFMO derivatives into the HDAC1 and HDAC4 binding sites provided an explanation for their selectivity profiles.

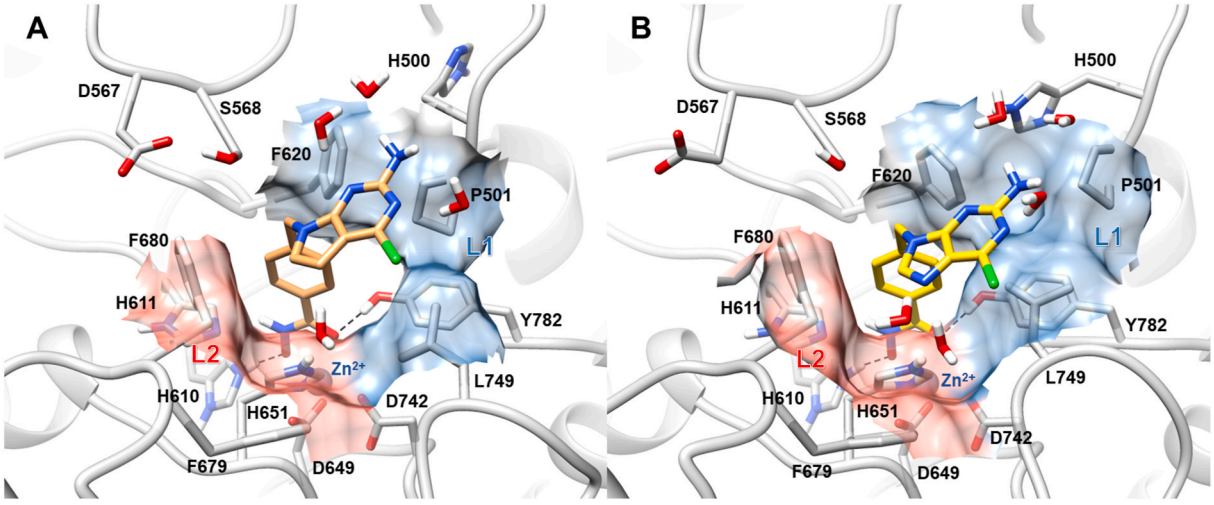

Fig. 4. Representative binding modes of compounds **37** (**panel A**) and **38** (**panel B**) in complex with HDAC6, resulting from the MD simulations. The hydrogen bonds are shown as black dashed lines. Only relevant water molecules are shown.

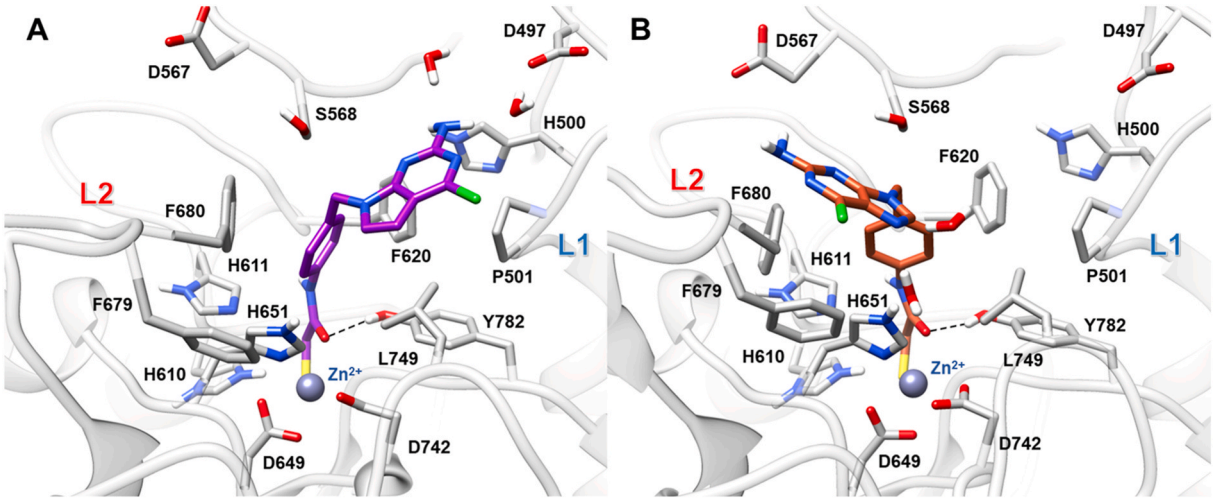

Fig. 5. Representative binding mode of compounds **59** (**panel A**) and **60** (**panel B**) in complex with HDAC6 resulting from the MD simulations. The hydrogen bonds are shown as dashed lines. Only relevant water molecules are shown.

Table 4
GI_{50} values ± SEM (n = 3) determined by MTT assay on LNCaP (cancer) and RWPE-1 (normal) cells treated for 72 h. (a) Selectivity Index (SI) values calculated as the ratio of GI_{50} (RWPE-1)/GI_{50} (LNCaP) values. SI values higher than 1 are indicative of compounds selective for cancer vs normal cells. (b) Compounds not characterized by dose-response cellular effects (Fig. S9). (c) Anti-proliferative activities against RWPE-1 cell lines were determined only for compounds with GI_{50} (LNCaP) values ≤ 30 μM. The fourteen compounds with GI_{50} (LNCaP) values ≤ 30 μM are marked in bold. Of these, the eight compounds with GI_{50} (LNCaP) values ≤ 30 μM and SI values > 1 are underscored. Tubastatin A, SAHA and TMP269 were used as positive controls.

Compound	GI_{50} (μM) Mean ± SEM		Selectivity Index [(a)]
	LNCaP	RWPE-1	
10	**10.6 ± 4.1**	4.0 ± 3.9	0.4
11	32.3 ± 8.0	(c)	(c)
12	**12.5 ± 5.5**	7.2 ± 1.4	0.6
13	**0.32 ± 0.02**	1.1 ± 0.8	**3.4**
14	**20.7 ± 11.9**	2.7 ± 1.3	0.1
15	**8.0 ± 3.1**	17.0 ± 16.1	**2.1**
16	**24.6 ± 11.5**	16.0 ± 7.2	0.6
17	**12.5 ± 2.4**	13.9 ± 7.9	**1.1**
18	**15.9 ± 2.4**	13.5 ± 2.3	0.9
19	**5.5 ± 3.2**	43.0 ± 40.5	**7.8**
20	**7.0 ± 2.5**	81.7 ± 1.3	**11.7**
21	80.8 ± 33.6	(c)	(c)
22	>100	(c)	(c)
37	**5.8 ± 1.4**	9.9 ± 0.8	**1.7**
38	(b)		
39	74.7 ± 20.7	(c)	(c)
40	**18.3 ± 7.5**	10.4 ± 4.4	0.6
41	(b)		
42	57.9 ± 11.9	(c)	(c)
43	>100	(c)	(c)
44	>100	(c)	(c)
45	**12.1 ± 2.4**	44.9 ± 2.4	**3.7**
46	(b)		
47	>100	(c)	(c)
48	**12.7 ± 3.3**	79.2 ± 60.5	**6.3**
51	41.9 ± 15.0	(c)	(c)
59	48.8 ± 21.8	(c)	(c)
60	>100	(c)	(c)
65	(b)		
Tubastatin A	5.0 ± 1.7	20.2 ± 1.1	4.0
SAHA	1.3 ± 0.2	1.6 ± 0.3	1.2
TMP269	21.3 ± 0.4	8.0 ± 0.6	0.4

2.4. Selective anti-proliferative activity on prostate adenocarcinoma cells

To determine the potential anti-tumor activity of the synthesized compounds, we performed dose-response cell viability assays on LNCaP cells, which are one of the most representative *in vitro* models of PCA deriving from a metastatic lymph node lesion. By MTT assays, we assessed the proliferation/viability of LNCaP cells treated for 72 h with 3-fold serial dilutions, starting from a compound concentration of 100 μM. Dose-response anti-proliferative effects were observed for all compounds except for **38**, **41**, **46** and **65** (Fig. S10). The GI_{50} values, calculated as the concentrations inhibiting the growth of cancer cells by 50% following 72 h of treatment, are reported in Table 4. Four reference compounds were used, *i.e.* the *pan*-HDACis SAHA and TSA, the class IIa-HDACi TMP269, and the HDAC6-HDACi Tubastatin A. Although the HDAC6 inhibitory activities of the HA derivatives were significantly higher compared to those of the corresponding analogues of the TFMO series (Tables 1 and 2), a clear superiority of the HA compounds could not be observed in the cellular assays (Table 4). The three compounds of the MCA series were poorly active in cellular assays. To gain more insights into such behaviour, we predicted the solubility and Caco-2 permeability, used as a model of human intestinal absorption of drugs, with QikProp [72] (Table S1). Interestingly, compounds of the HA series had predicted higher solubility but lower Caco-2 cell permeability, with respect to compounds of the TFMO series. Therefore, it is possible that the higher *in vitro* inhibitory activity of the HA derivatives is counterbalanced by a lower membrane permeability in cellular assays. Only the compounds characterized by a dose-response cellular effect and GI_{50} values lower than 30 μM were further investigated (*i.e.*, fourteen compounds marked in bold in Table 4). Firstly, we tested their anti-proliferative activity on human normal prostate RWPE-1 cells through dose-response MTT assays (Fig. S11). Noteworthy, eight molecules, namely **13**, **15**, **17**, **19**, **20**, **37**, **45** and **48**, were considerably selective for cancer *versus* normal cells, as demonstrated by a Selectivity Index (SI), defined as GI_{50} (RWPE-1, normal cell line)/GI_{50} (LNCaP, cancer cell line), higher than 1 (*i.e.*, eight underscored compounds in Table 4).

2.5. HDACs-targeting in prostate cancer cells

To assess whether the anti-proliferative activity of the fourteen compounds with GI_{50} (LNCaP) values ≤ 30 μM was a consequence of HDAC6-targeting, we determined the effect of cell treatments on the expression levels of acetylated tubulin (AcTub), a well-known HDAC6 target. We analyzed cellular extracts from LNCaP cells treated for 24 h at

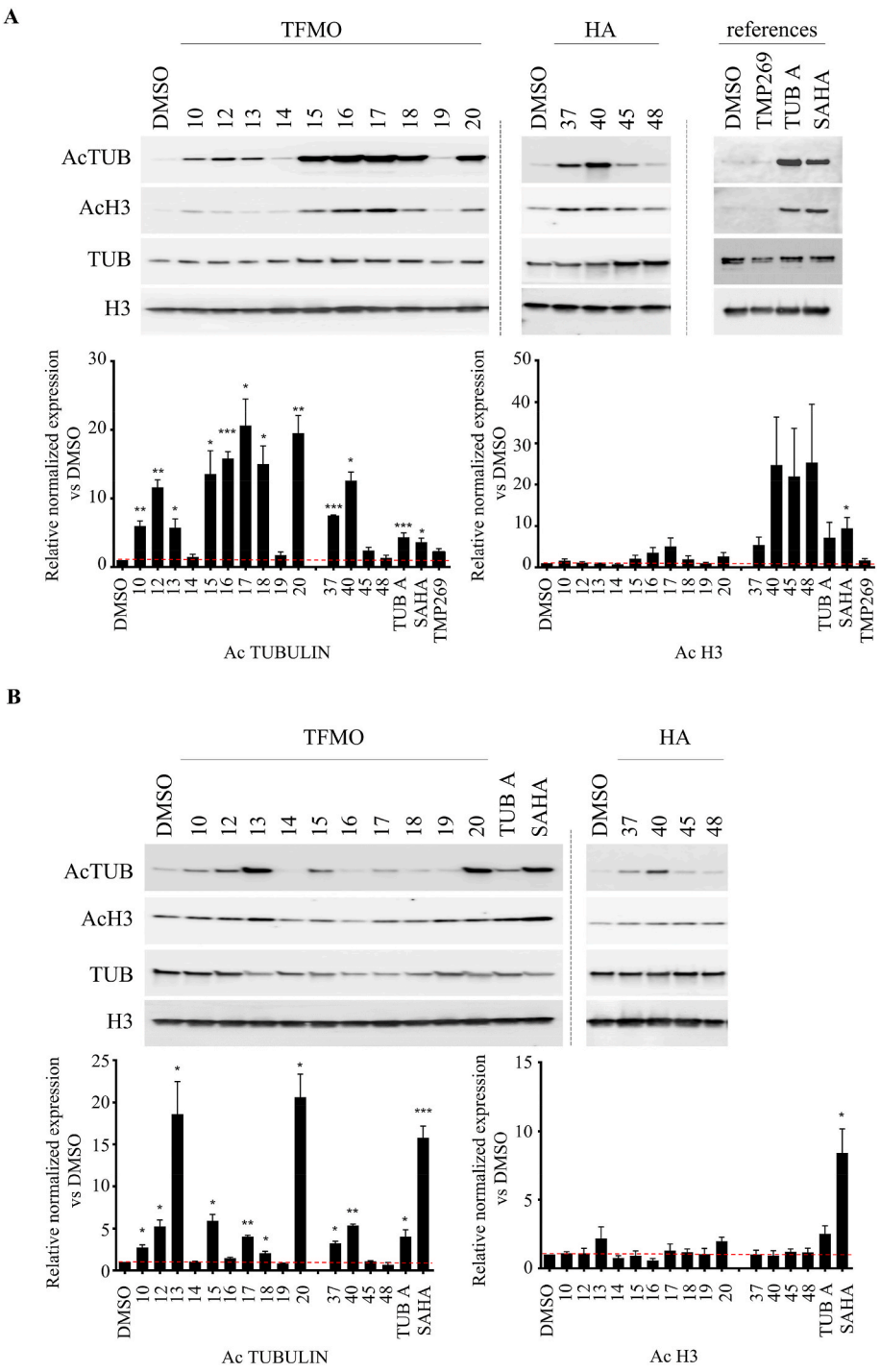

Fig. 6. Western blot analysis of the expression levels of acetylated-Tubulin (AcTub) and acetylated H3 (AcH3) in LNCaP cells treated for 24 h at the GI_{50} doses (A) or at a 3 μM dose (B). Lower panels represent relative quantification of protein expression normalized to tubulin and reported as fold change in treated cells versus DMSO, arbitrarily set at 1 (*t*-test p-values: *p < 0.05, **p < 0.01, ***p < 0.001; n = 3). Tubastatin A (TUB A) was used as HDAC6-specific positive control, TMP269 as class IIa-specific negative control and SAHA as pan-HDACs inhibitor. Tubulin (TUB) and Histone H3 (H3) were used as loading controls.

Table 5
Inhibition of HDAC Class IIa activity measured in LNCaP cells by cellular HDAC-Glo Class IIa Assay (Promega) after 1 h of incubation. IC_{50} values were calculated for compounds **13** and **20**, using TMP269 as reference compound.

Compound	IC_{50} (nM)
20	59
13	<5
TMP269	432

GI_{50} doses by Western blot and we normalized the levels of AcTub *versus* total Tubulin, which was used as loading control (Fig. 6A). Although with different efficiency, all the compounds induced an increase in AcTub, with the exception of **14**, **19**, **45** and **48**. The analysis of γH2AX expression ruled out possible genotoxic effects (Fig. S12).

The effect of treatments on the expression levels of AcTub in LNCaP cells was evaluated also at a lower concentration (3 μM) to avoid possible toxic side effects, non-specific drug targeting and drug resistance [73]. Western blot analysis highlighted that most compounds were able to inhibit HDAC6 activity even at lower doses (Fig. 6B). The effect of the molecules on the levels of acetylated histone H3 (AcH3)

Table 6
In vitro drug-like profiles of representative compounds 13 (TFMO) and 37 (HA). (a) Low, medium and high with Papp $\leq 10^{-6}$ cm/s, 10^{-6} cm/s < Papp $\leq 10 \times 10^{-6}$ cm/s and Papp $> 10 \times 10^{-6}$ cm/s, respectively. (b) An efflux ratio >2 suggests P-Glycoprotein (P-gp) mediated or other transporters efflux phenomena [74]. (c) Low, medium, and high clearance in mouse microsomes is ≤ 2.5, 2.5–66, >66 [75,76]. respectively. (d) Low, medium, and high clearance in human microsomes is ≤ 1.8, 1.8–48, >48 [75,76].

Cpd	Solubility (μM) pH 7.4	Solubility (μM) pH 4.5	Papp AB[a] 10^{-6} cm/s	Papp BA[a] 10^{-6} cm/s	Efflux ratio [b] (BA/AB)	Intrinsic Clearance[c] (μL/min/mg protein) mouse	Intrinsic Clearance [d] (μL/min/mg protein) human
13 (TFMO series)	3.4 ± 0.9	3.8 ± 0.4	20.6 ± 8.01	10.3 ± 0.05	0.5	30.2 ± 1.5	30.7 ± 12.9
37 (HA series)	434.2 ± 84.2	507.1 ± 0.67	2.5 ± 0.06	2.4 ± 0.1	0.9	7.4 ± 2.0	26.3 ± 7.0

normalized to total Tubulin was informative of a possible non-specific activity of the compounds on nuclear class I HDACs. Importantly, we did not observe a significant increase in AcH3. Compound **13**, which showed the lowest GI_{50} value in LNCaP cells, confirmed its HDCA6-targeting activity also after treatment at sub-GI_{50} concentration (Fig. S13). We further profiled the HDACi activity of the two more promising compounds based on GI_{50} data and HDAC6 inhibitory activity, namely compounds **13** and **20**. Using an HDAC-Glo Class IIa Assay based on an acetylated, live-cell-permeant, luminogenic peptide substrate specific for class IIa HDACs, we observed a robust Class IIa-HDACs inhibition in LNCaP cells (Table 5). Taken together, these results indicate that compounds **13** and **20** specifically target HDAC6 and Class IIa HDACs when administered to PCA cells.

2.6. In vitro evaluation of drug-like profiles of selected TFMO and HA compounds

Water solubility, cell permeability and metabolic stability are essential requirements for developing effective inhibitors with therapeutic potential. To this aim, we assessed the drug-like properties of representative TFMO and HA compounds (**13** and **37**, respectively). In particular, *in vitro* studies were performed to evaluate aqueous kinetic solubility, bidirectional intestinal permeability in Caco-2 cells [74] and metabolic stability in mouse and human liver microsomes. The results are reported in Table 6. The HA compound **37** exhibited an excellent water solubility of 434.2 and 507.1 μM at pH 7.4 and 5.4, respectively. Although compound **13** (TFMO) displayed sub-optimal water solubility, it showed 10-fold higher Caco-2 membrane permeability compared to compound **37** (HA). This finding may explain why TFMO compounds performed better than HA in the cellular assays. The *in vitro* results are in agreement with the *in silico* QikProp predictions discussed above (Table S1).

In both cases, the efflux ratio was lower than 1, indicating that the two compounds neither are substrates for P-Glycoproteins (P-gp), nor are affected by other transporters efflux phenomena [74]. Compounds **13** and 37 were also tested for their *in vitro* metabolic stability to Phase 1 oxidative metabolism in human and mouse liver microsomes, using NADP, Glc6P, Glc6P-DH as co-factors. As reported in Table 6, compound **37** displayed a clearance of 7.4 ± 2.0 μL/min/mg in mouse and 26.3 ± 7.0 μL/min/mg in human microsomes, while compound 13 showed a clearance of 30.2 ± 1.5 μL/min/mg in mouse and 30.7 ± 12.9 μL/min/mg in human microsomes. According to the literature [75,76], both compounds showed an acceptable intrinsic clearance in human and mouse microsomes. Overall, these results highlight favorable drug-like profiles.

2.7. Effects of selected compounds on the invasive behaviour of CSPC and CRPC cells

Since the acetylation of tubulin controls the dynamics of focal adhesion and promotes cell migration of cancer cells, we decided to investigate the compounds for their possible inhibitory effect on cell invasive behaviour. On the basis of HDAC6-targeting (Fig. 6) and selective activity on cancer *versus* normal cells (Table 4), we tested four TFMO molecules (*i.e.*, **13**, **15**, **17** and **20**) and one HA compound (*i.e.*, **37**) in transwell migration assays. LNCaP cells treated at 3 μM dose showed a significant decrease in cell migration by compound **13**, similarly to Tubastatin A used as HDAC6-specific positive control (Fig. 7). A slight but significant reduction was noted also for compound **15**. Even though the experimental condition in Transwell assays allowed to measure cell migration in the absence of proliferation (low serum cell culture medium), we explored whether a 3 μM dose could also affect cell proliferation in normal growth conditions. As expected from GI_{50} values (Table 4), compound **13** was the only one to severely inhibit cell growth, while the administration of compounds **15**, **17** and **20** at subGI_{50} dose reduced of about 30–40% the proliferation of LNCaP cells (Fig. 7B).

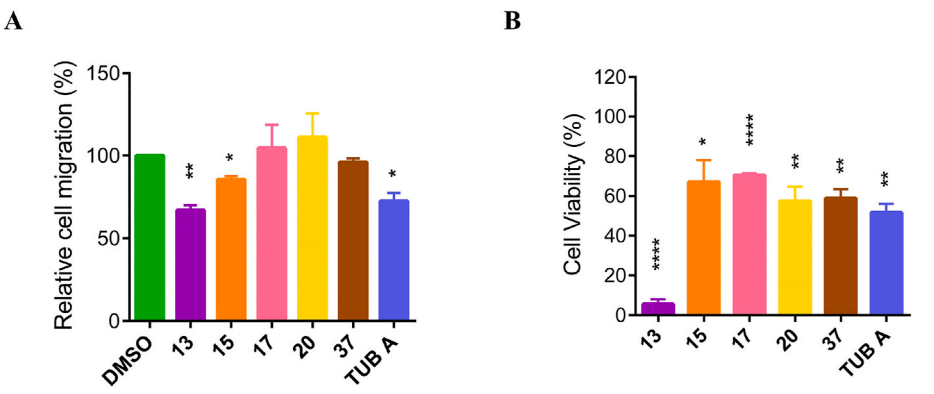

Fig. 7. Panel A. Percentage of cell migration of LNCaP cells treated at 3 μM for 72 h measured by Transwell assays. The percentage of cell migration in DMSO-treated cells was arbitrarily set at 100%. Tubastatin A (TUB A) was used as HDAC6-specific positive control. Data represent mean ± SEM (one-sample *t*-test vs DMSO: *p < 0.05, **p < 0.01; n = 3). Panel B. Anti-proliferative activity of the indicated compounds in LNCaP cells at 3 μM for 72 h. Data represent mean ± SEM (one-sample *t*-test vs DMSO: *p < 0.05, **p < 0.01; ****p < 0.0001; n = 3).

The major cause of PCA-associated death is the development of metastatic CRPC, which is characterized by a highly invasive behaviour. The results on AR-sensitive LNCaP cells reported above encouraged us to test the anti-cancer activity of the compounds on AR-insensitive PC3 cells, a cellular model for CRPC. Firstly, we verified whether the compounds were able to inhibit HDAC6 activity in the PC3 cell line. Western blot analysis of AcTub and AcH3 was performed following treatments at 3 μM dose for 24 h (Fig. 8). The compounds **12**, **13**, **15**, **17**, **20**, **37**, **40** and **45** showed a robust activity also in PC3 cells.

We then determined the activity of the five previously investigated compounds on the migration of PC3 cells. Wound healing assays demonstrated that **13**, **15** and **20** were able to significantly inhibit cell migration after 18 and 24 h compared to control cells treated with DMSO (Fig. 9A). Although the wound healing assay was performed in low serum conditions to avoid the interference of possible modulation of cell proliferation, we determined the anti-proliferative activity of the selected molecules at 3 μM in complete growth medium. As shown in Fig. 9B, compound **13** was the only to partially inhibit cell proliferation (about 20%), once again suggesting its therapeutic value against advanced PCA.

2.8. *Complete profiling of HDACs inhibitory activity of compound **13***

Based on these analyses, compound **13** combined the best anti-proliferative and anti-migratory abilities in PCA cells with promising drug-like properties. Therefore, we performed a complete profiling of its inhibitory activity on all HDAC isoforms (Table 7).

The *in vitro* profiling of **13** pointed out that the compound is significantly active against both HDAC6 and class IIa HDACs (HDAC4, HDAC5, HDAC7 and HDAC9). On the contrary, low or no inhibition was observed for other HDACs, indicating that compound **13** is selective for HDAC6 and class IIa HDACs. Such multi-target activity profile can be explained considering the structural differences present in the binding site of HDAC1, HDAC4 and HDAC6 isoforms. In particular, HDAC1 and

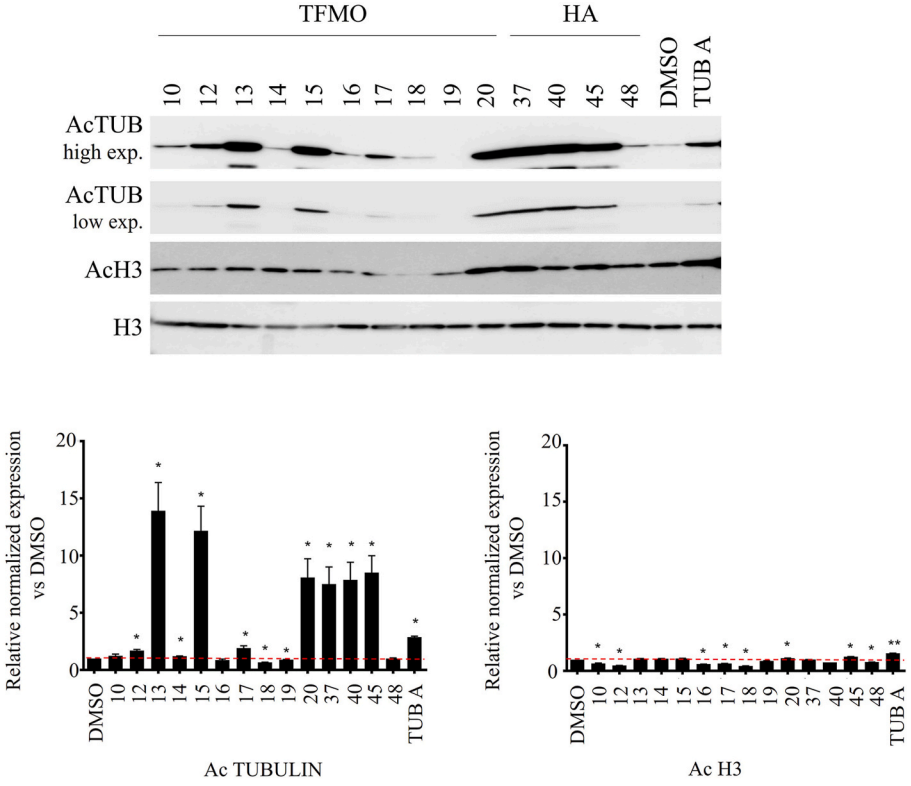

Fig. 8. Western blot analysis of AcTub and AcH3 in total extracts from PC3 cells treated with the compounds at 3 μM dose for 24 h. Tubastatin A (TUB A) was used as HDAC6-specific positive control. H3 was used as loading control. Lower panels represent relative quantification of protein expression normalized to total H3 and reported as fold change in treated cells versus DMSO, arbitrarily set at 1. T-test p-values: *p < 0.05, **p < 0.01; n = 3.

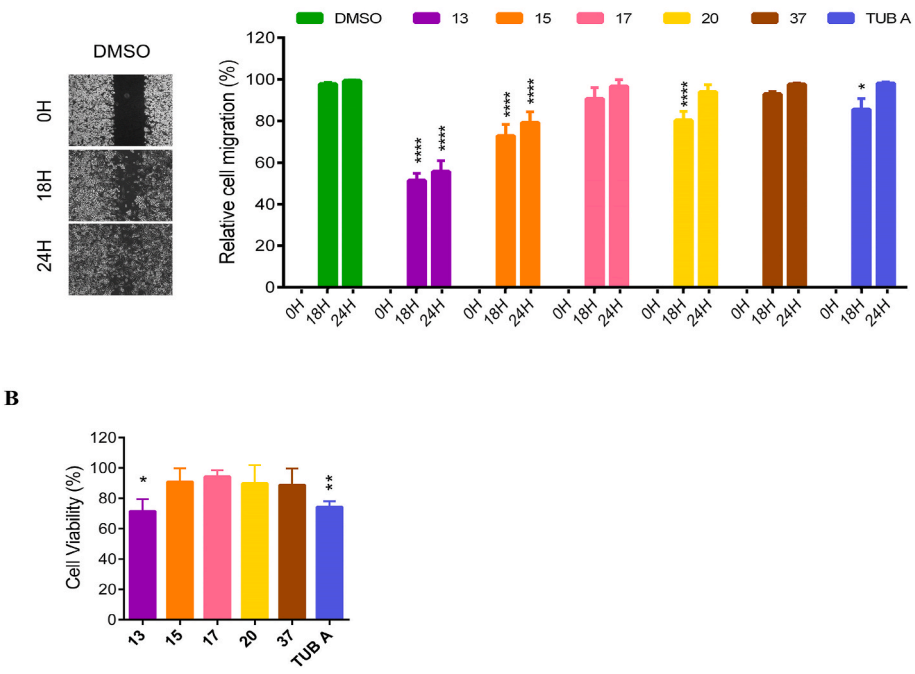

Fig. 9. Panel A. Wound healing assays on PC3 cells treated with the indicated compounds (3 μM) for 18h and 24h. Cell migration (% wound closure) at time 0 h has been arbitrarily set at 0%. Tubastatin A (TUB A) was used as HDAC6-specific positive control. Data represent mean ± SEM (Two-way ANOVA with Fisher's LSD test: *$p < 0.05$, ****$p < 0.0001$; $n = 3$). Representative images of wound closure in control cells (DMSO) are shown in left panel. Panel B. Anti-proliferative activity of the indicated compounds in PC3 cells at 3 μM for 72h. Data represent mean ± SEM (one-sample t-test vs DMSO: *$p < 0.05$, **$p < 0.01$; $n = 3$).

HDAC6 display three residues at the entrance of their catalytic tunnel (*i.e.*, His28, Pro29 and Met30 in HDAC1; His500, Pro501 and Glu502 in HDAC6), not present in HDAC4, which hamper the binding of ligands with sterically hindered linkers (Fig. S15) [79]. Indeed, this effect is particularly evident for HDAC1, in which these residues (*i.e.*, Met30) extend towards the inner part of the catalytic tunnel (Fig. S15), impairing the ability of the TMFO moiety of **13** to fit into the enzyme binding site.

Considering that the investigated compounds possess a pyrrolo-pyrimidine or purine scaffold, we reasoned that they could inhibit

Table 7
In vitro inhibitory activity (IC_{50}, nM) of compound **13** against Class I, IIa, IIb and IV HDACs. HDAC isoforms are grouped according to class membership. IC_{50} values of the control compounds Trichostatin A, TMP269 and Quisinostat are also reported. Titration curves of the compounds on the different histone deacetylases are reported in Fig. S14 and S1–S3.

Class I				
Compound	HDAC1	HDAC2	HDAC3	HDAC8
13	38800	3600	860	45100
Trichostatin A	7.2	9	4	650
TMP269	>100[d]	>100[d]	>100[d]	4200[d]
Quisinostat	0.1[b]	0.3[b]	4.86[c]	4[b]
Class IIa				
Compound	HDAC4	HDAC5	HDAC7	HDAC9
13	24	45	31	37
Trichostatin A	12[a]	16[a]	22[a]	38[a]
TMP269	13	191	44	17
Quisinostat	0.6[b]	4[b]	119[b]	32[b]
Class IIb				
Compound		HDAC6		HDAC10
13		85		2200
Trichostatin A		1.9		20[a]
TMP269		8200[d]		>100[d]
Quisinostat		77[b]		14
Class IV				
Compound				HDAC11
13				98700
Trichostatin A				4700
TMP269				>100[d]
Quisinostat				0.4[b]

Note: Assays were performed in singlicate. [a] activity values taken from Ref. [77]. [b] activity values taken from Ref. [12]. [c] activity values taken from Ref. [78]. [d] activity values taken from Ref. [70].

protein kinases. To investigate this possibility, extensive 2D ligand-based analyses were performed within ChEMBL (www.ebi.ac.uk/chembl/, accessed on June 21st, 2023) [80] as detailed in the Supporting Information. The performed chemoinformatics analyses led to the identification of MSK1, c-Mer, AXL, P38a, c-Met and VEGFR2 kinases as putative secondary targets of compound **13** (Supporting Information). Remarkably, results of *in vitro* assays performed on these kinases did not highlight any relevant inhibitory activity, suggesting that the effects of **13** observed in the cellular assays can be ascribed to modulation of HDACs.

3. Conclusions

In this study, we designed and synthesized novel HDAC inhibitors as an effort toward the identification of promising lead candidates against advanced PCA. Three series of compounds based on the trifluoromethyloxadiazole, hydroxamic acid, and 2-mercaptoacetamide zinc-binding groups were developed. The three warheads were conveniently tethered to variously substituted phenyl linkers and decorated with differently substituted pyrrolo-pyrimidine and purine cap groups, resulting in the synthesis of twenty-nine compounds that were submitted to biological tests.

Most of the tested compounds showed nanomolar HDAC6 inhibitory activities (Tables 1–3). Compounds of the HA and MCA series were highly selective for HDAC6, while compounds of the TFMO series were active on both HDAC6 (class IIb) and HDAC4 (class IIa), but poorly active on HDAC1 (class I). The *in silico* studies conducted on HDAC6 highlighted that the three zinc-binding groups were firmly anchored to the catalytic zinc ion, the phenyl linkers were sandwiched between Phe620 and Phe680, and the cap groups explored the L1 or the L2 subpockets depending on the hydrogen bonding features of the cap group.

When tested for their anti-proliferative activity on prostate adenocarcinoma cells, fourteen compounds showed GI_{50} values lower than 30 μM. Eight of these compounds, namely **13**, **15**, **17**, **19**, **20**, **37**, **45** and **48**, were consistently selective towards PCA cells with respect to normal RWPE-1 cells. Remarkably, compounds **15**, **19**, **20** and **37** showed single digit micromolar cellular activity, and one (compound **13**) had submicromolar cellular activity. Therefore, we tested the inhibition of HDACs in PCA cells through the analysis of the expression levels of the HDAC6-specific target AcTub and the class I HDACs-selective AcH3 (Figs. 6 and 8), and we also assessed class IIa-HDACs activity in LNCaP cells (Table 5). The results showed that ten of the fourteen tested compounds targeted HDAC6 in LNCaP cells, compounds **13** and **20** targeting also class IIa HDACs. The analysis of γH2AX expression ruled out possible genotoxic effects.

Representative compounds of the TFMO and HA series (compounds **13** and **37**, respectively) were then tested for *in vitro* kinetic solubility, Caco-2 cell permeability, and phase I metabolic stability. While compound **37** displayed higher water solubility compared to **13**, the latter was characterized by higher cellular membrane permeability. These findings suggest that the higher *in vitro* HDAC6 inhibitory activities exhibited by HA derivatives (*e.g.*, **37**) are likely counterbalanced by a lower cellular permeability with respect to compounds of the TFMO series (*e.g.*, **13**). Lead optimization of hydroxamic acid derivatives will require a careful fine-tuning of *in vitro* potency and cellular permeability. However, both compounds displayed an acceptable intrinsic clearance in human and mouse microsomes and were not affected by efflux phenomena.

The best performing compounds were further tested in the CRPC PC3 cells. Most of them efficiently targeted HDAC6 at 3 μM dose, as demonstrated by increased levels of AcTub. The increased acetylation of α-tubulin is an indicator of impairment of the metastatic potential that relies on cell migration. Since PCA cells acquire migratory invasive phenotype in several ways, including single cell and collective migration, we investigated the effect of the molecules on cell migration by transwell and scratch assays, which provide a measure of single cell and collective migration, respectively. Compounds **13** and **15** showed a significant effect on single cell migration of LNCaP cells, which are characterized by modest collective migration [81]. Interestingly, compounds **13**, and to a lesser extent **15** and **20**, showed a robust inhibitory activity on collective migration as well, as demonstrated by wound healing assays on PC3 cells, which primarily invade in a collective manner.

Overall, compound **13** combined favorable drug-like properties, excellent anti-proliferative activity and marked anti-migration properties on PCA cells, thus representing a valuable lead candidate. *In vitro* profiling against all HDAC recombinant enzymes (Table 7) and HDACi profiling in LNCaP cells (Figs. 6 and 8 and Table 5) demonstrated that compound **13** has potent anti-cancer effects through selective inhibition of HDAC6 and class IIa HDACs.

The analysis of the prognostic value of HDACs expression in PCA patients from the Cancer Genome Atlas project (TCGA-PRAD, data obtained through GEPIA2-web server) highlighted that high HDAC6, HDAC7 and HDAC10 transcriptional levels are linked to worse overall survival, as indicated by a positive Hazard Ratio (Fig. S16A). Moreover, the expression levels of HDAC6, HDAC7 and HDAC10 are significantly increased in pathological N1 with respect to healthy or N0 samples (Fig. S16B), where Node stage N0 represents localized tumors, while N1 describes regional lymph node involvement. Besides, HDAC4 is involved in aggressive PCA and, in particular, in androgen response [21]. Therefore, the combination of HDAC6 and class IIa HDACs inhibitory activity may be particularly relevant to tackle PCA disease.

Taken together, this study led to the identification of several potent inhibitors, some of which proved to be very promising in terms of cellular potency and anti-migration properties. We believe that this study provides insightful advances into the discovery of targeted drugs against aggressive forms of advanced PCA.

4. Experimental section

4.1. Chemistry/synthesis

All the reagents, solvents, and other chemicals were used as purchased without further purification, unless otherwise specified. Air or moisture sensitive reactions were performed under nitrogen atmosphere. The reaction mixtures were monitored by thin-layer chromatography on silica gel plates (60F-254, E. Merck) and visualized with UV-light, cerium ammonium sulfate, alkaline $KMnO_4$ aqueous solution, or 1% $FeCl_3$ ethanolic solution. Column liquid chromatography (LC) purifications were carried out using Merck silica gel 60 (230–400 mesh, ASTM). Flash chromatography purifications were performed with the ISOLERA-Biotage system. The structures of all isolated compounds were ensured by nuclear magnetic resonance (NMR) and mass spectrometry. ^{1}H and ^{13}C NMR (1D and 2D experiments) spectra were recorded on a DPX-400 Avance (Bruker) spectrometer at 400 MHz or on a DPX-600 Avance (Bruker) spectrometer at 600 MHz. Chemical shifts are expressed in ppm (δ) and calibrated on the residue signal of the solvent: $CDCl_3$ δ 77.04, CD_3OD δ 49.8, DMSO-d_6 δ 39.5. NMR data are reported as follows: chemical shift, multiplicity (s, singlet; d, doublet; t, triplet; q, quartet; qnt, quintet; sxt, sextet; m, multiplet; br, broad), coupling constants (Hz) and number of protons/carbons. ^{1}H–^{1}H correlation spectroscopy (COSY), ^{1}H–^{13}C heteronuclear multiple quantum coherence (HMQC) and heteronuclear multiple bond connectivity (HMBC) experiments were recorded for the determination of ^{1}H–^{1}H and ^{1}H–^{13}C correlations, respectively. The melting points were determined with Stuart SMP3 apparatus and are uncorrected. The purity of the compounds was determined by elemental analysis (C, H, N), which was performed on a Carlo Erba 1106 Analyzer and the results are within ±0.4% of the theoretical value. All final compounds are >95% pure by HPLC-UV/Vis (1260 Infinity II, Agilent Technologies (Waldbronn, Germany) column Poroshell 120 EC-C18 (4.6 × 100 mm, 4 μm (Agilent Technologies, Santa Clara, CA, U.S.A.). Low resolution MS analysis was

performed on a 6310 A Ion Trap (Agilent Technologies) whereas high resolution mass spectra were recorded on a UHPLC-HRMS 3000-Q Exactive (Thermo Scientific, Massachusetts, U.S.A.), both equipped with an electrospray ionization source (ESI).

*4.1.1. General procedure for preparation of cyanobenzyl-acetates **2a-e***

To a solution of properly substituted cyanobenzyl bromide (1 equiv) in DMF (0.1–0.2 M), potassium acetate (1.5 equiv) was added one pot and the resulting mixture was left stirring at room temperature. After 3 h, the solvent was removed under reduced pressure, the crude was taken up in ethyl acetate and washed with brine; the organic layer was dried over anhydrous Na_2SO_4, filtered and the solvent was removed under reduced pressure to afford the pure title compounds **2a-e** that were used in the next step without further purification.

*4.1.1.1. 4-cyanobenzyl acetate (**2a**).* The product was obtained as a clear oil, following the general procedure, in 83% yield (372 mg).

^{1}H NMR δ/ppm (400 MHz, $CDCl_3$): 7.66 (s, 1H, Ar), 7.61 (d, $J = 7.9$ Hz, 1H, Ar), 7.58 (d, $J = 7.9$ Hz, 1H, Ar), 7.48 (t, $J = 7.9$ Hz, 1H, Ar), 5.12 (s, 2H, –CH_2), 2.13 (s, 3H, –CH_3).

^{13}C NMR δ/ppm (100 MHz, $CDCl_3$): 170.2, 141.9, 136.0 (2C), 127.7 (2C), 119.3, 111.0, 66.4, 21.2.

ESI-MS, *m/z*: 176.1 $[M + H]^+$

*4.1.1.2. 4-cyano-3-fluorobenzyl acetate (**2b**).* The product was obtained as a clear oil, following the general procedure, in 96% yield (440 mg).

^{1}H NMR δ/ppm (400 MHz, $CDCl_3$): 7.56 (s, 1H, Ar), 7.49 (d, $J = 7.8$ Hz, 1H, Ar), 7.44 (d, $J = 7.7$ Hz, 1H, Ar), 5.13 (s, 2H, –CH_2), 2.14 (s, 3H, –CH_3).

^{13}C NMR δ/ppm (100 MHz, $CDCl_3$): 171.3, 158.9, 147.3, 135.5, 122.9, 121.2, 114.3, 111.1, 68.2, 20.9.

ESI-MS, *m/z*: 194.1 $[M + H]^+$

*4.1.1.3. 4-cyano-2-fluorobenzyl acetate (**2c**).* The product was obtained as a clear oil, following the general procedure, in 95% yield (430 mg).

^{1}H NMR δ/ppm (400 MHz, $CDCl_3$): 7.52 (d, $J = 7.7$, 1H, Ar), 7.46 (d, $J = 8.9$ Hz, 1H, Ar), 7.38 (d, $J = 8.9$ Hz, 1H, Ar), 5.20 (s, 2H, –CH_2), 2.13 (s, 3H, –CH_3).

^{13}C NMR δ/ppm (100 MHz, $CDCl_3$): 170.8, 161.3, 137.1, 129.5, 128.9, 119.2, 118.0, 113.4, 64.1, 21.3.

ESI-MS, *m/z*: 194.1 $[M + H]^+$.

*4.1.1.4. 3-chloro-4-cyanobenzyl acetate (**2d**).* The product was obtained as a clear oil, following the general procedure, in 91% yield (820 mg).

^{1}H NMR δ/ppm (400 MHz, $CDCl_3$): 7.74 (s, 1H, Ar), 7.51 (d, $J = 7.7$ Hz, 1H, Ar), 7.42 (d, $J = 7.7$ Hz, 1H, Ar), 5.19 (s, 2H, –CH_2), 2.18 (s, 3H, –CH_3).

^{13}C NMR δ/ppm (100 MHz, $CDCl_3$): 169.9, 144.0, 136.3, 132.5, 127.2, 125.8, 117.3, 111.9, 65.9, 20.8.

ESI-MS, *m/z*: 210.1 $[M + H]^+$.

*4.1.1.5. 3-cyanobenzyl acetate (**2e**).* The product was obtained as a clear oil, following the general procedure, in 95% yield (869 mg).

^{1}H NMR δ/ppm (400 MHz, $CDCl_3$): 7.66 (s, 1H, Ar), 7.61 (d, $J = 7.9$ Hz, 1H, Ar), 7.58 (d, $J = 7.9$ Hz, 1H, Ar), 7.48 (t, $J = 7.9$ Hz, 1H, Ar), 5.12 (s, 2H, –CH_2), 2.13 (s, 3H, –CH_3).

^{13}C NMR δ/ppm (100 MHz, $CDCl_3$): 170.6, 142.3, 131.2, 130.9, 130.2, 129.4, 118.5, 111.9, 65.4, 20.7.

ESI-MS, *m/z*: 176.1 $[M + H]^+$.

*4.1.2. General procedure for preparation of (Z/E)-4-(N′-hydroxycarbamimidoyl)benzyl acetates **3a-e***

To a suspension of **2a-e** (1 equiv) and $NH_2OH{\cdot}HCl$ (1.2 equiv) in EtOH, TEA (1.5 equiv) was added dropwise, and the reaction mixture was left overnight at room temperature under stirring. After complete conversion of the starting material, monitored by TLC, the solvent was removed under reduced pressure; the crude was taken up in ethyl acetate and the organic layer was washed several times with brine, then dried over anhydrous Na_2SO_4, filtered and the solvent was removed under reduced pressure. The resulting title compounds **3a-e** were used in the next step without further purification.

*4.1.2.1. (Z/E)-4-(N′-hydroxycarbamimidoyl)benzyl acetate (**3a**).* The product was obtained as a yellow oil, following the general procedure, in 77% yield (240 mg).

^{1}H NMR δ/ppm (400 MHz, $CDCl_3$): 10.84 (bs, 1H, –OH), 7.54 (m, 4H, Ar), 5.19 (s, 2H, –CH_2), 4.91 (bs, 2H, –NH_2), 2.18 (s, 3H, –CH_3).

^{13}C NMR δ/ppm (100 MHz, $CDCl_3$): 170.3, 161.2, 141.6, 131.1 (2C), 130.2 (2C), 128.2, 66.1, 20.4.

ESI-MS, *m/z*: 209.1 $[M + H]^+$

*4.1.2.2. (Z/E)-3-fluoro-4-(N′-hydroxycarbamimidoyl)benzyl acetate (**3b**).* The product was obtained as a yellow oil, following the general procedure, in 60% yield (204 mg).

^{1}H NMR δ/ppm (400 MHz, $CDCl_3$): 10.42 (bs, 1H, –OH), 7.57 (s, 1H, Ar), 7.47 (d, $J = 7.8$ Hz, 1H, Ar), 7.43 (d, $J = 7.9$ Hz, 1H, Ar), 5.19 (s, 2H, –CH_2), 4.99 (bs, 2H, –NH_2), 2.13 (s, 3H, –CH_3).

^{13}C NMR δ/ppm (100 MHz, $CDCl_3$): 170.1, 163.7, 155.4, 143.2, 128.8, 123.5, 117.5, 113.8, 65.2, 22.0.

ESI-MS, *m/z*: 227 $[M + H]^+$

*4.1.2.3. (Z/E)-2-fluoro-4-(N′-hydroxycarbamimidoyl)benzyl acetate (**3c**).* The product was obtained as a yellow oil, following the general procedure, in 81% yield (275 mg).

^{1}H NMR δ/ppm (400 MHz, $CDCl_3$): 9.98 (bs, 1H, –OH), 7.50 (t, $J = 7.7$, 1H, Ar), 7.48 (d, $J = 8.9$ Hz, 1H, Ar), 7.40 (d, $J = 8.9$ Hz, 1H, Ar), 5.18 (s, 2H, –CH_2), 4.92 (bs, 2H, –NH_2), 2.11 (s, 3H, –CH_3).

^{13}C NMR δ/ppm (100 MHz, $CDCl_3$): 170.8, 163.2, 158.7, 129.4127.9 (2C), 126.0, 110.9, 62.7, 20.2.

ESI-MS, *m/z*: 227.1 $[M + H]^+$

*4.1.2.4. (Z/E)-3-chloro-4-(N′-hydroxycarbamimidoyl)benzyl acetate (**3d**).* The product was obtained as a yellow oil, following the general procedure, in 58% yield (211 mg).

^{1}H NMR δ/ppm (400 MHz, $CDCl_3$): 10.28 (bs, 1H, –OH), 7.70 (s, 1H, Ar), 7.44 (d, $J = 7.7$ Hz, 1H, Ar), 7.29 (d, $J = 7.7$ Hz, 1H, Ar), 5.20 (s, 2H, –CH_2), 4.48 (s, 2H, –NH_2), 2.21 (s, 3H, –CH_3).

^{13}C NMR δ/ppm (100 MHz, $CDCl_3$): 170.7, 161.8, 142.0, 131.4, 127.7 (2C), 126.5, 120.3, 64.8, 20.9.

ESI-MS, *m/z*: 243.1 $[M + H]^+$

*4.1.2.5. (Z/E)-3-(N′-hydroxycarbamimidoyl)benzyl acetate (**3e**).* The product was obtained as a yellow oil, following the general procedure, in 72% yield (225 mg).

^{1}H NMR δ/ppm (400 MHz, $CDCl_3$): 10.32 (bs, 1H, –OH), 7.63 (s, 1H, Ar), 7.59 (d, $J = 7.8$ Hz, 1H, Ar), 7.58 (d, $J = 7.8$ Hz, 1H, Ar), 7.41 (t, $J = 7.8$ Hz, 1H, Ar), 5.12 (s, 2H, –CH_2), 4.97 (bs, 2H, –NH_2), 2.11 (s, 3H, –CH_3).

^{13}C NMR δ/ppm (100 MHz, $CDCl_3$): 171.1, 162.0, 140.7, 129.5, 128.3 (2C), 126.9, 123.8, 66.3, 22.0.

ESI-MS, *m/z*: 209.1 $[M + H]^+$.

*4.1.3. General procedure for preparation of 5-(trifluoromethyl)-1,2,4-oxadiazol-3-yl)benzyl acetates **4a-e***

A suspension of **3a-e** (1 equiv) in dry DCM (0.2 M) was cooled to 0 °C and TFAA (2 equiv) was added dropwise. The reaction mixture was left stirring for 3 h. After complete conversion of the starting material monitored by TLC, the solvent was removed under reduced pressure; the crude was taken up in ethyl acetate and the organic layer was washed several times with brine, then dried over anhydrous Na_2SO_4 and filtered.

The solvent was removed under reduced pressure to afford the pure title compounds **4a-e** which were used in the next step without further purification.

*4.1.3.1. 4-(5-(trifluoromethyl)-1,2,4-oxadiazol-3-yl)benzyl acetate (**4a**).* The product was obtained as a yellow oil, following the general procedure, in 58% yield (287 mg).

^{1}H NMR δ/ppm (400 MHz, $CDCl_3$): 7.77 (d, J = 7.7 Hz, 2H, Ar), 7.42 (d, J = 7.7 Hz, 2H, Ar), 5.20 (s, 2H, –CH_2), 2.21 (s, 3H, –CH_3).

^{13}C NMR δ/ppm (100 MHz, $CDCl_3$): 170.4, 168.8, 162.2, 136.3, 127.9 (2C), 126.3 (2C), 125.8, 120.1, 66.2, 20.3.

ESI-MS, *m/z*: 287.1 $[M + H]^+$

*4.1.3.2. 2-fluoro-4-(5-(trifluoromethyl)-1,2,4-oxadiazol-3-yl)benzyl acetate (**4b**).* The product was obtained as a yellow oil, following the general procedure, in 89% yield (650 mg).

^{1}H NMR δ/ppm (400 MHz, $CDCl_3$): 7.58 (t, J = 7.9 Hz, 1H, Ar), 7.40 (d, J = 8.6 Hz, 1H, Ar), 7.40 (d, J = 8.6 Hz, 1H, Ar), 5.11 (s, 2H, –CH_2), 2.11 (s, 3H, –CH_3).

^{13}C NMR δ/ppm (100 MHz, $CDCl_3$): 170.4, 168.7, 164.5, 160.5, 131.4, 129.6, 127.7, 122.3, 121.8, 116.4, 61.3, 20.4.

ESI-MS, *m/z*: 305.1 $[M + H]^+$

*4.1.3.3. 3-fluoro-4-(5-(trifluoromethyl)-1,2,4-oxadiazol-3-yl)benzyl acetate (**4c**).* The product was obtained as a yellow oil, following the general procedure, in 82% yield (600 mg).

^{1}H NMR δ/ppm (400 MHz, $CDCl_3$): 7.60 (s, 1H, Ar), 7.50 (d, J = 7.8 Hz, 1H, Ar), 7.47 (d, J = 7.8 Hz, 1H, Ar), 5.19 (s, 2H, –CH_2), 2.11 (s, 3H, –CH_3).

^{13}C NMR δ/ppm (100 MHz, $CDCl_3$): 171.2, 165.8, 163.2, 157.9, 142.4, 129.2, 123.3, 122.8, 121.4, 115.3, 65.6, 20.4.

ESI-MS, *m/z*: 305.1 $[M + H]^+$.

*4.1.3.4. 3-chloro-4-(5-(trifluoromethyl)-1,2,4-oxadiazol-3-yl)benzyl acetate (**4d**).* The product was obtained as a yellow oil, following the general procedure, in 94% yield (490 mg).

^{1}H NMR δ/ppm (400 MHz, $CDCl_3$): 7.66 (s, 1H, Ar), 7.62 (d, J = 7.7 Hz, 1H, Ar), 7.30 (d, J = 7.7 Hz, 1H, Ar), 5.18 (s, 2H, –CH_2), 2.20 (s, 3H, –CH_3).

^{13}C NMR δ/ppm (100 MHz, $CDCl_3$): 170.8, 166.4, 161.9, 139.4, 138.2, 132.7, 129.2, 127.3, 125.4, 121.7, 65.8, 20.7.

ESI-MS, *m/z*: 321.1 $[M + H]^+$

*4.1.3.5. 3-(5-(trifluoromethyl)-1,2,4-oxadiazol-3-yl)benzyl acetate (**4e**).* The product was obtained as a yellow oil, following the general procedure, in 89% yield (437 mg).

^{1}H NMR δ/ppm (400 MHz, $CDCl_3$): 8.12 (s, 1H, Ar), 8.08 (d, J = 7.9 Hz, 1H, Ar), 7.57 (d, J = 7.9 Hz, 1H, Ar), 7.53 (t, J = 7.9 Hz, 1H, Ar), 5.18 (s, 2H, –CH_2), 2.14 (s, 3H, –CH_3).

^{13}C NMR δ/ppm (100 MHz, $CDCl_3$): 170.4, 167.8, 162.4, 140.2, 131.1, 129.2, 128.4, 127.7, 126.4, 121.9, 66.6, 20.9.

ESI-MS, *m/z*: 287.1 $[M + H]^+$.

*4.1.4. General procedure for preparation of 5-(trifluoromethyl)-1,2,4-oxadiazol-3-yl)phenyl)methanoles **5a-e***

To a suspension of **4a-e** in THF/MeOH 3:1 (0.2 M v/v), NaOH 1 N (3 equiv) was added dropwise. The reaction mixture was stirred for 1 h, then the solvent was removed under reduced pressure. The crude was taken up in ethyl acetate and the organic layer was washed several times with brine, then dried over anhydrous Na_2SO_4 and filtered. The solvent was removed under reduced pressure to afford the pure title compounds **5a-e** which were used in the next step without further purification.

*4.1.4.1. (4-(5-(trifluoromethyl)-1,2,4-oxadiazol-3-yl)phenyl)methanol (**5a**).* The product was obtained as a yellow oil, following the general procedure, in 98% yield (240 mg).

^{1}H NMR δ/ppm (400 MHz, $CDCl_3$): 7.71 (d, J = 7.7 Hz, 2H, Ar), 7.40 (d, J = 7.7 Hz, 2H, Ar), 4.81 (s, 2H, –CH_2).

^{13}C NMR δ/ppm (100 MHz, $CDCl_3$): 168.3, 163.5, 140.8, 128.1 (2C), 126.7 (2C), 125.5, 121.0, 64.8.

ESI-MS, *m/z*: 245.1 $[M + H]^+$

*4.1.4.2. 2-fluoro-(4-(5-(trifluoromethyl)-1,2,4-oxadiazol-3-yl)phenyl) methanol (**5b**).* The product was obtained as a yellow oil, following the general procedure, in 90% yield (480 mg).

^{1}H NMR δ/ppm (400 MHz, $CDCl_3$): 7.58 (d, J = 7.9 Hz, 1H, Ar), 7.40 (d, J = 8.6 Hz, 1H, Ar), 7.33 (d, J = 8.2 Hz, 1H, Ar), 4.81 (s, 2H, –CH_2).

^{13}C NMR δ/ppm (100 MHz, $CDCl_3$): 168.2, 163.5, 160.9, 132.0, 128.8, 127.6, 121.8, 121.0, 115.4, 60.8.

ESI-MS, *m/z*: 263.0 $[M + H]^+$

*4.1.4.3. 3-fluoro-(4-(5-(trifluoromethyl)-1,2,4-oxadiazol-3-yl)phenyl) methanol (**5c**).* The product was obtained as a yellow oil, following the general procedure, in 75% yield (400 mg).

^{1}H NMR δ/ppm (400 MHz, $CDCl_3$): 7.59 (m, 1H, Ar), 7.20 (d, J = 7.8 Hz, 1H, Ar), 7.15 (d, J = 7.8 Hz, 1H, Ar), 4.82 (s, 2H, –CH_2).

^{13}C NMR δ/ppm (100 MHz, $CDCl_3$): 167.1, 164.1, 159.9, 140.9, 128.9, 123.5, 122.2, 121.5, 114.7, 64.4.

ESI-MS, *m/z*: 263.0 $[M + H]^+$.

*4.1.4.4. (3-chloro-4-(5-(trifluoromethyl)-1,2,4-oxadiazol-3-yl)phenyl) methanol (**5d**).* The product was obtained as a yellow oil, following the general procedure, in 82% yield (350 mg).

^{1}H NMR δ/ppm (400 MHz, $CDCl_3$): 7.76 (s, 1H, Ar), 7.70 (d, J = 7.7 Hz, 1H, Ar), 7.29 (d, J = 7.7 Hz, 1H, Ar), 4.80 (s, 2H, –CH_2).

^{13}C NMR δ/ppm (100 MHz, $CDCl_3$): 166.8, 163.1, 142.4, 138.0, 132.8, 129.3, 126.5, 125.5, 121.8, 64.8.

ESI-MS, *m/z*: 279.0 $[M + H]^+$

*4.1.4.5. (3-(5-(trifluoromethyl)-1,2,4-oxadiazol-3-yl)phenyl)methanol (**5e**).* The product was obtained as a yellow oil, following the general procedure, in 75% yield (272 mg).

^{1}H NMR δ/ppm (400 MHz, $CDCl_3$): 8.12 (s, 1H, Ar), 8.04 (d, J = 8.0 Hz, 1H, Ar), 7.59 (d, J = 8.0 Hz, 1H, Ar), 7.53 (t, J = 8.0 Hz, 1H, Ar), 4.80 (s, 2H, –CH_2).

^{13}C NMR δ/ppm (100 MHz, $CDCl_3$): 168.8, 162.7, 140.9, 130.8, 129.3, 128.4, 126.8, 125.4, 121.1, 65.3.

ESI-MS, *m/z*: 245.0 $[M + H]^+$

*4.1.5. General procedure for preparation of chloromethyl)phenyl)-5-(trifluoromethyl)-1,2,4-oxadiazoles **6a-e***

A suspension of **5a-e** (1 equiv) and $SOCl_2$ (10 equiv) was refluxed at 65 °C for 3 h. The solution was quenched with a sat. aqueous solution of $NaHCO_3$ and the mixture was extracted with ethyl acetate; the organic layer was washed with brine, dried over Na_2SO_4, filtered and the solvent was removed under reduced pressure to afford the pure title compounds **6a-e** which were used in the next step without further purification.

*4.1.5.1. 3-(4-(chloromethyl)phenyl)-5-(trifluoromethyl)-1,2,4-oxadiazole (**6a**).* The product was obtained as a brown oil, following the general procedure, in 98% yield (240 mg).

^{1}H NMR δ/ppm (400 MHz, $CDCl_3$): 8.13 (d, J = 7.8 Hz, 2H, Ar), 7.56 (d, J = 7.7 Hz, 2H, Ar), 4.64 (s, 2H, –CH_2).

^{13}C NMR δ/ppm (100 MHz, $CDCl_3$) 167.8, 163.1, 139.2, 129.3 (2C), 127.2, 126.4 (2C), 121.7, 46.6.

ESI-MS, *m/z*: 263.0 $[M + H]^+$.

*4.1.5.2. 3-(2-fluoro-4-(chloromethyl)phenyl)-5-(trifluoromethyl)-1,2,4-oxadiazole (**6b**).* The product was obtained as a brown oil, following the

general procedure, in 78% yield (263 mg).

^{1}H NMR δ/ppm (400 MHz, $CDCl_3$): 7.88 (1H, Ar), 7.53 (d, $J = 7.4$ Hz, 1H, Ar), 7.47 (d, $J = 7.2$ Hz, 1H, Ar), 4.66 (s, 2H, $–CH_2$).

^{13}C NMR δ/ppm (100 MHz, $CDCl_3$) 168.9, 163.4, 161.1, 133.4, 131.2, 125.3, 122.2, 121.8, 115.2, 40.3.

ESI-MS, *m/z*: 281.0 $[M + H]^+$

*4.1.5.3. 3-(3-fluoro-4-(chloromethyl)phenyl)-5-(trifluoromethyl)-1,2,4-oxadiazole (**6c**).* The product was obtained as a brown oil, following the general procedure, in 90% yield (303 mg).

^{1}H NMR δ/ppm (400 MHz, $CDCl_3$): 7.94 (d, $J = 8.5$ Hz, 1H, Ar), 7.81 (d, $J = 8.5$ Hz, 1H, Ar), 7.64 (d, $J = 7.8$ Hz, 1H, Ar), 4.76 (s, 2H, $–CH_2$).

^{13}C NMR δ/ppm (100 MHz, $CDCl_3$) 167.4, 163.1, 157.2, 139.8, 130.4, 125.1, 123.7, 121.2, 116.4, 45.8.

ESI-MS, *m/z*: 281.0 $[M + H]^+$.

*4.1.5.4. 3-(2-chloro-4-(chloromethyl)phenyl)-5-(trifluoromethyl)-1,2,4-oxadiazole (**6d**).* The product was obtained as a brown oil, following the general procedure, in 85% yield (320 mg).

^{1}H NMR δ/ppm (400 MHz, $CDCl_3$): 7.80 (s, 1H, Ar), 7.78 (d, $J = 7.7$ Hz, 1H, Ar), 7.28 (d, $J = 7.7$ Hz, 1H, Ar), 4.65 (s, 2H, $–CH_2$).

^{13}C NMR δ/ppm (100 MHz, $CDCl_3$) 166.3, 163.6, 140.0, 138.4, 132.2, 128.9, 128.2, 127.5, 121.5, 46.8.

ESI-MS, *m/z*: 298.0 $[M + H]^+$

*4.1.5.5. 3-(3-(chloromethyl)phenyl)-5-(trifluoromethyl)-1,2,4-oxadiazole (**6e**).* The product was obtained as a brown oil, following the general procedure, in 92% yield (120 mg).

^{1}H NMR δ/ppm (400 MHz, $CDCl_3$): 8.15 (s, 1H, Ar), 8.08 (d, $J = 7.8$ Hz, 1H, Ar), 7.61 (d, $J = 7.8$ Hz, 1H, Ar), 7.54 (t, $J = 7.8$ Hz, 1H, Ar), 4.66 (s, 2H, $–CH_2$).

^{13}C NMR δ/ppm (100 MHz, $CDCl_3$): 169.2, 162.4, 141.3, 131.2, 129.7, 128.9, 127.4, 126.7, 121.8, 64.9.

ESI-MS, *m/z*: 263.0 $[M + H]^+$.

*4.1.6. General procedure for preparation of the final compounds **10–22***

To a suspension of **6a-e** (1 equiv) and **7–9** (1.1 equiv) in dry DMF (0.2 M), K_2CO_3 (2 equiv) was added. The suspension was stirred at room temperature overnight, then the solvent was evaporated under reduced pressure, and the residue was purified by column chromatography to afford the pure title compounds **10–22**.

*4.1.6.1. 4-chloro-7-(4-(5-(trifluoromethyl)-1,2,4-oxadiazol-3-yl)benzyl)-7H-pyrrolo [2,3-d]pyrimidin-2-amine (**10**).* The product was obtained following the general procedure and after column chromatography with 40% EtOAc/*n*-Hexane; 47% yield corresponding to 140 mg of a white solid; mp = 151–152 °C.

^{1}H NMR δ/ppm (400 MHz, DMSO-d_6): 8.03 (d, $J = 8.2$ Hz, 2H, Ar), 7.36 (d, $J = 8.2$ Hz, 2H, Ar), 7.27 (d, $J = 3.7$ Hz, 1H, Ar), 6.39 (d, $J = 3.7$ Hz, 1H, Ar), 6.69 (s, 2H, $–NH_2$), 5.38 (s, 2H, $–CH_2$).

^{13}C NMR δ/ppm (100 MHz, DMSO-d_6): 168.2, 165.2, 159.5, 153.6, 151.4, 142.5, 127.9 (2C), 127.8, 126.6 (2C), 123.5, 115.9, 108.5, 99.1, 46.8.

HRMS (ESI), *m/z*: calcd. for $C_{16}H_{11}ClF_3N_6O^+$: 395.0629 $[M+H]^+$; found: 395.0627.

Anal. Calcd for $C_{16}H_{10}ClF_3N_6O$: C, 48.68; H, 2.55; N, 21.29. Found: C, 48.60; H, 2.53; N, 21.30.

*4.1.6.2. 6-chloro-9-(4-(5-(trifluoromethyl)-1,2,4-oxadiazol-3-yl)benzyl)-9H-purin-2-amine (**11**).* The product was obtained following the general procedure and after column chromatography with 50% EtOAc/*n*-Hexane; 36% yield corresponding to 70 mg of a white solid; mp = 248–250 °C.

^{1}H NMR δ/ppm (600 MHz, DMSO-d_6): 8.28 (s, 1H, Ar), 8.04 (d, $J =$ 8.1 Hz, 2H, Ph Ar), 7.45 (d, $J = 8.1$ Hz, 2H, Ar), 6.95 (s, 2H, $–NH_2$), 5.42 (s, 2H, $–CH_2$).

^{13}C NMR δ/ppm (150 MHz, DMSO-d_6): 168.1, 165.0, 160.0, 154.1, 149.6, 143.3, 141.2, 128.0 (2C), 127.8, 123.8 (2C), 123.3, 115.7, 45.8.

HRMS (ESI), *m/z*: calcd. for $C_{15}H_{10}ClF_3N_7O^+$: 396.0582 $[M+H]^+$; found: 396.0579.

Anal. Calcd for $C_{15}H_9ClF_3N_7O$: C, 45.53; H, 2.29; N, 24.78. Found: C, 45.52; H, 2.29; N, 24.80.

*4.1.6.3. 4-chloro-7-(2-fluoro-4-(5-(trifluoromethyl)-1,2,4-oxadiazol-3-yl) benzyl)-7H-pyrrolo [2,3-d]pyrimidin-2-amine (**12**).* The product was obtained following the general procedure and after column chromatography with 5% MeOH/DCM; 34% yield corresponding to 50 mg of a white solid; mp = 146–147 °C.

^{1}H NMR δ/ppm (600 MHz, DMSO-d_6): 7.89 (d, $J = 8.5$ Hz, 1H, Ar), 7.86 (d, $J = 8.5$ Hz, 1H, Ar), 7.30 (t, $J = 7.1$ Hz, 1H, Ar), 7.20 (d, $J = 4.0$ Hz, 1H, Ar), 6.43 (d, $J = 3.7$ Hz, 1H, Pyr), 6.01 (s, 2H, $–NH_2$), 5.47 (s, 2H, $–CH_2$).

^{13}C NMR δ/ppm (150 MHz, DMSO-d_6): 168.9, 162.5, 160.7, 160.1, 154.9, 152.9, 132.3, 130.3, 128.2, 126.9, 124.6, 115.2, 115.0, 110.4, 100.5, 42.2.

HRMS (ESI), *m/z*: calcd. for $C_{16}H_{10}ClF_4N_6O^+$: 413.0535 $[M+H]^+$; found: 413.0532.

Anal. Calcd for $C_{16}H_9ClF_4N_6O$: C, 46.56; H, 2.20; N, 20.36. Found: C, 46.57; H, 2.21; N, 20.36.

*4.1.6.4. 6-chloro-9-(2-fluoro-4-(5-(trifluoromethyl)-1,2,4-oxadiazol-3-yl) benzyl)-9H-purin-2-amine (**13**).* The product was obtained following the general procedure and after column chromatography with 5% MeOH/DCM; 50% yield corresponding to 169 mg of a white solid; mp = 201–203 °C.

^{1}H NMR δ/ppm (400 MHz, DMSO-d_6): 8.24 (s, 1H, Ar), 7.89 (d, $J =$ 8.5 Hz, 1H, Ar), 7.87 (d, $J = 8.5$ Hz, 1H, Ar), 7.29 (t, $J = 7.1$ Hz, 1H, Ar), 6.96 (s, 2H, $–NH_2$), 5.47 (s, 2H, $–CH_2$).

^{13}C NMR δ/ppm (100 MHz, DMSO-d_6): 178.7, 172.4, 170.7, 167.8, 159.9, 154.1, 149.6, 143.2, 130.4, 128.11, 126.4, 123.9, 123.2, 114.2, 40.4.

HRMS (ESI), *m/z*: calcd. for $C_{15}H_9ClF_4N_7O^+$: 414.0488 $[M+H]^+$; found: 414.0485.

Anal. Calcd for $C_{15}H_8ClF_4N_7O$: C, 43.55; H, 1.95; N, 23.70. Found: C, 43.49; H, 1.91; N, 23.77.

*4.1.6.5. 4-chloro-7-(3-fluoro-4-(5-(trifluoromethyl)-1,2,4-oxadiazol-3-yl) benzyl)-7H-pyrrolo [2,3-d]pyrimidin-2-amine (**14**).* The product was obtained following the general procedure and after column chromatography with 50% EtOAc/*n*-Hexane; 27% yield corresponding to 50 mg of a white solid; mp = 156–158 °C.

^{1}H NMR δ/ppm (400 MHz, DMSO-d_6): 8.03 (t, $J = 7.5$ Hz, 1H, Ar), 7.31 (d, $J = 8.5$ Hz, 1H, Ar), 7.29 (d, $J = 3.8$ Hz, 1H, Ar), 7.17 (d, $J = 7.5$ Hz, 1H, Ar), 6.71 (s, 2H, $–NH_2$), 6.40 (d, $J = 3.8$ Hz, 1H, Ar), 5.39 (s, 2H, $–CH_2$).

^{13}C NMR δ/ppm (100 MHz, DMSO-d_6): 165.0, 161.1, 159.3, 158.6, 153.6, 151.4, 145.2, 131.1, 126.4, 123.6, 115.3, 111.7, 108.6, 99.3, 46.4.

HRMS (ESI), *m/z*: calcd. for $C_{16}H_{10}ClF_4N_6O^+$: 413.0535 $[M+H]^+$; found: 413.0530.

Anal. Calcd for $C_{15}H_9ClF_4N_6O$: C, 46.56; H, 2.20; N, 20.36. Found: C, 46.56; H, 2.19; N, 20.38.

*4.1.6.6. 6-chloro-9-(3-fluoro-4-(5-(trifluoromethyl)-1,2,4-oxadiazol-3-yl) benzyl)-9H-purin-2-amine (**15**).* The product was obtained following the general procedure and after column chromatography with 5% MeOH/DCM; 49% yield corresponding to 180 mg of a white solid; mp = 203–204 °C.

^{1}H NMR δ/ppm (600 MHz, DMSO-d_6): 8.27 (s, 1H, Ar), 8.05 (t, $J =$

7.5 Hz, 1H, Ar), 7.43 (d, $J = 11.2$ Hz, 1H, Ar), 7.26 (d, $J = 7.5$ Hz, 1H, Ar), 6.96 (s, 2H, $–NH_2$), 5.43 (s, 2H, $–CH_2$).

^{13}C NMR δ/ppm (150 MHz, DMSO-d_6): 164.9, 162.3, 161.1, 160.1, 158.5, 151.1, 149.6, 145.3, 143.6, 143.7, 137.6, 131.2, 123.6, 115.7, 45.4.

HRMS (ESI), *m/z*: calcd. for $C_{15}H_9ClF_4N_7O^+$: 414.0488 $[M+H]^+$; found: 414.0486.

Anal. Calcd for $C_{15}H_8ClF_4N_7O$: C, 43.55; H, 1.95; N, 23.70. Found: C, 43.49; H, 1.90; N, 23.72.

*4.1.6.7. 3-(4-((6-chloro-9H-purin-9-yl)methyl)phenyl)-5-(trifluoromethyl)-1,2,4-oxadiazole **(16)***. The product was obtained following the general procedure and after column chromatography with 50% EtOAc/*n*-Hexane; 52% yield corresponding to 30 mg of a white solid; mp = 153–155 °C.

^{1}H NMR δ/ppm (600 MHz, DMSO-d_6): 8.89 (s, 1H, Ar), 8.79 (s, 1H, Ar), 8.04 (d, $J = 8.2$ Hz, 2H, Ar), 7.56 (d, $J = 8.2$ Hz, 2H, Ar), 5.67 (s, 2H, $–CH_2$).

^{13}C NMR δ/ppm (150 MHz, DMSO-d_6): 168.1, 164.8, 151.9, 151.8, 149.2, 147.6, 140.5, 130.9, 128.6 (2C), 127.8 (2C), 114.4, 46.7.

HRMS (ESI), *m/z*: calcd. for $C_{15}H_9ClF_3N_6O^+$: 381.0473 $[M+H]^+$; found: 381.0471.

Anal. Calcd for $C_{15}H_8ClF_3N_6O$: C, 47.32; H, 2.12; N, 22.07. Found: C, 47.30; H, 2.11; N, 22.10.

*4.1.6.8. 3-(4-((6-chloro-9H-purin-9-yl)methyl)-3-fluorophenyl)-5-(trifluoromethyl)-1,2,4-oxadiazole **(17)***. The product was obtained following the general procedure and after column chromatography with 2% MeOH/DCM; 33% yield corresponding to 48 mg of a white solid; mp = 150–152 °C.

^{1}H NMR δ/ppm (400 MHz, acetone-d_6): 8.72 (s, 1H, Ar), 8.67 (s, 1H, Ar), 7.93 (d, $J = 8.5$ Hz, 1H, Ar), 7.88 (d, $J = 8.5$ Hz, 1H, Ar), 7.65 (t, $J = 7.1$ Hz, 1H, Ar), 5.81 (s, 2H, $–CH_2$).

^{13}C NMR δ/ppm (100 MHz, acetone-d_6): 168.6, 162.9, 160.4, 153.2, 152.7, 151.0, 147.6, 132.5, 132.3, 128.3, 128.0, 124.7, 118.3, 115.5, 42.2.

HRMS (ESI), *m/z*: calcd. for $C_{15}H_8ClF_4N_6O^+$: 399.0379 $[M+H]^+$; found: 399.0376.

Anal. Calcd for $C_{15}H_7ClF_4N_6O$: C, 45.19; H, 1.77; N, 21.08. Found: C, 45.17; H, 1.76; N, 21.08.

*4.1.6.9. 3-(4-((6-chloro-9H-purin-9-yl)methyl)-2-fluorophenyl)-5-(trifluoromethyl)-1,2,4-oxadiazole **(18)***. The product was obtained following the general procedure and after column chromatography with 5% MeOH/DCM; 48% yield corresponding to 170 mg of a white solid; mp = 125–127 °C.

^{1}H NMR δ/ppm (600 MHz, DMSO-d_6): 8.87 (s, 1H, Ar), 8.69 (s, 1H, Ar), 8.04 (t, $J = 8.3$ Hz, 1H, Ar), 7.54 (d, $J = 10.9$ Hz, 1H, Ar), 7.37 (d, $J = 8.0$ Hz, 1H, Ar), 5.68 (s, 2H, $–CH_2$).

^{13}C NMR δ/ppm (150 MHz, DMSO-d_6): 164.9, 163.4161.1, 158.6, 151.9, 149.2, 147.5, 143.2, 131.1, 124.3, 117.1, 116.2, 114.4, 112.2, 46.2.

HRMS (ESI), *m/z*: calcd. for $C_{15}H_8ClF_4N_6O^+$: 399.0379 $[M+H]^+$; found: 399.0377.

Anal. Calcd for $C_{15}H_7ClF_4N_6O$: C, 45.19; H, 1.77; N, 21.08. Found: C, 45.20; H, 1.77; N, 21.07.

*4.1.6.10. 4-chloro-7-(3-chloro-4-(5-(trifluoromethyl)-1,2,4-oxadiazol-3-yl)benzyl)-7H-pyrrolo [2,3-d]pyrimidin-2-amine **(19)***. The product was obtained following the general procedure and after column chromatography with 50% EtOAc/*n*-Hexane; 14% yield corresponding to 120 mg of a white solid; mp = 232–234 °C.

^{1}H NMR δ/ppm (400 MHz, DMSO-d_6): 7.92 (d, $J = 8.1$ Hz, 1H, Ar), 7.55 (d, $J = 1.2$ Hz, 1H, Ar), 7.25 (d, $J = 3.7$ Hz, 1H, Ar), 7.21 (dd, $J = 8.1$ Hz, $J = 1.2$ Hz, 1H, Ar), 6.71 (s, 2H, $–NH_2$), 6.39 (d, $J = 3.7$ Hz, 1H, Ar), 5.36 (s, 2H, $–CH_2$).

^{13}C NMR δ/ppm (100 MHz, DMSO-d_6): 167.4, 159.5, 153.6, 151.5, 149.3, 145.6, 135.5, 135.0, 131.3, 128.2, 126.3, 115.8, 110.9, 108.5, 99.4, 46.3.

HRMS (ESI), *m/z*: calcd. for $C_{16}H_{10}Cl_2F_3N_6O^+$: 429.0240 $[M+H]^+$; found: 429.0237.

Anal. Calcd for $C_{16}H_9Cl_2F_3N_6O$: C, 44.78; H, 2.11; N, 19.58. Found: C, 44.69; H, 2.01; N, 19.67.

*4.1.6.11. 6-chloro-9-(3-chloro-4-(5-(trifluoromethyl)-1,2,4-oxadiazol-3-yl)benzyl)-9H-purin-2-amine **(20)***. The product was obtained following the general procedure and after column chromatography with 3% MeOH/DCM; 5% yield corresponding to 14 mg of a white solid; mp = 267–268 °C.

^{1}H NMR δ/ppm (400 MHz, $CDCl_3$): 8.09 (s, 1H, Ar), 7.92 (m, 1H, Ar), 7.90 (m, 1H, Ar), 7.12 (t, $J = 7.5$ Hz, 1H, Ar), 5.67 (s, 2H, $–CH_2$), 5.16 (s, 2H, $–NH_2$).

^{13}C NMR δ/ppm (100 MHz, $CDCl_3$): 166.6, 161.4, 153.0, 152.1, 145.1, 135.9, 134.8, 131.8, 129.2, 126.9, 113.4, 110.8, 109.1, 97.5, 47.2.

HRMS (ESI), *m/z*: calcd. for $C_{15}H_9Cl_2F_3N_7O^+$: 430.0192 $[M+H]^+$; found: 430.0197.

Anal. Calcd for $C_{15}H_8Cl_2F_3N_7O$: C, 41.88; H, 1.87; N, 22.79. Found: C, 41.88; H, 1.85; N, 22.80.

*4.1.6.12. 4-chloro-7-(3-(5-(trifluoromethyl)-1,2,4-oxadiazol-3-yl) benzyl)-7H-pyrrolo [2,3-d]pyrimidin-2-amine **(21)***. The product was obtained following the general procedure and after column chromatography with 50% EtOAc/*n*-Hexane; 43% yield corresponding to 100 mg of a white solid; mp = 177–178 °C.

^{1}H NMR δ/ppm (400 MHz, $CDCl_3$): δ 8.03 (d, $J = 8.1$ Hz, 1H, Ar), 8.03 (s, 1H, Ar), 7.48 (t, $J = 8.1$ Hz, 1H, Ar), 7.36 (d, $J = 8.0$ Hz, 1H, Ar), 6.86 (d, $J = 3.9$ Hz, 1H, Ar), 6.45 (d, $J = 3.9$ Hz, 1H, Ar), 5.33 (s, 2H, $–CH_2$), 5.08 (s, 2H, $–NH_2$).

^{13}C NMR δ/ppm (100 MHz, $CDCl_3$): 168.9, 166.1, 158.7, 153.6, 152.9, 137.5, 131.2, 131.5, 130.0, 127.7, 125.7, 117.2, 114.7, 110.8, 100.9, 47.7.

HRMS (ESI), *m/z*: calcd. for $C_{16}H_{11}ClF_3N_6O^+$: 395.0629 $[M+H]^+$; found: 395.0629.

Anal. Calcd for $C_{16}H_{10}ClF_3N_6O$: C, 48.68; H, 2.55; N, 21.29. Found: C, 48.66; H, 2.50; N, 21.33.

*4.1.6.13. 6-chloro-9-(3-(5-(trifluoromethyl)-1,2,4-oxadiazol-3-yl) benzyl)-9H-purin-2-amine **(22)***. The product was obtained following the general procedure and after column chromatography with 50% EtOAc/*n*-Hexane; 26% yield corresponding to 70 mg of a white solid; mp = 237–239 °C.

^{1}H NMR δ/ppm (400 MHz, DMSO-d_6): δ 8.30 (s, 1H, Ar), 7.99 (d, $J = 8.2$ Hz, 1H, Ar), 7.99 (s, 1H, Ar), 7.61 (t, $J = 8.2$ Hz, 1H, Ar), 7.54 (d, $J = 8.1$ Hz, 1H, Ar), 6.95 (s, 2H, $–NH_2$), 5.43 (s, 2H, $–CH_2$).

^{13}C NMR δ/ppm (100 MHz, DMSO-d_6): 168.1, 165.1, 160.0, 154.1, 149.6, 143.2, 138.2, 131.3, 130.1, 126.8, 126.0, 124.9, 123.0, 115.6, 47.7.

HRMS (ESI), *m/z*: calcd. for $C_{15}H_{10}ClF_3N_7O^+$: 396.0582 $[M+H]^+$; found: 396.0580.

Anal. Calcd for $C_{15}H_9ClF_3N_7O$: C, 45.53; H, 2.29; N, 24.78. Found: C, 45.39; H, 2.11; N, 24.89.

*4.1.7. General procedure for preparation of methyl-4-benzoates **25–36, 50***

To a suspension of **7–9**, **23** (1 equiv) and **24a-d** (1.1 equiv) in dry DMF (0.2 M), K_2CO_3 was added. The suspension was stirred at room temperature overnight, then the reaction solvent was removed under reduced pressure, and the residue was purified by column chromatography to afford the pure title compounds **25–36** and **50**.

*4.1.7.1. Methyl 4-((2-amino-4-chloro-7H-pyrrolo [2,3-d]pyrimidin-7-yl) methyl)benzoate (**25**).* The product was obtained following the general procedure and after column chromatography with 10%–50% EtOAc/*n*-Hexane; 44% yield corresponding to 139 mg of a white solid; mp = 188–189 °C.

^{1}H NMR δ/ppm (400 MHz, DMSO-d_6): δ 7.91 (d, J = 8.37 Hz, 2H, Ar), 7.26 (d, J = 8.35 Hz, 2H, Ar), 7.23 (d, J = 3.83 Hz, 1H, Ar), 6.68 (s, 2H, –NH_2), 6.37 (d, J = 3.48 Hz, 1H, Ar), 5.35 (s, 2H, –CH_2), 3.83 (s, 3H, –OCH_3).

^{13}C NMR δ/ppm (100 MHz, DMSO-d_6): 167.3, 159.4, 151.6, 151.0, 142.3, 130.2 (2C), 128.4 (2C), 125.9, 123.0, 114.1, 98.7, 61.1, 49.3.

ESI-MS, *m/z*: 317.1 $[M + H]^+$.

*4.1.7.2. Methyl 4-((2-amino-6-chloro-9H-purin-9-yl)methyl)benzoate (**26**).* The product was obtained following the general procedure and after column chromatography with 40%–100% EtOAc/*n*-Hexane; 45% yield corresponding to 285 mg of a white solid; mp = 200–202 °C.

^{1}H NMR δ/ppm (400 MHz, DMSO-d_6): 8.25 (s, 1H, Ar), 7.93 (d, J = 8.37 Hz, 2H, Ar), 7.34 (d, J = 8.07 Hz, 2H, Ar), 6.94 (s, 2H, –NH_2), 5.39 (s, 2H, –CH_2), 3.83 (s, 3H, –OCH_3).

^{13}C NMR δ/ppm (100 MHz, DMSO-d_6): 165.9, 159.6, 150.7, 150.3, 145.6, 142.8, 132.2, 129.9 (2C), 129.0 (2C), 128.3, 50.3, 48.7.

ESI-MS, *m/z*: 318.1 $[M + H]^+$.

*4.1.7.3. Methyl 4-((2-amino-9H-purin-9-yl)methyl)benzoate (**27**).* The product was obtained following the general procedure and after column chromatography with 30%–70% EtOAc/*n*-Hexane; 46% yield corresponding to 260 mg of a white solid; mp = 177–179 °C.

^{1}H NMR δ/ppm (400 MHz, DMSO-d_6): 8.61, (s, 1H, Ar), 8.18 (s, 1H, Ar), 7.93 (d, J = 7.35 Hz, 2H, Ar), 7.35 (d, J = 8.10 Hz, 2H, Ar), 6.54 (s, 2H, –NH_2), 5.39 (s, 2H, –CH_2), 3.83 (s, 3H, –OCH_3).

^{13}C NMR δ/ppm (100 MHz, DMSO-d_6): 165.2, 160.6, 150.7, 149.3, 145.6, 141.7, 134.8, 134.2, 133.5 (2C), 130.1 (2C), 52.5 50.3.

ESI-MS, *m/z*: 284.1 $[M + H]^+$.

*4.1.7.4. Methyl 4-((2-amino-4-chloro-7H-pyrrolo [2,3-d]pyrimidin-7-yl) methyl)-3-fluorobenzoate (**28**).* The product was obtained following the general procedure and after column chromatography with 30%–60% EtOAc/*n*-Hexane; 46% yield corresponding to 303 mg of a yellow solid; mp = 188–190 °C.

^{1}H NMR δ/ppm (400 MHz, DMSO-d_6): 7.72 (d, J = 8.88 Hz, 2H, Ar), 7.21 (d, J = 3.51 Hz, 1H, Ar), 6.98 (t, J = 7.32 Hz, 1H, Ar), 6.71 (s, 2H, –NH_2), 6.39 (d, J = 3.51 Hz, 1H, Ar), 5.39 (s, 2H, –CH_2), 3.84 (s, 3H, –OCH_3).

^{13}C NMR δ/ppm (100 MHz, DMSO-d_6): 167.3, 159.4, 151.6, 151.0, 142.3, 130.2 (2C), 128.4 (2C), 125.9, 123.0, 114.1, 98.7, 61.1, 49.3.

ESI-MS, *m/z*: 335.1 $[M + H]^+$.

*4.1.7.5. Methyl 4-((2-amino-6-chloro-9H-purin-9-yl)methyl)-3-fluorobenzoate (**29**).* The product was obtained following the general procedure and after column chromatography with 40%–100% EtOAc/*n*-Hexane; 42% yield corresponding to 303 mg of a white solid; mp = 199–200 °C.

^{1}H NMR δ/ppm (400 MHz, DMSO-d_6): 8.21 (s, 1H, Ar), 7.74 (m, 2H, Ar), 7.17 (t, J = 8.02 Hz, 1H, Ar), 6.95 (s, 2H, –NH_2), 5.43 (s, 2H, –CH_2), 3.85 (s, 3H, –OCH_3).

^{13}C NMR δ/ppm (100 MHz, DMSO-d_6): 165.4, 161.2, 158.9, 150.0 (2C), 146.3, 131.4, 130.6, 129.1 (2C), 124.8, 114.6, 58.4, 48.3.

ESI-MS, *m/z*: 336.1 $[M + H]^+$.

*4.1.7.6. Methyl 4-((2-amino-9H-purin-9-yl)methyl)-3-fluorobenzoate (**30**).* The product was obtained following the general procedure and after column chromatography with 30%–50% EtOAc/*n*-Hexane; 38% yield corresponding to 220 mg of a white solid; mp = 181–183 °C.

^{1}H NMR δ/ppm (400 MHz, DMSO-d_6): 8.62 (s, 1H, Ar), 8.15 (s, 1H, Ar), 7.74 (m, 2H, Ar), 7.15 (t, J = 8.54 Hz, 1H, Ar), 6.56 (s, 2H, –NH_2), 5.44 (s, 2H, –CH_2), 3.86 (s, 3H, –OCH_3).

^{13}C NMR δ/ppm (100 MHz, DMSO-d_6): 166.1, 161.8, 160.3, 150.4, 148.5, 145.3, 133.8, 130.4, 128.7 (2C), 125.2, 114.1, 55.0, 48.7.

ESI-MS, *m/z*: 302.1 $[M + H]^+$.

*4.1.7.7. Methyl 4-((6-chloro-9H-purin-9-yl)methyl)-3-fluorobenzoate (**31**).* The product was obtained following the general procedure and after column chromatography with 40%–80% EtOAc/*n*-Hexane; 28% yield corresponding to 130 mg of a yellow solid; mp = 182–183 °C.

^{1}H NMR δ/ppm (400 MHz, DMSO-d_6): 8.83 (s, 1H, Ar), 8.77 (s, 1H, Ar), 7.74 (m, 2H, Ar), 7.41 (t, J = 8.02 Hz, 1H, Ar), 5.69 (s, 2H, –CH_2), 3.85 (s, 3H, –OCH_3).

^{13}C NMR δ/ppm (100 MHz, DMSO-d_6): 165.4, 161.1, 153.8, 151.7, 150.8, 145.1, 132.4, 131.2, 130.0 (2C), 126.1, 115.8, 54.2, 49.2.

ESI-MS, *m/z*: 321.1 $[M + H]^+$.

*4.1.7.8. Methyl 4-((6-chloro-9H-purin-9-yl)methyl)benzoate (**32**).* The product was obtained following the general procedure and after column chromatography with 20%–50% EtOAc/*n*-Hexane; 43% yield corresponding to 260 mg of a white solid; mp = 166–168 °C.

^{1}H NMR δ/ppm (400 MHz, DMSO-d_6): 8.87 (s, 1H, Ar), 8.79 (s, 1H, Ar), 7.93 (d, J = 7.98 Hz, 2H, Ar), 7.45 (d, J = 8.02 Hz, 2H, Ar), 5.64 (s, 2H, –CH_2), 3.83 (s, 3H, –OCH_3).

^{13}C NMR δ/ppm (100 MHz, DMSO-d_6): 166.7, 151.1, 150.8, 148.3, 145.0, 141.6, 132.8, 129.4 (2C), 128.1 (2C), 126.9, 52.2, 47.9.

ESI-MS, *m/z*: 303.1 $[M + H]^+$.

*4.1.7.9. Methyl 6-((2-amino-4-chloro-7H-pyrrolo [2,3-d]pyrimidin-7-yl) methyl)nicotinate (**33**).* The product was obtained following the general procedure and after column chromatography with 30%–60% EtOAc/*n*-Hexane; 28% yield corresponding to 130 mg of a white solid; mp = 174–175 °C.

^{1}H NMR δ/ppm (400 MHz, DMSO-d_6): 9.03 (s, 1H, Ar), 8.24 (d, J = 8.61 Hz, 1H, Ar), 7.26 (d, J = 3.83 Hz, 1H, Ar), 7.04 (d, J = 8.46 Hz, 1H, Ar), 6.68 (s, 2H, –NH_2), 6.40 (d, J = 3.56 Hz, 1H, Ar), 5.46 (s, 2H, –CH_2), 3.87 (s, 3H, –OCH_3).

^{13}C NMR δ/ppm (100 MHz, DMSO-d_6): 165.7, 160.2 (2C), 151.1, 150.8, 150.0, 138.3, 125.0, 121.6, 120.8, 113.2, 98.7, 61.1, 49.9.

ESI-MS, *m/z*: 318.1 $[M + H]^+$.

*4.1.7.10. Methyl 6-((2-amino-6-chloro-9H-purin-9-yl)methyl)nicotinate (**34**).* The product was obtained following the general procedure and after column chromatography with 60%–100% EtOAc/*n*-Hexane; 13% yield corresponding to 60 mg of a white solid; mp = 166–168 °C.

^{1}H NMR δ/ppm (400 MHz, DMSO-d_6): 9.05 (s, 1H, Ar), 8.33 (m, 2H, Ar), 7.40 (d, J = 8.11 Hz, 1H, Ar), 6.96 (s, 2H, –NH_2), 5.58 (s, 2H, –CH_2), 3.93 (s, 3H, –OCH_3).

^{13}C NMR δ/ppm (100 MHz, DMSO-d_6): 166.6, 160.5 (2C), 150.6, 150.2, 149.4, 145.2, 137.1, 131.4, 122.4 (2C), 60.4, 50.9.

ESI-MS, *m/z*: 319.1 $[M + H]^+$.

*4.1.7.11. Methyl 2-(4-((2-amino-4-chloro-7H-pyrrolo [2,3-d]pyrimidin-7-yl)methyl)phenyl)acetate (**35**).* The product was obtained following the general procedure and after column chromatography with 30%–60% EtOAc/*n*-Hexane; 51% yield corresponding to 334 mg of a white solid; mp = 181–183 °C.

^{1}H NMR δ/ppm (400 MHz, DMSO-d_6): 7.21 (m, 3H, Ar), 7.13 (m, 2H), 6.67 (s, 2H, –NH_2), 6.34 (d, J = 3.58 Hz, 1H, Ar), 5.24 (s, 2H, –CH_2), 3.64 (s, 2H, –CH_2), 3.59 (s, 3H, –OCH_3).

^{13}C NMR δ/ppm (100 MHz, DMSO-d_6): 174.1, 162.2, 152.6, 151.8, 137.8, 133.2, 128.9 (2C), 126.6 (2C), 120.3, 117.5, 101.2, 60.8, 52.3, 40.2.

ESI-MS, *m/z*: 331.1 $[M + H]^+$.

*4.1.7.12. Methyl 2-(4-((2-amino-6-chloro-9H-purin-9-yl)methyl)phenyl) acetate (**36**).* The product was obtained following the general procedure and after column chromatography with 60%–100% EtOAc/*n*-Hexane; 25% yield corresponding to 160 mg of a white solid; mp = 190–191 °C.

^{1}H NMR δ/ppm (400 MHz, DMSO-d_6): 8.23 (s, 1H, Ar), 7.22 (m, 4H, Ar), 6.94 (s, 2H, –NH_2), 5.28 (s, 2H, –CH_2), 3.66 (s, 2H, –CH_2), 3.59 (s, 3H, –OCH_3).

^{13}C NMR δ/ppm (100 MHz, DMSO-d_6): 173.8, 158.7, 151.8, 150.7145.7, 137.2, 131.4.129.5, 128.3 (2C), 127.1 (2C), 51.1, 47.3, 40.4.

ESI-MS, *m/z*: 332 $[M + H]^+$.

*4.1.7.13. Methyl 2-((2-amino-4-chloro-7H-pyrrolo [2,3-d]pyrimidin-7-yl) methyl)oxazole-4-carboxylate (**50**).* The product was obtained following the general procedure and after column chromatography with 70%–100% EtOAc/*n*-Hexane; 54% yield corresponding to 331 mg of a white solid; mp = 217–218 °C.

^{1}H NMR δ/ppm (400 MHz, DMSO-d_6): 8.83 (s, 1H, Ar), 7.25 (d, J = 4.4 Hz, 1H, Ar), 6.74 (s, 2H, –NH_2), 6.38 (d, J = 4.01 Hz, 1H, Ar), 5.48 (s, 2H, –CH_2), 3.78 (s, 3H, –OCH_3).

^{13}C NMR δ/ppm (100 MHz, DMSO-d_6): 161.4, 159.2, 151.6, 151.1, 150.8, 141.3, 135.2, 122.4, 117.2, 100.6, 59.7, 50.9.

ESI-MS, *m/z*: 308.1 $[M + H]^+$.

*4.1.8. General procedure for preparation of the final compounds **37–48, 51***

To a solution of **25**–**36** or **50** (1 equiv) in 1,4-dioxane (0.2 M), were added aqueous 50 wt % in H_2O (5 equiv) followed by a solution of NaOH 1 N (5 equiv). The formed solution was stirred at room temperature for 5 h, then the dioxane was removed under reduced pressure and the pH was adjusted to 4–5 with 1 N HCl. The formed precipitate was filtered off, washed with water and recrystallized from MeOH/Et_2O to afford the pure titled compounds **37–48** and **51**.

*4.1.8.1. 4-((2-amino-4-chloro-7H-pyrrolo [2,3-d]pyrimidin-7-yl)methyl)-N-hydroxybenzamide (**37**).* The product was obtained as a white solid following the general procedure; 55% yield (70 mg); mp = 246–248 °C.

^{1}H NMR δ/ppm (400 MHz, DMSO-d_6): 8.93 (m, 2H, –NH –OH), 7.69 (d, J = 7.70 Hz, 2H, Ar), 7.18 (d, J = 8.03 Hz, 2H, Ar), 6.75 (d, J = 3.31 Hz, 1H, Ar), 6.28 (m, 3H, Ar, –NH_2), 5.18 (s, 2H, –CH_2).

^{13}C NMR δ/ppm (100 MHz, DMSO-d_6): 165.9, 160.7, 153.0, 149.3, 142.8, 142.3.129.6 (2C), 128.9, 127.2 (2C), 126.7, 52.2, 45.2.

HRMS (ESI), *m/z*: calcd. for $C_{14}H_{13}ClN_5O_2^+$: 318.0752 $[M+H]^+$; found: 318.0740.

Anal. Calcd. for $C_{14}H_{12}ClN_5O_2$: C, 52.92; H, 3.81; N, 22.04. Found: C, 53.10; H, 4.08; N, 21.84.

*4.1.8.2. 4-((2-amino-6-chloro-9H-purin-9-yl)methyl)-N-hydroxybenzamide (**38**).* The product was obtained as a white solid following the general procedure; 61% yield (174 mg); mp = 252–254 °C.

^{1}H NMR δ/ppm (400 MHz, DMSO-d_6): 11.18 (bs, 1H, –OH), 9.02 (bs, 1H, –NH), 7.79 (s, 1H, Ar), 7.71 (d, J = 8.47 Hz, 2H, Ar), 7.26 (d, J = 8.17 Hz, 2H, Ar), 6.47 (s, 2H, –NH_2), 5.23 (s, 2H, –CH_2).

^{13}C NMR δ/ppm (100 MHz, DMSO-d_6): 163.8, 156.8, 153.7, 151.2140.2, 137.6, 132.1, 127.3 (2C), 126.8 (2C), 116.5, 45.4.

HRMS (ESI), *m/z*: calcd. for $C_{13}H_{12}ClN_6O_2^+$: 319.0705 $[M+H]^+$; found: 319.0700.

Anal. Calcd for $C_{13}H_{11}ClN_6O_2$: C, 48.99; H, 3.48; N, 26.37. Found: C, 49.29; H, 3.61; N, 26.15.

*4.1.8.3. 4-((2-amino-9H-purin-9-yl)methyl)-N-hydroxybenzamide (**39**).* The product was obtained as a white solid following the general procedure; 42% yield (108 mg); mp = 225–226 °C.

^{1}H NMR δ/ppm (400 MHz, DMSO-d_6): 11.17 (bs, 1H, –OH), 9.03 (bs, 1H, –NH), 8.61 (s, 1H, Ar), 8.18 (s, 1H, Ar), 7.70 (d, J = 8.89, Hz 2H, Ar), 7.30 (d, J = 8.29 Hz, 2H, Ar), 6.53 (s, 2H, –NH_2), 5.34 (s, 2H, –CH_2).

^{13}C NMR δ/ppm (100 MHz, DMSO-d_6): 163.9, 160.7, 153.0, 149.2, 142.7, 140.9, 132.1, 127.3 (2C), 127.0 (2C), 126.7, 45.2.

HRMS (ESI), *m/z*: calcd. for $C_{13}H_{13}N_6O_2^+$: 285.1095 $[M+H]^+$; found: 285.1077.

Anal. Calcd for $C_{13}H_{12}N_6O_2$: C, 54.93; H, 4.25; N, 29.56. Found: C, 54.76; H, 4.08; N, 29.58.

*4.1.8.4. 4-((2-amino-4-chloro-7H-pyrrolo [2,3-d]pyrimidin-7-yl)methyl)-3-fluoro-N-hydroxybenzamide (**40**).* The product was obtained as a white solid following the general procedure; 59% yield (170 mg); mp = 249–251 °C.

^{1}H NMR δ/ppm (400 MHz, DMSO-d_6): 11.29 (bs, 1H, –OH), 9.17 (bs, 1H, –NH), 7.54 (m, 2H, Ar), 6.90 (t, J = 7.22 Hz, 1H, Ar), 6.75 (d, J = 3.28 Hz, 1H, Ar), 6.31, (d, J = 3.12 Hz, 1H, Ar), 6.25 (s, 2H, –NH_2), 5.24 (s, 2H, –CH_2).

^{13}C NMR δ/ppm (100 MHz, DMSO-d_6): 162.6, 160.4, 158.6, 157.9, 152.5, 150.5, 128.8, 128.3, 123.1, 120.3, 113.7, 101.9, 99.9, 41.0.

HRMS (ESI), *m/z*: calcd. for $C_{14}H_{12}ClFN_5O_2^+$: 336.0658 $[M+H]^+$; found: 336.0642.

Anal. Calcd for $C_{14}H_{11}ClFN_5O_2$: C, 50.09; H, 3.30; N, 20.86. Found: C, 50.23; H, 3.38; N, 20.80.

*4.1.8.5. 4-((2-amino-6-chloro-9H-purin-9-yl)methyl)-3-fluoro-N-hydroxybenzamide (**41**).* The product was obtained as a white solid following the general procedure; 76% yield (205 mg); mp = 223–225 °C.

^{1}H NMR δ/ppm (400 MHz, DMSO-d_6): 11.21 (bs, 1H, –OH), 9.23 (bs, 1H, –NH), 7.76 (s, 1H, Ar), 7.56 (m, 2H, Ar), 7.06 (t, J = 6.16 Hz, 1H, Ar), 6.53 (s, 2H, –NH_2), 5.28 (s, 2H, –CH_2).

^{13}C NMR δ/ppm (100 MHz, DMSO-d_6): 162.8, 160.4, 158.3, 157.1, 153.8, 151.4, 137.8, 134.5, 129.2, 127.1, 123.2, 116.7, 113.7.

HRMS (ESI), *m/z*: calcd. for $C_{13}H_{11}ClFN_6O_2^+$: 337.0611 $[M+H]^+$; found: 337.0599.

Anal. Calcd for $C_{13}H_{10}ClFN_6O_2$: C, 46.37; H, 2.99; N, 24.96. Found: C, 46.32; H, 2.78; N, 24.99.

*4.1.8.6. 4-((2-amino-9H-purin-9-yl)methyl)-3-fluoro-N-hydroxybenzamide (**42**).* The product was obtained as a white solid following the general procedure; 58% yield (140 mg); mp = 210–211 °C.

^{1}H NMR δ/ppm (400 MHz, DMSO-d_6): 11.31 (bs, 1H, –OH), 9.19 (bs, 1H, –NH), 8.62 (s, 1H, Ar), 8.15 (s, 1H Ar), 7.57 (m, 2H, Ar), 7.15 (t, J = 7.71 Hz, 1H, Ar), 6.54 (s, 2H, –NH_2), 5.39 (s, 2H, –CH_2).

^{13}C NMR δ/ppm (100 MHz, DMSO-d_6): 162.4, 160.7, 160.5, 158.1, 152.9, 149.3, 142.7, 134.4, 129.3, 126.9, 126.6, 123.1, 113.8.

HRMS (ESI), *m/z*: calcd. for $C_{13}H_{12}FN_6O_2^+$: 303.1006 $[M+H]^+$; found: 303.0993.

Anal. Calcd for $C_{13}H_{11}FN_6O_2$: C, 51.66; H, 3.67; N, 27.80. Found: C, 51.59; H, 3.55; N, 27.81.

*4.1.8.7. 4-((6-chloro-9H-purin-9-yl)methyl)-3-fluoro-N-hydroxybenzamide (**43**).* The product was obtained as a white solid following the general procedure; 37% yield (47 mg); mp = 225–227 °C.

^{1}H NMR δ/ppm (400 MHz, DMSO-d_6): 11.38 (bs, 1H, –OH), 9.21 (bs, 1H, –NH), 8.19 (s, 1H, Ar), 8.03 (s, 1H Ar), 7.58 (m, 2H, Ar), 7.25 (t, J = 7.62 Hz, 1H, Ar), 5.53 (s, 2H, –CH_2).

^{13}C NMR δ/ppm (100 MHz, DMSO-d_6): 162.4, 160.6, 158.1, 156.5, 148.4, 145.9, 140.1, 134.7, 129.8, 126.4, 124.0, 123.9, 113.9.

HRMS (ESI), *m/z*: calcd. for $C_{13}H_{10}ClFN_5O_2^+$: 322.0502 $[M+H]^+$; found: 322.0503.

Anal. Calcd for $C_{13}H_9ClFN_5O_2$: C, 48.54; H, 2.82; N, 21.77. Found: C, 48.69; H, 3.02; N, 21.84.

*4.1.8.8. 4-((6-chloro-9H-purin-9-yl)methyl)-N-hydroxybenzamide (**44**).* The product was obtained as a white solid following the general procedure; 26% yield (64 mg); mp = 264–267 °C.

^{1}H NMR δ/ppm (400 MHz, DMSO-d_6): 11.18 (bs, 1H, –OH), 9.03 (bs, 1H, –NH), 8.23 (s, 1H, Ar), 8.04 (s, 1H Ar), 7.72 (d, J = 8.23 Hz, 2H, Ar), 7.34 (d, J = 8.20 Hz, 2H, Ar), 5.43 (s, 2H, –CH_2).

^{13}C NMR δ/ppm (100 MHz, DMSO-d_6): 163.9, 156.6, 148.3, 145.9 (2C), 140.4 (2C), 139.6, 132.1, 127.1 (2C), 124.1, 46.3.

HRMS (ESI), *m/z*: calcd. for $C_{13}H_{11}ClN_5O_2^+$: 304.0596 $[M+H]^+$; found: 304.0576.

Anal. Calcd for $C_{13}H_{10}ClN_5O_2$: C, 51.41; H, 3.32; N, 23.06. Found: C, 51.48; H, 3.59; N, 23.05.

*4.1.8.9. 6-((2-amino-4-chloro-7H-pyrrolo [2,3-d]pyrimidin-7-yl)methyl)-N-hydroxynicotinamide (**45**).* The product was obtained as a brown solid following the general procedure; 60% yield (76 mg); mp = 206–208 °C.

^{1}H NMR δ/ppm (400 MHz, DMSO-d_6): 11.35 (bs, 1H, –OH), 9.20 (bs, 1H, –NH), 8.85 (d, J = 1.94 Hz, 1H, Ar), 8.04 (dd, J = 8.18, 2.20 Hz, 1H Ar), 6.89 (d, J = 8.13 Hz, 1H, Ar), 6.80 (d, J = 2.96 Hz, 1H, Ar), 6.32 (d, J = 3.32 Hz, 1H, Ar), 6.23, (s, 2H, –NH_2), 5.30 (s, 2H, –CH_2).

^{13}C NMR δ/ppm (100 MHz, DMSO-d_6): 162.3, 160.4, 158.8, 152.7, 150.7, 147.4, 135.8, 127.2, 120.8, 120.2, 101.9, 100.1, 48.6.

HRMS (ESI), *m/z*: calcd. for $C_{13}H_{12}ClN_6O_2^+$: 319.0710 $[M+H]^+$; found: 319.0696.

Anal. Calcd for $C_{13}H_{11}ClN_6O_2$: C, 48.99; H, 3.48; N, 26.37. Found: C, 48.71; H, 3.11; N, 26.17.

*4.1.8.10. 6-((2-amino-6-chloro-9H-purin-9-yl)methyl)-N-hydroxynicotinamide (**46**).* The product was obtained as a white solid following the general procedure; 27% yield (19 mg); mp = 247–249 °C.

^{1}H NMR δ/ppm (400 MHz, DMSO-d_6): 11.34 (bs, 1H, –OH), 9.22 (bs, 1H, –NH), 8.82 (s, 1H, Ar), 8.07 (dd, J = 8.16, 2.21 Hz, 1H Ar), 7.79 (s, 1H, Ar), 7.16 (d, J = 7.34 Hz, 1H, Ar), 6.43 (s, 2H, –NH_2), 5.35 (s, 2H, –CH_2).

^{13}C NMR δ/ppm (100 MHz, DMSO-d_6): 162.8, 158.9, 156.9, 153.5, 151.7, 147.9, 138.1, 136.1, 127.4, 120.6, 116.7, 47.1.

HRMS (ESI), *m/z*: calcd. for $C_{12}H_{11}ClN_7O_2^+$: 320.0657 $[M+H]^+$; found: 320.0651.

Anal. Calcd for $C_{12}H_{10}ClN_7O_2$: C, 45.08; H, 3.15; N, 30.67. Found: C, 44.73; H, 2.94; N, 30.51.

*4.1.8.11. 2-(4-((2-amino-4-chloro-7H-pyrrolo [2,3-d]pyrimidin-7-yl) methyl)phenyl)-N-hydroxyacetamide (**47**).* The product was obtained as a white solid following the general procedure; 74% yield (86 mg); mp = 221–222 °C.

^{1}H NMR δ/ppm (400 MHz, DMSO-d_6): 10.64 (bs, 1H, –OH), 8.78 (bs, 1H, –NH), 7.20 (d, J = 8.59 Hz, 2H, Ar), 7.08 (d, J = 7.64 Hz, 2H Ar), 6.71 (d, J = 3.58 Hz, 1H, Ar), 6.25 (m, 3H, Ar–NH_2), 5.11 (s, 2H, –CH_2), 3.24 (s, 2H, –CH_2).

^{13}C NMR δ/ppm (100 MHz, DMSO-d_6): 166.9, 158.9, 152.6, 150.2, 136.4, 134.9, 129.2 (2C), 127.0 (2C), 120.1, 101.6, 100.1, 46.7, 39.0.

HRMS (ESI), *m/z*: calcd. for $C_{15}H_{15}ClN_5O_2^+$: 332.0909 $[M+H]^+$; found: 332.0892.

Anal. Calcd for $C_{15}H_{14}ClN_5O_2$: C, 54.30; H, 4.25; N, 21.11. Found: C, 54.39; H, 4.25; N, 21.04.

*4.1.8.12. 2-(4-((2-amino-6-chloro-9H-purin-9-yl)methyl)phenyl)-N-hydroxyacetamide (**48**).* The product was obtained as a white solid following the general procedure; 77% yield (128 mg); mp = 267–268 °C.

^{1}H NMR δ/ppm (400 MHz, DMSO-d_6): 10.63 (bs, 1H, –OH), 8.80 (bs, 1H, –NH), 7.78 (s, 1H, Ar), 7.22 (d, J = 7.84 Hz, 2H, Ar), 7.15 (d, J = 8.23 Hz, 2H Ar), 6.44 (s, 2H, –NH_2), 5.15 (s, 2H, –CH_2), 3.25 (s, 2H, –CH_2).

^{13}C NMR δ/ppm (100 MHz, DMSO-d_6): 167.0, 156.9, 153.5, 151.1, 137.5, 135.6 (2C), 129.4 (2C), 127.2 (2C), 116.7, 45.4, 38.9.

HRMS (ESI), *m/z*: calcd. for $C_{14}H_{14}ClN_6O_2^+$: 333.0861 $[M+H]^+$; found: 333.0852.

Anal. Calcd for $C_{14}H_{13}ClN_6O_2$: C, 50.53; H, 3.94; N, 25.26. Found; C, 50.63; H, 4.21; N, 25.09.

*4.1.8.13. 2-((2-amino-4-chloro-7H-pyrrolo [2,3-d]pyrimidin-7-yl)methyl)-N-hydroxyoxazole-4-carboxamide (**51**).* The product was obtained as a white solid following the general procedure; 65% yield (223 mg); mp = 235–236 °C.

^{1}H NMR δ/ppm (400 MHz, DMSO-d_6): 10.92 (bs, 1H, –OH), 9.03 (bs, 1H, –NH), 8.47 (s, 1H, Ar), 6.78 (d, J = 3.16 Hz, 1H, Ar), 6.28 (m, 3H Ar–NH_2), 5.33 (s, 2H, –CH_2).

^{13}C NMR δ/ppm (100 MHz, DMSO-d_6): 159.7, 158.5, 157.4, 152.7, 150.5, 141.9, 134.6, 120.4, 102.2, 99.9, 40.5.

HRMS (ESI), *m/z*: calcd. for $C_{11}H_{10}ClN_6O_3^+$: 309.0497 $[M+H]^+$; found: 309.0500.

Anal. Calcd for $C_{11}H_9ClN_6O_3$: C, 42.80; H, 2.94; N, 27.23. Found: C, 42.51; H, 2.77; N, 27.44.

*4.1.9. General procedure for preparation of compounds **53** and **54***

To a suspension of **7** or **8** (1 equiv) and **52** (1.1 equiv) in dry DMF (0.2 M), K_2CO_3 (2 equiv) was added. The suspension was stirred at room temperature overnight, then the reaction solvent was removed under reduced pressure, and the residue was purified by column chromatography to afford the pure title compounds **53** and **54**.

*4.1.9.1. 4-chloro-7-(4-nitrobenzyl)-7H-pyrrolo [2,3-d]pyrimidin-2-amine (**53**).* The product was obtained following the general procedure and after column chromatography with 30%–60% EtOAc/*n*-Hexane; 43% yield corresponding to 458 mg of a yellow solid; mp = 197–199 °C.

^{1}H NMR δ/ppm (400 MHz, $CDCl_3$): 8.18 (d J = 8.69 Hz, 2H, Ar), 7.32 (d, J = 8.61 Hz, 2H, Ar), 6.83 (d, J = 3.50 Hz, 1H, Ar), 6.47 (d, J = 3.66 Hz, 1H, Ar) 5.36 (s, 2H, –CH_2), 5.05 (s, 2H, –NH_2).

^{13}C NMR δ/ppm (100 MHz, $CDCl_3$): 161.8, 152.3, 151.8, 145.1, 143.8, 129.2 (2C), 121.2 (2C), 122.4, 115.9, 100.7, 61.3.

ESI-MS, *m/z*: 304.1 $[M + H]^+$.

*4.1.9.2. 6-chloro-9-(4-nitrobenzyl)-9H-purin-2-amine (**54**).* The product was obtained following the general procedure and after column chromatography with 70%–100% EtOAc/*n*-Hexane; 40% yield corresponding to 433 mg of a yellow solid; mp = 203–205 °C.

^{1}H NMR δ/ppm (400 MHz, DMSO-d_6): 8.28 (s, 1H, Ar), 8.21 (d, J = 8.13 Hz, 2H, Ar), 7.47 (d, J = 8.60 Hz, 2H, Ar), 6.96 (s, 2H, –NH_2), 5.47 (s, 2H, –CH_2).

^{13}C NMR δ/ppm (100 MHz, DMSO-d_6): 160.8, 151.2, 151.0, 145.1, 144.8, 143.6, 131.2, 127.4 (2C), 125.9 (2C), 48.3.

ESI-MS, *m/z*: 305.1 $[M + H]^+$.

*4.1.10. General procedure for preparation of compounds **55** and **56***

To a solution of **53** or **54** (1 equiv) in EtOH/H_2O 1:1 (0.2 M v/v), Fe (5 equiv) and NH_4Cl (5 equiv) were added. The suspension was refluxed for 5 h, then the reaction solvent was filtered through Celite and washed several times with EtOH. The solvent was evaporated under reduced pressure, and the residue was purified by column chromatography to afford the pure title compounds **55** and **56**.

*4.1.10.1. 7-(4-aminobenzyl)-4-chloro-7H-pyrrolo [2,3-d]pyrimidin-2-amine (**55**).* The product was obtained following the general procedure and after column chromatography with 50%–80% EtOAc/*n*-Hexane; 85% yield corresponding to 300 mg of a white solid; mp = 203–205 °C.

^{1}H NMR δ/ppm (400 MHz, DMSO-d_6): 7.16 (d, J = 3.73 Hz, 1H, Ar), 6.99 (d, J = 8.36 Hz, 2H, Ar), 6.69 (s, 2H, –NH_2), 6.54 (d, J = 8.36 Hz, 2H, Ar), 6.33 (d, J = 3.93, 1H, Ar), 5.10 (bs, 2H, –NH_2), 5.08 (s, 2H, –CH_2).

^{13}C NMR δ/ppm (100 MHz, DMSO-d_6): 160.1, 152.2, 151.4, 145.7, 130.6 (2C), 128.4, 123.1, 115.4 (2C), 113.2, 100.3, 61.2.

ESI-MS, *m/z*: 274.1 $[M + H]^+$.

*4.1.10.2. 9-(4-aminobenzyl)-6-chloro-9H-purin-2-amine (**56**).* The product was obtained following the general procedure and after column chromatography with 80%–100% EtOAc/*n*-Hexane; 41% yield corresponding to 120 mg of a white solid; mp = 227–229 °C.

^{1}H NMR δ/ppm (400 MHz, DMSO-d_6): 8.19 (s, 1H, Ar), 7.06 (d, J = 8.32 Hz, 2H, Ar), 6.97 (s, 2H, –NH_2), 6.56 (d, J = 8.32 Hz, 2H, Ar), 5.16 (bs, 2H, –NH_2), 5.11 (s, 2H, –CH_2).

^{13}C NMR δ/ppm (100 MHz, DMSO-d_6): 160.1, 151.4, 151.1, 145.8, 145.0, 131.4, 129.8 (2C), 127.7, 115.8 (2C), 47.8.

ESI-MS, *m/z*: 275.1 $[M + H]^+$.

*4.1.11. General procedure for preparation of compounds **57** and **58***

To a solution of 2-[(triphenylmethyl)thio]acetic acid (1.1 equiv) in dry DMF (0.2 M), EDCI (1.2 equiv) and HOBt (1.2 equiv) were added. The solution was stirred at 25 °C for 20 min, then **55** or **56** was added. The reaction mixture was stirred at 25 °C overnight, then the solvent was evaporated under reduced pressure. The residue was quenched with water and the mixture was extracted with ethyl acetate; the organic layer was washed with brine, dried over Na_2SO_4 and the solvent was removed under reduced pressure. The crudes were purified by column chromatography to afford the pure title compounds **57** and **58**.

*4.1.11.1. N-(4-((2-amino-4-chloro-7H-pyrrolo [2,3-d]pyrimidin-7-yl) methyl)phenyl)-2-(tritylthio)acetamide (**57**).* The product was obtained following the general procedure and after column chromatography with 40%–60% EtOAc/*n*-Hexane; 38% yield corresponding to 120 mg of a white solid; mp = 201–203 °C.

^{1}H NMR δ/ppm (400 MHz, $CDCl_3$): 7.78 (bs, 1H, –NH), 7.47 (m, 6H, Ar), 7.30 (m, 6H, Ar), 7.23 (m, 5H, Ar), 7.11 (m, 2H, Ar), 6.80 (d, J = 3.59 Hz, 1H, Ar), 6.42 (d, J = 3.64 Hz, 1H, Ar), 5.20 (s, 2H, –CH_2), 5.14 (bs, 2H, –NH_2), 3.31 (s, 2H, –CH_2).

^{13}C NMR δ/ppm (100 MHz, $CDCl_3$): 168.4, 160.3, 152.4, 151.8, 144.0 (3C), 135.2, 133.6, 130.3 (4C), 129.7 (4C), 127.4 (6C), 125.9 (3C), 121.4, 120.8 (2C), 116.3, 100.1, 66.4, 60.3, 36.6.

ESI-MS, *m/z*: 590.2 $[M + H]^+$.

*4.1.11.2. N-(4-((2-amino-6-chloro-9H-purin-9-yl)methyl)phenyl)-2-(tritylthio)acetamide (**58**).* The product was obtained following the general procedure and after column chromatography with 60%–80% EtOAc/*n*-Hexane; 34% yield corresponding to 130 mg of a white solid; mp = 213–215 °C.

^{1}H NMR δ/ppm (400 MHz, $CDCl_3$): 7.81 (bs, 1H, –NH), 7.73 (s, 1H, Ar), 7.54 (m, 1H, Ar), 7.47 (m, 5H, Ar), 7.32 (m, 10H, Ar), 7.23 (m, 3H, Ar), 5.23 (s, 2H, –CH_2), 4.87 (bs, 2H, –NH_2), 3.33 (s, 2H, –CH_2).

^{13}C NMR δ/ppm (100 MHz, $CDCl_3$): 168.2, 159.4, 151.2, 150.4, 145.3, 144.2 (3C), 135.7, 133.1, 132.5, 130.4 (4C), 129.2 (4C), 128.2 (6C), 126.4 (3C), 121.3 (2C), 66.7, 50.1, 36.2.

ESI-MS, *m/z*: 591.1 $[M + H]^+$.

*4.1.12. General procedure for preparation of the final compounds **59** and **60***

To a solution of **57** or **58** (1 equiv) in dry DCM, TFA (5 equiv) was added dropwise at 0 °C, followed by Et_3SiH (1.2 equiv). The reaction mixture was stirred at 0 °C for 20 min, then warmed to room temperature. The solvent was removed under reduced pressure and the residue was treated with Et_2O. The formed precipitate was filtered off and washed with cold Et_2O to afford the pure title compounds **59** and **60**.

*4.1.12.1. N-(4-((2-amino-4-chloro-7H-pyrrolo [2,3-d]pyrimidin-7-yl) methyl)phenyl)-2-mercaptoacetamide (**59**).* The product was obtained as a white solid following the general procedure; 93% yield (60 mg); mp = 153–155 °C.

^{1}H NMR δ/ppm (400 MHz, DMSO-d_6): 10.09 (s, 1H, –NH), 7.52 (d, J = 8.43 Hz, 2H, Ar), 7.17 (m, 3H Ar), 6.44 (s, 2H, –NH_2), 6.33 (d, J = 3.27 Hz, 1H, Ar), 5.20 (s, 2H, –CH_2), 3.28 (d, J = 8.77 Hz, 2H, –CH_2), 2.92 (t, J = 8.04 Hz, 1H, –SH).

^{13}C NMR δ/ppm (100 MHz, DMSO-d_6): 166.6, 159.8, 153.5, 151.4, 138.1, 132.7, 127.7 (2C), 126.2, 119.4 (2C), 108.9, 99.2, 47.1, 43.0.

HRMS (ESI), *m/z*: calcd. for $C_{15}H_{15}ClN_5OS^+$: 348.0680 $[M+H]^+$; found: 348.0651.

Anal. Calcd for $C_{15}H_{14}ClN_5OS$: C, 51.80; H, 4.06; N, 20.13. Found: C, 51.70; H, 4.02; N, 20.10.

*4.1.12.2. N-(4-((2-amino-6-chloro-9H-purin-9-yl)methyl)phenyl)-2-mercaptoacetamide (**60**).* The product was obtained as a white solid following the general procedure; 88% yield (63 mg); mp = 185–187 °C.

^{1}H NMR δ/ppm (400 MHz, DMSO-d_6): 10.13 (s, 1H, –NH), 8.21 (s, 1H, Ar), 7.56 (d, J = 8.60 Hz, 2H, Ar), 7.27 (d, J = 8.78 Hz, 2H, Ar), 6.92 (s, 2H, –NH_2), 5.28 (s, 2H, –CH_2), 3.29 (d, J = 7.97 Hz, 2H, –CH_2), 2.93 (t, J = 7.97 Hz, 1H, –SH).

^{13}C NMR δ/ppm (100 MHz, DMSO-d_6): 166.9, 160.1, 151.8, 151.2, 145.3, 139.0, 132.4, 131.8, 128.3 (2C), 120.7 (2C), 47.8, 43.2.

HRMS (ESI), *m/z*: calcd. for $C_{14}H_{14}ClN_6OS^+$: 349.0633 $[M+H]^+$; found: 349.0648.

Anal. Calcd for $C_{14}H_{13}ClN_6OS$: C, 48.21; H, 3.76; N, 24.09. Found: C, 48.37; H, 3.99; N, 24.40.

*4.1.12.3. tert-butyl (4-((2-amino-6-chloro-9H-purin-9-yl)methyl)benzyl) carbamate (**62**).* To a suspension of **8** (1 equiv) and **61** (1.1 equiv) in dry DMF (0.2 M), K_2CO_3 (2 equiv) was added. The suspension was stirred at room temperature overnight, then the reaction solvent was evaporated under reduced pressure, and the residue was purified by column chromatography (60%–100% EtOAc/*n*-Hexane) to afford 560 mg (52% yield) of the pure title compound **62** as a white solid; mp = 142–144 °C.

^{1}H NMR δ/ppm (400 MHz, DMSO-d_6): 8.21 (s, 1H, Ar), 7.36 (t, J = 6.10 Hz, 1H, –NH), 7.20 (m, 4H, Ar), 6.92 (s, 2H, –NH_2), 5.26 (s, 2H, –CH_2), 4.08 (d, J = 5.82 Hz, 2H, –CH_2), 1.38 (s, 9H, –CH_3).

^{13}C NMR δ/ppm (100 MHz, DMSO-d_6): 159.3, 157.2, 151.4, 150.7, 145.7, 135.1, 134.8, 131.6, 128.8 (2C), 126.9 (2C), 80.4, 50.7, 46.6, 28.6 (3C).

ESI-MS, *m/z*: 389.1 $[M + H]^+$.

*4.1.12.4. 9-(4-(aminomethyl)benzyl)-6-chloro-9H-purin-2-amine (**63**).* To a solution of **62** (1 equiv) in dry DCM (0.2 M), TFA (10 equiv) was added. The solution was stirred at room temperature overnight, then the reaction solvent was evaporated under reduced pressure, and the residue was treated with Et_2O. The formed solid was filtered off and washed with Et_2O to afford 544 mg (87% yield) of the pure title compound **63** as a white solid; mp = 267–268 °C.

^{1}H NMR δ/ppm (400 MHz, DMSO-d_6): 8.25 (s, 1H, Ar), 7.44 (d, J = 8.63 Hz, 2H, Ar), 7.35 (s, 2H, NH_2), 7.31 (d, J = 8.15 Hz, 2H, Ar), 6.93 (s, 2H, –NH_2), 5.31 (s, 2H, –CH_2), 4.01 (m, 2H, –CH_2).

^{13}C NMR δ/ppm (100 MHz, DMSO-d_6): 159.8, 151.1, 150.8, 147.2, 139.6, 135.2, 131.4, 128.5 (2C), 126.2 (2C),49.1, 45.4.

ESI-MS, *m/z*: 289.1 $[M + H]^+$.

*4.1.12.5. N-(4-((2-amino-6-chloro-9H-purin-9-yl)methyl)benzyl)-2-(tritylthio)acetamide (**64**).* To a solution of 2-[(triphenylmethyl)thio]acetic acid (1.1 equiv) in dry DMF (0.2 M), EDCI (1.2 equiv) and HOBt (1.2 equiv) were added. The solution was stirred at 25 °C for 20 min, then **63** was added. The reaction mixture was stirred at 25 °C overnight, then the solvent was evaporated under reduced pressure. The residue was quenched with water and the mixture was extracted with ethyl acetate; the organic layer was washed with brine, dried over Na_2SO_4, filtered and the solvent was removed under reduced pressure. The crude was purified by column chromatography (50%–100% EtOAc/*n*-Hexane) to afford 375 mg (62% yield) of the pure title compound **64** as a white solid; mp = 199–200 °C.

^{1}H NMR δ/ppm (400 MHz, $CDCl_3$): 7.75 (s, 1H, Ar), 7.40 (m, 7H, Ar), 7.25 (m, 12H, Ar), 7.14 (m, 2H, Ar), 6.27 (t, J = 5.37 Hz, 1H, –NH),

5.24 (s, 2H, –CH_2), 5.16 (s, 2H, –NH_2), 4.13 (d, J = 4.63 Hz, 2H, –CH_2).

^{13}C NMR δ/ppm (100 MHz, $CDCl_3$): 171.6, 160.4, 152.3, 151.7, 146.4, 142.5 (3C), 135.2, 134.7, 131.2, 130.1 (3C), 129.7 (3C), 128.8 (2C), 128.1 (6C), 127.5 (2C), 126.2 (3C), 67.2, 48.4, 43.1, 36.6.

ESI-MS, *m/z*: 605.2 $[M + H]^+$.

*4.1.12.6. N-(4-((2-amino-6-chloro-9H-purin-9-yl)methyl)benzyl)-2-mercaptoacetamide (**65**).* To a solution of **64** (1 equiv) in dry DCM, TFA (5 equiv) was added dropwise at 0 °C, followed by Et_3SiH. The reaction mixture was stirred at 0 °C for 20 min, then warmed to room temperature. The solvent was removed under reduced pressure and the residue was treated with Et_2O. The formed precipitate was filtered off and washed with cold Et_2O to afford 290 mg (82% yield) of the pure title compounds **65** as a white solid; mp = 174–176 °C.

^{1}H NMR δ/ppm (400 MHz, DMSO-d_6): 8.47 (t, J = 5.28 Hz, 1H, –NH), 8.22 (s, 1H, Ar), 7.23 (m, 4H, Ar), 6.92 (s, 2H, –NH_2), 5.27 (s, 2H, –CH_2), 4.24 (d, J = 6.05 Hz, 2H, –CH_2), 3.14 (d, J = 7.82 Hz, 2H, –CH_2), 2.78 (t, J = 8.26 Hz, 1H, –SH).

^{13}C NMR δ/ppm (100 MHz, DMSO-d_6): 171.4, 160.8, 151.1, 150.7, 145.9, 135.0, 134.7, 131.2, 128.6 (2C), 127.7 (2C), 49.2, 43.4, 33.6.

HRMS (ESI), *m/z*: calcd. for $C_{15}H_{16}ClN_6OS^+$: 363.0789 $[M+H]^+$; found: 363.0803.

Anal. Calcd for $C_{15}H_{15}ClN_6OS$: C, 49.65; H, 4.17; N, 23.16. Found: C, 49.60; H, 4.09; N, 23.22.

4.2. Molecular modelling

4.2.1. Protein preparation

All the molecular modelling analyses related to HDAC6 were conducted on the 5EDU crystal structure [43]. The crystal structure of the protein underwent an optimization process using the *Protein Preparation Wizard* tool implemented in Maestro of the Schrödinger Suite (release 2021–1) [82]. Missing hydrogen atoms were added, and bond orders were assigned. The prediction of the most suitable protonation states of the protein residues was accomplished by using PROPKA, with the pH set to 7.4. The same procedure was also adopted for the preparation of the crystal structures of HDAC1 (PDB code: 4BKX) [83] and HDAC4 (PDB code: 2VQJ) [84].

4.2.2. Molecular docking

Docking studies were performed by using the XP protocol of the Glide program [85], allowing for ligand flexibility. Default settings were used for the analyses, using the bound crystallographic ligand as the centroid of the box for generating the receptor grid. A metal coordination constraint was applied to allow the ligands to coordinate to the catalytic Zn^{2+} ion. The protonation state of His610 was set depending on whether or not an acidic hydrogen was present in the ZBGs. To this aim, the compounds bearing the hydroxamic acid and 2-mercaptoacetamide zinc binding groups were modelled as negatively charged and His610 as positively charged, while compounds of the TFMO series, which lack an acidic proton, were modelled as neutral and docked into the HDAC6 binding site with a neutral His610. Docking calculations in the HDAC4 binding site were performed for the TFMO representative compound **11** and its fluoro-substituted derivatives, with the default settings of the XP protocol available in Glide [85].

4.2.3. Molecular dynamics

All the MD simulations were carried out with AMBER20 starting from the structures of the docking complexes [86]. MD simulations were performed using the ff14SB force field. Zinc and potassium ions originally present in the HDAC6 crystal structure were maintained. A bonded model was used to simulate the interaction of the TFMO compounds **10**, **11**, and **16** with Zn^{2+}. The MCPB. py tool [87] was used to setup the system using the Empirical method to obtain the force constants. The RESP charges of the residues involved in the bonded model were calculated with GAMESS [88] at the B3LYP/6-31G* level of theory. Four bonds with the metal ion were defined among the side chains of Asp649, Asp742, His651 and the oxygen atom of the oxadiazole ring of **10**, **11** and **16**. The 12-6-4 LJ-Type nonbonded model [89,90] was used to model zinc complexes of **37**, **38**, **44**, **59**, **60**. General Amber force field (GAFF) [91] parameters were assigned to the ligands, while RESP partial charges were fitted using the RED tools [92]. Geometry optimization and electrostatic potential calculations of the ligands were performed at the HF level with a 6-31G*(1d) basis set using GAMESS [88]. For all simulations, the TIP3P explicit water model was used by solvating the complexes into a cubic 10 Å water box. Prior to the MD simulations, two steps of minimization were carried out; in the first stage, heavy atoms were kept fixed with a position restraint of 100 kcal/mol. In the second stage, the entire system was minimized with 10,000 steps of steepest descent minimization. PME electrostatics and periodic boundary conditions were used in the simulation [93]. The MD simulation was run using the minimized structure as the starting conformation. The time step was set to 2.0 fs, with a cut-off of 8 Å for the non-bonded interaction, and SHAKE was employed to keep all bonds involving hydrogen atoms rigid. Constant volume periodic boundary MD was carried out for 1 ns, during which the temperature was gradually raised from 0 to 300 K. A positional restraint of 10 kcal/mol was applied to heavy atoms except for water molecules. Then, 1 ns constant pressure MD at 300 K with gradually decreasing constraints were performed. After equilibration, production runs of 100 ns were performed. In the simulations of TFMO and MCA derivatives, positional restraints were applied to the ZBG-metal complexes to maintain the interactions similar to those of crystallographic complexes. For TFMO derivatives **10**, **11** and **16**, the distance and angle values were referred to the 3ZNR [70] crystal structure, while the positional restraints of the 2-mercaptoacetamide derivatives **59** and **60** were taken from the 6MR5 [54] crystal structure.

4.3. Histone deacetylases inhibitory activity assays

In vitro assays on recombinant HDACs enzymes were performed with the same procedure described in our previous work [44]. Briefly, the reactions were carried out in a solution of 50 mM Tris–HCl (pH 8.0), 137 mM NaCl, 2.7 mM KCl, 1 mM MgCl2, and 1 mg/ml BSA, by using: (i) the fluorogenic peptide from p53 residues 379–382 (RHKK-Ac-AMC) as a substrate for the assays on HDAC1, HDAC2, HDAC3, HDAC6, HDAC10; (ii) trifluoroacetyl lysine as a substrate for the assays on HDAC4, HDAC5, HDAC7, HDAC9 and HDAC11; (iii) the fluorogenic peptide from p53 residues 379–382 (RHK-Ac-K-Ac-AMC) as a substrate for the assays on HDAC8. The compounds were tested with a 3-fold serial dilution in DMSO, starting from 100 μM. Moreover, compounds **37–41**, **43** and **45** that showed high potency in the HDAC6 assays were also re-tested with a 3-fold serial dilution in DMSO, starting from 1 μM. The enzymatic assays were performed by adding to the reaction buffer, the recombinant protein and ligand solutions. Then, a 2 μM volume of the reference compound, 16 mg/mL trypsin in 50 mM Tris–HCl, pH 8.0, 137 mM NaCl, 2.7 mM KCl, 1 mM $MgCl_2$ was added to record the fluorescence signal (Ex 360 nm/Em 460 nm). A concentration equal to 1.00×10^{-12} M was used for curve fitting of the blank (*i.e.*, DMSO). IC_{50} values were calculated by using the GraphPad Prism 4 program based on a sigmoidal dose–response equation. Trichostatin A was used as a reference compound for the assays on HDAC1, HDAC2, HDAC3, HDAC6, HDAC8 and HDAC11. The reference compound TMP269 was tested on HDAC4, HDAC5, HDAC7 and HDAC9, while Quisinostat was used as a control in HDAC10 assays. Tubastatin A and Vorinostat (SAHA) were also assayed against HDAC6.

4.4. Inhibition of class IIa HDAC activity in LNCaP cells by means of cellular HDAC-Glo Class IIa assay

The evaluation of specific Class IIa isoenzyme activity in LNCaP was performed with Cellular HDAC-Glo Class IIa Assay (Promega), according

to the protocol provided by the manufacturer. LNCaP cells were seeded into the wells of 384-well plate. Cells were treated with reference compound TMP269 and compounds **13** and **20** for 1 h, in 10-dose IC_{50} mode in duplicate with 3-fold serial dilution starting at 100 μM. HDAC Class IIa activity was measured with HDAC-Glo Class IIa Assay on an Envision 2104 Multilabel Reader (PerkinElmer). IC_{50} values were calculated using the GraphPad Prism 4 program based on a sigmoidal dose-response equation.

4.5. Cell lines and treatments

Three human prostate cell lines were analyzed. Cancer LNCaP cells (ATCC #CRL-1740, RRID:CVCL_1379) were grown in RPMI 1640 Medium and PC3 cells (ATCC #CRL-1435, RRID:CVCL_0035) were maintained in Ham's F12 Medium. All media (Biowest) were supplemented with 2 mM glutamine, 100 IU/mL penicillin, 100 μg/mL streptomycin and 10% Foetal Bovine Serum (Gibco). Normal RWPE-1 cells (ATCC #CRL-11609, RRID:CVCL_3791) were grown in Keratinocyte Serum Free Medium (K-SFM; # 17,005,042, Gibco), supplemented with 0.05 mg/mL bovine pituitary extract (Gibco) and 5 ng/mL human recombinant epidermal growth factor (Gibco). All above-mentioned cell lines were authenticated by Short Tandem Repeat (STR) Analysis (Eurofins Genomics), verified to be mycoplasma free and passaged <3 months. All cells were grown at 37 °C in a humidified incubator containing 5% CO_2. Synthesized compounds, Tubastatin A, SAHA, TSA and TMP269 were dissolved in DMSO (Sigma-Aldrich, St. Louis, MO, USA) and added to the cell medium at the concentrations described in the text for 24–72 h, as indicated in figure legends. DMSO was used as control.

4.6. Cell viability

Cells were treated with the candidate compounds at different concentrations and viability was measured by colorimetric 3-(4,5-Dimethylthiazol-2-yl)-2,5-diphenyltetrazolium bromide (MTT) assay after 72 h [94]. Dose-response curves were analyzed in GraphPad PRISM 6 software (GraphPad Prism) based on a log (inhibitor) *vs* response (variable slope) equation and the concentration at which cellular growth is inhibited by 50% (GI_{50}) was determined. In dose-response experiments, the compounds were tested at 8 concentrations, starting at 300 μM (RWPE-1) or 100 μM (LNCaP), with 3-fold serial dilutions.

4.7. Migration assays

Migration assays were performed with Transwell membranes for LNCaP cells and wound healing assays for PC3 cells. LNCaP cells were pre-treated with the indicated compounds (3 μM for 24 h) and 7×10^4 cells were seeded in 100 μl of serum-free medium into the upper chamber of the Transwell (pore size 8 μm; #3464, Corning). Complete RPMI medium containing 10% FBS was used as chemoattractant in the lower chamber. 3 μM of the selected compounds were added to either the lower and upper chamber. After 24 h, the cells on the upper chambers were removed with a cotton swab, while cells on the underside of the inserts were fixed and stained with 0.5% crystal violet solution in 20% Methanol, for 15 min. Following visual inspection under a light microscope, the bound crystal violet was eluted using 33% acetic acid and quantified by measuring the absorbance at 590 nm, according to the manufacturer's protocol. For wound healing cell migration assay, 4×10^5 PC3 cells were plated in a 12-well plate. Approximately 24 h later, the cells were pre-treated with the indicated compounds (3 μM, for 24 h) and the confluent monolayer was scratched using a 200 μL pipette tip. Medium and non-adherent cells were removed and new medium containing 1% FBS and 3 μM of the indicated compounds was added. Cells were observed under the microscope and the inhibition of migration was assessed after 18 h and 24 h. Two random pictures were taken for each treated well per experiment and the areas of the wounds measured using ImageJ software. Cell migration (%) was then calculated using the formula: (initial gap area - final gap area/initial gap area) × 100%.

4.8. Protein extraction and immunoblotting

Whole-cell protein extracts were prepared by lysis of control or treated-cells into 1X SDS sample buffer [95]. Equivalent amounts of cellular extracts were resolved by SDS-PAGE, transferred to PVDF or nitrocellulose membrane with *Trans*-Blot Turbo Transfer System (Bio--Rad) and immunoblotted with the following primary antibodies, diluted 1:1000 in 1X TBS with 1 mg/mL BSA: *anti*-αTubulin (#PA5-19489, Invitrogen) *anti*-βActin (#66009, Proteintech Europe), anti-Acetylated Histone H3 (#518011, Santa Cruz), anti-Acetylated α-Tubulin (#sc-23950, Santa Cruz), anti-Histone H3 (#ab1791, Abcam) and *anti*-γ-H2AX (#05–636, Millipore). Membranes were blotted and scanned with an Amersham Imager AI680 RGB (GE Healthcare), using detection reagents Westar ηC and Supernova HRP substrates (Cyanagen). ImageJ software has been used to quantify protein bands from western blots.

4.9. TCGA data analysis

Expression levels and prognostic impact of HDACs were evaluated based on RNA-seq and clinical data of TCGA- Prostate Adenocarcinoma (PRAD).

The overall survival Hazard Ratios of HDACs, estimated using Mantel–Cox test, were obtained using Gene Expression Profiling Interactive Analysis - GEPIA2 (http://gepia2.cancer-pku.cn/, accessed on April 7th, 2023) [96]. a web server for analysis of the RNA sequencing expression data of the TCGA project using a standard processing pipeline. Expression thresholds Cutoff-High/Cutoff-Low of 40%/60% were used.

Box plots of the transcriptional expression levels of class II HDACs in patients with PRAD, stratified according to pathological N stage, were obtained using the UALCAN database (https://ualcan.path.uab.edu/, accessed on April 7th, 2023) [97]. UALCAN is an interactive web resource for analyzing transcriptome data from The Cancer Genome Atlas project (TCGA). $p < 0.05$ was considered statistically significant.

4.10. Statistical analysis

All statistical analyses were performed using GraphPad PRISM 6 software (GraphPad Prism, RRID: SCR_002798), using *t*-test or ANOVA with post-hoc tests, as specified in the figure legends. Graphs represent Means ± Standard Error of the Mean (SEM). Data are considered to be statistically significant if $p < 0.05$ (*), $p < 0.01$ (**), $p < 0.001$ (***) and $p < 0.0001$ (****).

4.11. Solubility evaluation

50 mM stock solutions of the test compounds were prepared in 100% DMSO. 500 μM samples were made up by a direct dilution of the stock solution in phosphate buffer pH 7.4 and citric buffer pH 4.5 (1% DMSO final concentration). Reference solutions were made up in 100% MeOH. Solutions in buffers (200 μL) were incubated at room temperature at 200 rpm for 1.5 h directly in a Multiscreen solubility plate (Millipore) and then filtrated under vacuum for 5 min. Reference solutions and samples were than diluted 1:1000 in MeOH with 1 μM Verapamil before analysis. Samples were analyzed on a UPLC Acquity (Waters) coupled with an API 3200 Triple Quadrupole AB Sciex. Compound **13**: mobile phase A: ammonium bicarbonate pH 8, mobile phase B: MeOH. Column: Gemini NX C18 50 × 2.1 mm 5 μm. Temperature 35 °C, injection volume 10 μL. Compound **37**: mobile phase A: 0.1% formic acid in water, mobile phase B acetonitrile 0.1% formic acid. Column: Synergy Polar 2.5 μm 50 × 2.1 mm. Temperature 35 °C, injection volume 10 μL. Final concentrations were evaluated by comparing the AUC of the reference solutions in organic solvent (500 μM) with those of the filtered test compounds

after 1.5 h of incubation.

4.12. Permeability in Caco-2 cells

4.12.1. Cell culture

Caco-2 cells (ECACC) were acquired from Readycells (Barcelona, Spain) after 21 days of culture (Fig. S17). Three days before the assay the 24-Insert HTS plates were placed into a cell culture incubator kept at 37 °C, in a highly humidified atmosphere of 95% air/5% CO_2 for 4 h to allow shipping medium to completely liquefy. The shipping medium was removed from the basal and apical compartments of the Caco-Ready™ plate *via* aspiration and was replaced with fresh culture medium DMEM (1 g/L glucose, 10% FCS, 1% glutamine 200 mM, 1% penicillin (10,000 U/mL) – streptomycin (10/mg/mL) in HBSS). Cells were kept at 37 °C with 5% CO_2 in an incubator up to the day of the experiment. Prior to perform the experiments, transendothelial electrical resistance (TEER) was >1000Ωcm^2, as measured with a Millicell-ERS Millipore. Stock solutions were prepared in DMSO at 5 mM concentrations for the TI. HBSS buffer was placed in the apical compartments (250 μL) and in the basolateral compartments (750 μL). Stock solutions were spiked in the apical compartments (2.5 μL) for apical to basolateral transport (A→B) and in the basolateral compartments 7.5 μL for basolateral to apical transport (B→A) to reach the final concentration of 5 μM. Samples at T = 0 from the donor compartments were diluted with 150 μL of Internal Standard (IS) solution (Verapamil, 10 ng/mL in acetonitrile). After 2 h incubation period at 37 °C and 5% CO_2, the basolateral and the apical sides were diluted with IS solutions as reported above. Samples were collected in plates and stored at −20 °C up to the analysis. At the end of the experiment integrity of the cellular junction was measured by incubating 250 μL of Lucifer yellow (LY) at the apical side (at the concentration of 0.02 mg/mL in MEM medium) and with 0.75 mL of DMEM medium in the basolateral compartment for 1 h at 37 °C. At the end of incubation, 100 μL of the solution at the apical side were placed in a 96-black plate with 100 μL of buffer. 200 μL of the solution at the basolateral side were placed in a 96 well black plate. The control wells were made by 100 μL of DMEM and 100 μL of LY starting solution (0.02 mg/mL). The plate was read on a fluorimeter at λ 430–538 nm. Samples were analyzed on a UPLC Acquity (Waters) coupled with a API 3200 Triple Quadrupole AB Sciex. Compound **13**: mobile phase A: ammonium bicarbonate pH 8, mobile phase B: MeOH Column: Gemini NX C18 50 × 2.1 mm 5 μm, Temperature 35 °C, injection volume 10 μL. Compound **37**: mobile phase A: 0.1% Formic acid in water, mobile phase B acetonitrile 0.1%Formic acid. Column: Synergy Polar 2.5 μm 50 × 2.1 mm. Temperature 35 °C, injection volume 10 μL.

4.12.2. Data analysis

The apparent permeability (Papp) was calculated according to the following formula:

$$\text{Papp} = \frac{dQ}{dT} * \frac{1}{A * C_0}$$

dQ: amount of transporter test drug in μmol/cm.^{3}
dT: incubation time in seconds.
A: surface of porous membrane in cm^2 (0.33).
C_0:initial concentration of TA in the donor chamber in μmol/cm.^{3}
The efflux ratio (ER) is calculated according to following formula:

$$\text{Efflux Ratio} = \frac{\text{Papp}(B\rightarrow A)}{\text{Papp}(A\rightarrow B)}$$

Data were processed with Microsoft Excel. Data are expressed as mean of n = 2 (±SD). To assure suitable functionality of the monolayers, the permeability of Lucifer Yellow (LY), known as low permeability compound, was measured at the end of the assay. The permeability value of LY indicates the proper integrity of the monolayer. LY values are accepted if below 0.7% permeability.

5. Metabolic stability in liver microsomes

5.1. Assay protocol

Test compounds in duplicate were dissolved in DMSO to obtain 1 mg/mL solutions, which were pre-incubated, at the final concentration of 1 μM, for 10 min at 37 °C in potassium phosphate buffer 50 mM pH 7.4, 3 mM $MgCl_2$, with mouse and human liver microsomes (Sigma) at the final concentration of 0.5 mg/mL. After the pre-incubation period, reactions were started by adding the cofactors mixture (NADP, Glc6P, Glc6P-DH in 2% Sodium bicarbonate); samples (25 μL) were taken at time 0, 10, 20, 30 and 60 min and added to 150 μL of acetonitrile with verapamil 0.1 μM as Internal Standard (IS) to stop the reaction. After centrifugation the supernatants were analyzed by LC-MS/MS. A control sample without cofactors was added in order to check the stability of test compounds in the matrix after 60min. 7-Ethoxycoumarin (7-EC) was added as positive reference standard. Samples were analyzed on Acquity UPLC (Waters) coupled with an API 3200 Triple Quadrupole ABSciex.

Column: Synergy Polar 2.5 μm 50 × 2.1 mm. Temperature 35 °C, injection volume 10 μL. Mobile phase A: Deionized water +0.1% HCOOH, mobile phase B: acetonitrile +0.1% HCOOH. Temperature: RT.

5.2. Data analysis

The percentage of the area of the test compound remaining at the various incubation times were calculated with respect to the area of compound at time 0 min. The rate constant, k (min^{-1}) derived from the exponential decay equation (peak area/IS *vs* time) was used to calculate the rate of Intrinsic clearance (Cli) of the compound, using the following equation: Cli (μL/min/mg) = k/microsomal conc. X 1000, where k is the rate constant (min^{-1}) and the microsomal protein concentration is 0.5 mg protein/mL.

Declaration of competing interest

The authors declare that they have no known competing financial interests or personal relationships that could have appeared to influence the work reported in this paper.

Data availability

Data will be made available on request.

Acknowledgements

The research leading to these results has received funding from AIRC (Fondazione Italiana per la Ricerca sul Cancro) under IG 2019- I.D. 23635 project – P.I. Giulio Rastelli and IG 2018 – I.D. 21323 project – P. I. Carol Imbriano. We thank OpenEye Scientific Software, Inc. for a free academic license.

Appendix A. Supplementary data

Supplementary data to this article can be found online at https://doi.org/10.1016/j.ejmech.2023.115730.

Abbreviations

AcH3	Acetylated Histone H3
AcTub	Acetylated Tubulin
AR	Androgen Receptor
Cli	Intrinsic Clearance
CRPC	Castration-Resistant Prostate Cancer
CSPC	Castration-Sensitive Prostate Cancer
EDCI	N'-ethylcarbodiimide Hydrochloride
EMT	Epithelial-Mesenchymal Transition

FDA	Food and Drug Administration
GAFF	General Amber Force Field
HA	Hydroxamic Acid
HAT	Histone Acetyltransferase
HDAC	Histone Deacetylase
HOBt	Hydroxybenzotriazole
Hsp	Heat Shock Protein
HSPC	Hormone-Sensitive Prostatic Carcinoma
IS	Internal Standard
LY	Lucifer Yellow
MCA	2-mercaptoacetamide
MD	Molecular Dynamics
MEF2	Myocyte Enhancer Factor-2
MTT	3-(4,5-Dimethylthiazol-2-yl)-2,5-diphenyltetrazolium bromide
NAD	Nicotinamide Adenine Dinucleotide
NEPC	Neuroendocrine Prostate Cancer
Papp	Apparent Permeability
PCA	Prostate Cancer
PRAD	Prostate Adenocarcinoma
RMSD	Root-Mean-Square Deviation
SAHA	Vorinostat
SAR	Structure-Activity Relationships
STR	Short Tandem Repeat
TEER	Transendothelial electrical resistance
TFAA	Trifluoroacetic Anhydride
TFMO	Trifluoromethyloxadiazole
TUB	Tubulin
TUB A	Tubastatin A
ZBG	Zinc-Binding Group

References

[1] P. Rawla, Epidemiology of prostate cancer, World J. Oncol. 10 (2019) 63–89, https://doi.org/10.14740/wjon1191.

[2] D.F. Penson, Re: comparison of gonadotropin-releasing hormone agonists and orchiectomy: effects of androgen-deprivation therapy, J. Urol. 196 (2016) 104–106, https://doi.org/10.1016/j.juro.2016.04.029.

[3] S. Gleicher, B.A. Porter, D. Nath, G. Li, R. Khanna, H. Goldberg, M. Kortylewski, G. Bratslavsky, L. Kotula, Novel target opportunities in non-metastatic castrate resistant prostate cancer, Cancers 13 (2021) 2426, https://doi.org/10.3390/cancers13102426.

[4] J. de Bono, J. Mateo, K. Fizazi, F. Saad, N. Shore, S. Sandhu, K.N. Chi, O. Sartor, N. Agarwal, D. Olmos, A. Thiery-Vuillemin, P. Twardowski, N. Mehra, C. Goessl, J. Kang, J. Burgents, W. Wu, A. Kohlmann, C.A. Adelman, M. Hussain, Olaparib for metastatic castration-resistant prostate cancer, N. Engl. J. Med. 382 (2020) 2091–2102, https://doi.org/10.1056/NEJMoa1911440.

[5] N. Mitsiades, A road map to comprehensive androgen receptor axis targeting for castration-resistant prostate cancer, Cancer Res. 73 (2013) 4599–4605, https://doi.org/10.1158/0008-5472.CAN-12-4414.

[6] T.M. Beer, A.J. Armstrong, D.E. Rathkopf, Y. Loriot, C.N. Sternberg, C.S. Higano, P. Iversen, S. Bhattacharya, J. Carles, S. Chowdhury, I.D. Davis, J.S. de Bono, C. P. Evans, K. Fizazi, A.M. Joshua, C.-S. Kim, G. Kimura, P. Mainwaring, H. Mansbach, K. Miller, S.B. Noonberg, F. Perabo, D. Phung, F. Saad, H.I. Scher, M.-E. Taplin, P.M. Venner, B. Tombal, PREVAIL Investigators, Enzalutamide in metastatic prostate cancer before chemotherapy, N. Engl. J. Med. 371 (2014) 424–433, https://doi.org/10.1056/NEJMoa1405095.

[7] N.D. James, J.S. de Bono, M.R. Spears, N.W. Clarke, M.D. Mason, D.P. Dearnaley, A.W.S. Ritchie, C.L. Amos, C. Gilson, R.J. Jones, D. Matheson, R. Millman, G. Attard, S. Chowdhury, W.R. Cross, S. Gillessen, C.C. Parker, J.M. Russell, D. R. Berthold, C. Brawley, F. Adab, S. Aung, A.J. Birtle, J. Bowen, S. Brock, P. Chakraborti, C. Ferguson, J. Gale, E. Gray, M. Hingorani, P.J. Hoskin, J.F. Lester, Z.I. Malik, F. McKinna, N. McPhail, J. Money-Kyrle, J. O'Sullivan, O. Parikh, A. Protheroe, A. Robinson, N.N. Srihari, C. Thomas, J. Wagstaff, J. Wylie, A. Zarkar, M.K.B. Parmar, M.R. Sydes, STAMPEDE investigators, Abiraterone for prostate cancer not previously treated with hormone therapy, N. Engl. J. Med. 377 (2017) 338–351, https://doi.org/10.1056/NEJMoa1702900.

[8] Y. Mulati, Y. Fan, W. Yu, Q. Zhang, Z. He, Novel androgen receptor inhibitors in non-metastatic, castration-resistant prostate cancer: a systematic review and network meta-analysis, Front. Oncol. 11 (2021), 733202, https://doi.org/10.3389/fonc.2021.733202.

[9] P.A. Watson, V.K. Arora, C.L. Sawyers, Emerging mechanisms of resistance to androgen receptor inhibitors in prostate cancer, Nat. Rev. Cancer 15 (2015) 701–711, https://doi.org/10.1038/nrc4016.

[10] Y. Yamada, H. Beltran, Clinical and biological features of neuroendocrine prostate cancer, Curr. Oncol. Rep. 23 (2021) 15, https://doi.org/10.1007/s11912-020-01003-9.

[11] J. Ai, Y. Wang, J.A. Dar, J. Liu, L. Liu, J.B. Nelson, Z. Wang, HDAC6 regulates androgen receptor hypersensitivity and nuclear localization via modulating Hsp90 acetylation in castration-resistant prostate cancer, Mol. Endocrinol. Baltim. Md 23 (2009) 1963–1972, https://doi.org/10.1210/me.2009-0188.

[12] T.C.S. Ho, A.H.Y. Chan, A. Ganesan, Thirty years of HDAC inhibitors: 2020 insight and hindsight, J. Med. Chem. 63 (2020) 12460–12484, https://doi.org/10.1021/acs.jmedchem.0c00830.

[13] A.J.M. de Ruijter, A.H. van Gennip, H.N. Caron, S. Kemp, A.B.P. van Kuilenburg, Histone deacetylases (HDACs): characterization of the classical HDAC family, Biochem. J. 370 (2003) 737–749, https://doi.org/10.1042/BJ20021321.

[14] I.V. Gregoretti, Y.-M. Lee, H.V. Goodson, Molecular evolution of the histone deacetylase family: functional implications of phylogenetic analysis, J. Mol. Biol. 338 (2004) 17–31, https://doi.org/10.1016/j.jmb.2004.02.006.

[15] F. Yang, N. Zhao, D. Ge, Y. Chen, Next-generation of selective histone deacetylase inhibitors, RSC Adv. 9 (2019) 19571–19583, https://doi.org/10.1039/C9RA02985K.

[16] C.M. Grozinger, S.L. Schreiber, Regulation of histone deacetylase 4 and 5 and transcriptional activity by 14-3-3-dependent cellular localization, Proc. Natl. Acad. Sci. U.S.A. 97 (2000) 7835–7840, https://doi.org/10.1073/pnas.140199597.

[17] A. Clocchiatti, C. Florean, C. Brancolini, Class IIa HDACs: from important roles in differentiation to possible implications in tumourigenesis, J. Cell Mol. Med. 15 (2011) 1833–1846, https://doi.org/10.1111/j.1582-4934.2011.01321.x.

[18] Y. Asfaha, C. Schrenk, L.A. Alves Avelar, A. Hamacher, M. Pflieger, M.U. Kassack, T. Kurz, Recent advances in class IIa histone deacetylases research, Bioorg. Med. Chem. 27 (2019), 115087, https://doi.org/10.1016/j.bmc.2019.115087.

[19] N.R. Bertos, A.H. Wang, X.J. Yang, Class II histone deacetylases: structure, function, and regulation, Biochem. Cell Biol. Biochim. Biol. Cell. 79 (2001) 243–252.

[20] A.H. Wang, M.J. Kruhlak, J. Wu, N.R. Bertos, M. Vezmar, B.I. Posner, D.P. Bazett-Jones, X.J. Yang, Regulation of histone deacetylase 4 by binding of 14-3-3 proteins, Mol. Cell Biol. 20 (2000) 6904–6912, https://doi.org/10.1128/MCB.20.18.6904-6912.2000.

[21] K. Halkidou, S. Cook, H.Y. Leung, D.E. Neal, C.N. Robson, Nuclear accumulation of histone deacetylase 4 (HDAC4) coincides with the loss of androgen sensitivity in hormone refractory cancer of the prostate, Eur. Urol. 45 (2004) 382–389, https://doi.org/10.1016/j.eururo.2003.10.005. ; author reply 389.

[22] B.-C. Jeong, C.Y. Hong, S. Chattopadhyay, J.H. Park, E.-Y. Gong, H.-J. Kim, S.-Y. Chun, K. Lee, Androgen receptor corepressor-19 kDa (ARR19), a leucine-rich protein that represses the transcriptional activity of androgen receptor through recruitment of histone deacetylase, Mol. Endocrinol. 18 (2004) 13–25, https://doi.org/10.1210/me.2003-0065.

[23] G. Ren, G. Zhang, Z. Dong, Z. Liu, L. Li, Y. Feng, D. Su, Y. Zhang, B. Huang, J. Lu, Recruitment of HDAC4 by transcription factor YY1 represses HOXB13 to affect cell growth in AR-negative prostate cancers, Int. J. Biochem. Cell Biol. 41 (2009) 1094–1101, https://doi.org/10.1016/j.biocel.2008.10.015.

[24] Y. Wang, R. Abrol, J.Y.W. Mak, K. Das Gupta, D. Ramnath, D. Karunakaran, D. P. Fairlie, M.J. Sweet, Histone deacetylase 7: a signalling hub controlling development, inflammation, metabolism and disease, FEBS J. (2022), https://doi.org/10.1111/febs.16437.

[25] C. Simões-Pires, V. Zwick, A. Nurisso, E. Schenker, P.-A. Carrupt, M. Cuendet, HDAC6 as a target for neurodegenerative diseases: what makes it different from the other HDACs? Mol. Neurodegener. 8 (2013) 7, https://doi.org/10.1186/1750-1326-8-7.

[26] G.I. Aldana-Masangkay, K.M. Sakamoto, The role of HDAC6 in cancer, J. Biomed. Biotechnol. 2011 (2011), 875824, https://doi.org/10.1155/2011/875824.

[27] Y. Li, D. Shin, S.H. Kwon, Histone deacetylase 6 plays a role as a distinct regulator of diverse cellular processes, FEBS J. 280 (2013) 775–793, https://doi.org/10.1111/febs.12079.

[28] C. Hubbert, A. Guardiola, R. Shao, Y. Kawaguchi, A. Ito, A. Nixon, M. Yoshida, X.-F. Wang, T.-P. Yao, HDAC6 is a microtubule-associated deacetylase, Nature 417 (2002) 455–458, https://doi.org/10.1038/417455a.

[29] C. Seidel, M. Schnekenburger, A. Mazumder, M.-H. Teiten, G. Kirsch, M. Dicato, M. Diederich, 4-Hydroxybenzoic acid derivatives as HDAC6-specific inhibitors modulating microtubular structure and HSP90α chaperone activity against prostate cancer, Biochem. Pharmacol. 99 (2016) 31–52, https://doi.org/10.1016/j.bcp.2015.11.005.

[30] C. Corno, N. Arrighetti, E. Ciusani, E. Corna, N. Carenini, N. Zaffaroni, L. Gatti, P. Perego, Synergistic interaction of histone deacetylase 6- and MEK-inhibitors in castration-resistant prostate cancer cells, Front. Cell Dev. Biol. 8 (2020) 610, https://doi.org/10.3389/fcell.2020.00610.

[31] S. Shen, A.P. Kozikowski, A patent review of histone deacetylase 6 inhibitors in neurodegenerative diseases (2014-2019), Expert Opin. Ther. Pat. 30 (2020) 121–136, https://doi.org/10.1080/13543776.2019.1708901.

[32] S.D. Pramanik, A. Kumar Halder, U. Mukherjee, D. Kumar, Y.N. Dey, M. R, Potential of histone deacetylase inhibitors in the control and regulation of prostate, breast and ovarian cancer, Front. Chem. 10 (2022), 948217, https://doi.org/10.3389/fchem.2022.948217.

[33] M. Zhou, H. Zheng, Y. Li, H. Huang, X. Min, S. Dai, W. Zhou, Z. Chen, G. Xu, Y. Chen, Discovery of a novel AR/HDAC6 dual inhibitor for prostate cancer treatment, Aging 13 (2021) 6982–6998, https://doi.org/10.18632/aging.202554.

[34] M.-J. Chuang, S.-T. Wu, S.-H. Tang, X.-M. Lai, H.-C. Lai, K.-H. Hsu, K.-H. Sun, G.-H. Sun, S.-Y. Chang, D.-S. Yu, P.-W. Hsiao, S.-M. Huang, T.-L. Cha, The HDAC inhibitor LBH589 induces ERK-dependent prometaphase arrest in prostate cancer

via HDAC6 inactivation and down-regulation, PLoS One 8 (2013), e73401, https://doi.org/10.1371/journal.pone.0073401.
[35] W. Weichert, A. Röske, V. Gekeler, T. Beckers, C. Stephan, K. Jung, F.R. Fritzsche, S. Niesporek, C. Denkert, M. Dietel, G. Kristiansen, Histone deacetylases 1, 2 and 3 are highly expressed in prostate cancer and HDAC2 expression is associated with shorter PSA relapse time after radical prostatectomy, Br. J. Cancer 98 (2008) 604–610, https://doi.org/10.1038/sj.bjc.6604199.
[36] A.P. Kozikowski, Y. Chen, A. Gaysin, B. Chen, M.A. D'Annibale, C.M. Suto, B. C. Langley, Functional differences in epigenetic modulators-superiority of mercaptoacetamide-based histone deacetylase inhibitors relative to hydroxamates in cortical neuron neuroprotection studies, J. Med. Chem. 50 (2007) 3054–3061, https://doi.org/10.1021/jm070178x.
[37] J.H. Kalin, J.A. Bergman, Development and therapeutic implications of selective histone deacetylase 6 inhibitors, J. Med. Chem. 56 (2013) 6297–6313, https://doi.org/10.1021/jm4001659.
[38] H.R. Gatla, Y. Zou, M.M. Uddin, B. Singha, P. Bu, A. Vancura, I. Vancurova, Histone deacetylase (HDAC) inhibition induces IκB kinase (IKK)-dependent interleukin-8/CXCL8 expression in ovarian cancer cells, J. Biol. Chem. 292 (2017) 5043–5054, https://doi.org/10.1074/jbc.M116.771014.
[39] G.-M. Jiang, H.-S. Wang, F. Zhang, K.-S. Zhang, Z.-C. Liu, R. Fang, H. Wang, S.-H. Cai, J. Du, Histone deacetylase inhibitor induction of epithelial-mesenchymal transitions via up-regulation of Snail facilitates cancer progression, Biochim. Biophys. Acta 1833 (2013) 663–671, https://doi.org/10.1016/j.bbamcr.2012.12.002.
[40] R.R. Shah, Safety and tolerability of histone deacetylase (HDAC) inhibitors in oncology, Drug Saf. 42 (2019) 235–245, https://doi.org/10.1007/s40264-018-0773-9.
[41] C. Zagni, A. Citarella, M. Oussama, A. Rescifina, A. Maugeri, M. Navarra, A. Scala, A. Piperno, N. Micale, Hydroxamic acid-based histone deacetylase (HDAC) inhibitors bearing a pyrazole scaffold and a cinnamoyl linker, Int. J. Mol. Sci. 20 (2019) 945, https://doi.org/10.3390/ijms20040945.
[42] M. Géraldy, M. Morgen, P. Sehr, R.R. Steimbach, D. Moi, J. Ridinger, I. Oehme, O. Witt, M. Malz, M.S. Nogueira, O. Koch, N. Gunkel, A.K. Miller, Selective inhibition of histone deacetylase 10: hydrogen bonding to the gatekeeper residue is implicated, J. Med. Chem. 62 (2019) 4426–4443, https://doi.org/10.1021/acs.jmedchem.8b01936.
[43] Y. Hai, D.W. Christianson, Histone deacetylase 6 structure and molecular basis of catalysis and inhibition, Nat. Chem. Biol. 12 (2016) 741–747, https://doi.org/10.1038/nchembio.2134.
[44] D. Moi, A. Citarella, D. Bonanni, L. Pinzi, D. Passarella, A. Silvani, C. Giannini, G. Rastelli, Synthesis of potent and selective HDAC6 inhibitors led to unexpected opening of a quinazoline ring, RSC Adv. 12 (2022) 11548–11556, https://doi.org/10.1039/d2ra01753a.
[45] M.S. Mohamed, R. Kamel, S.S. Fatahala, Synthesis and biological evaluation of some thio containing pyrrolo [2,3-d]pyrimidine derivatives for their anti-inflammatory and anti-microbial activities, Eur. J. Med. Chem. 45 (2010) 2994–3004, https://doi.org/10.1016/j.ejmech.2010.03.028.
[46] E.-J. Hao, G.-X. Li, Y.-R. Liang, M.-S. Xie, D.-C. Wang, X.-H. Jiang, J.-Y. Cheng, Z.-X. Shi, Y. Wang, H.-M. Guo, Design, synthesis, and activity evaluation of novel acyclic nucleosides as potential anticancer agents *in vitro* and *in vivo*, J. Med. Chem. 64 (2021) 2077–2109, https://doi.org/10.1021/acs.jmedchem.0c01717.
[47] S.J. Tangeda, A. Garlapati, Synthesis of new pyrrolo[2,3-d]pyrimidine derivatives and evaluation of their activities against human colon cancer cell lines, Eur. J. Med. Chem. 45 (2010) 1453–1458, https://doi.org/10.1016/j.ejmech.2009.12.050.
[48] H.-Y. Lee, A.-C. Tsai, M.-C. Chen, P.-J. Shen, Y.-C. Cheng, C.-C. Kuo, S.-L. Pan, Y.-M. Liu, J.-F. Liu, T.-K. Yeh, J.-C. Wang, C.-Y. Chang, J.-Y. Chang, J.-P. Liou, Azaindolylsulfonamides, with a more selective inhibitory effect on histone deacetylase 6 activity, exhibit antitumor activity in colorectal cancer HCT116 cells, J. Med. Chem. 57 (2014) 4009–4022, https://doi.org/10.1021/jm401899x.
[49] X. Liang, S. Tang, X. Liu, Y. Liu, Q. Xu, X. Wang, A. Saidahmatov, C. Li, J. Wang, Y. Zhou, Y. Zhang, M. Geng, M. Huang, H. Liu, Discovery of novel pyrrolo[2,3-d] pyrimidine-based derivatives as potent JAK/HDAC dual inhibitors for the treatment of refractory solid tumors, J. Med. Chem. 65 (2022) 1243–1264, https://doi.org/10.1021/acs.jmedchem.0c02111.
[50] Y. Li, Y. Liu, Z. Zhu, W. Yan, C. Zhang, Z. Yang, P. Bai, M. Tang, M. Shi, W. He, S. Fu, J. Liu, K. Han, J. Li, L. Xie, H. Ye, J. Yang, L. Chen, Structure-based design and synthesis of N-substituted 3-Amino-β-Carboline derivatives as potent αβ-tubulin degradation agents, J. Med. Chem. 65 (2022) 2675–2693, https://doi.org/10.1021/acs.jmedchem.1c02159.
[51] H. Suh, K. Choi, J. Lee, C. Ryou, H. Rhee, C.-H. Lee, Effects of a novel carbocyclic analog of pyrrolo[2,3-d]pyrimidine nucleoside on pleiotropic induction of cell death in prostate cancer cells with different androgen responsiveness, Bioorg. Med. Chem. Lett. 26 (2016) 1130–1135, https://doi.org/10.1016/j.bmcl.2016.01.057.
[52] K. Nepali, T.-Y. Chang, M.-J. Lai, K.-C. Hsu, Y. Yen, T.E. Lin, S.-B. Lee, J.-P. Liou, Purine/purine isoster based scaffolds as new derivatives of benzamide class of HDAC inhibitors, Eur. J. Med. Chem. 196 (2020), 112291, https://doi.org/10.1016/j.ejmech.2020.112291.
[53] P. Linciano, R. Benedetti, L. Pinzi, F. Russo, U. Chianese, C. Sorbi, L. Altucci, G. Rastelli, L. Brasili, S. Franchini, Investigation of the effect of different linker chemotypes on the inhibition of histone deacetylases (HDACs), Bioorg. Chem. 106 (2021), 104462, https://doi.org/10.1016/j.bioorg.2020.104462.
[54] N.J. Porter, S. Shen, C. Barinka, A.P. Kozikowski, D.W. Christianson, Molecular basis for the selective inhibition of histone deacetylase 6 by a mercaptoacetamide inhibitor, ACS Med. Chem. Lett. 9 (2018) 1301–1305, https://doi.org/10.1021/acsmedchemlett.8b00487.
[55] L. Zhang, J. Zhang, Q. Jiang, L. Zhang, W. Song, Zinc binding groups for histone deacetylase inhibitors, J. Enzym. Inhib. Med. Chem. 33 (2018) 714–721, https://doi.org/10.1080/14756366.2017.1417274.
[56] K.-C. Hsu, C.-Y. Liu, T.E. Lin, J.-H. Hsieh, T.-Y. Sung, H.-J. Tseng, J.-M. Yang, W.-J. Huang, Novel class IIa-selective histone deacetylase inhibitors discovered using an in silico virtual screening approach, Sci. Rep. 7 (2017) 3228, https://doi.org/10.1038/s41598-017-03417-1.
[57] D. Bonanni, A. Citarella, D. Moi, L. Pinzi, E. Bergamini, G. Rastelli, Dual targeting strategies on histone deacetylase 6 (HDAC6) and Heat Shock protein 90 (Hsp90), Curr. Med. Chem. (2021), https://doi.org/10.2174/0929867328666210902145102.
[58] L. Pinzi, R. Benedetti, L. Altucci, G. Rastelli, Design of dual inhibitors of histone deacetylase 6 and Heat Shock protein 90, ACS Omega 5 (2020) 11473–11480, https://doi.org/10.1021/acsomega.0c00559.
[59] A. Citarella, D. Moi, L. Pinzi, D. Bonanni, G. Rastelli, Hydroxamic acid derivatives: from synthetic strategies to medicinal chemistry applications, ACS Omega 6 (2021), 21843, https://doi.org/10.1021/acsomega.1c03628. –21849.
[60] F.F. Wagner, D.E. Olson, J.P. Gale, T. Kaya, M. Weïwer, N. Aidoud, M. Thomas, E. L. Davoine, B.C. Lemercier, Y.-L. Zhang, E.B. Holson, Potent and selective inhibition of histone deacetylase 6 (HDAC6) does not require a surface-binding motif, J. Med. Chem. 56 (2013) 1772–1776, https://doi.org/10.1021/jm301355j.
[61] S. Shen, A.P. Kozikowski, Why hydroxamates may not Be the best histone deacetylase inhibitors–what some may have forgotten or would rather forget? ChemMedChem 11 (2016) 15–21, https://doi.org/10.1002/cmdc.201500486.
[62] M.T. Tavares, A.P. Kozikowski, S. Shen, Mercaptoacetamide: a promising zinc-binding group for the discovery of selective histone deacetylase 6 inhibitors, Eur. J. Med. Chem. 209 (2021), 112887, https://doi.org/10.1016/j.ejmech.2020.112887.
[63] P. Linciano, L. Pinzi, S. Belluti, U. Chianese, R. Benedetti, D. Moi, L. Altucci, S. Franchini, C. Imbriano, C. Sorbi, G. Rastelli, Inhibitors of histone deacetylase 6 based on a novel 3-hydroxy-isoxazole zinc binding group, J. Enzym. Inhib. Med. Chem. 36 (2021) 2080–2086, https://doi.org/10.1080/14756366.2021.1981306.
[64] D.E. Olson, F.F. Wagner, T. Kaya, J.P. Gale, N. Aidoud, E.L. Davoine, F. Lazzaro, M. Weïwer, Y.-L. Zhang, E.B. Holson, Discovery of the first histone deacetylase 6/8 dual inhibitors, J. Med. Chem. 56 (2013) 4816–4820, https://doi.org/10.1021/jm400390r.
[65] J. Senger, J. Melesina, M. Marek, C. Romier, I. Oehme, O. Witt, W. Sippl, M. Jung, Synthesis and biological investigation of oxazole hydroxamates as highly selective histone deacetylase 6 (HDAC6) inhibitors, J. Med. Chem. 59 (2016) 1545–1555, https://doi.org/10.1021/acs.jmedchem.5b01493.
[66] L. Pinzi, G. Rastelli, Molecular docking: shifting paradigms in drug discovery, Int. J. Mol. Sci. 20 (2019) 4331, https://doi.org/10.3390/ijms20184331.
[67] J. Melesina, C.V. Simoben, L. Praetorius, E.F. Bülbül, D. Robaa, W. Sippl, Strategies to design selective histone deacetylase inhibitors, ChemMedChem 16 (2021) 1336–1359, https://doi.org/10.1002/cmdc.202000934.
[68] J. Roche, P. Bertrand, Inside HDACs with more selective HDAC inhibitors, Eur. J. Med. Chem. 121 (2016) 451–483, https://doi.org/10.1016/j.ejmech.2016.05.047.
[69] J.D. Osko, D.W. Christianson, Structural determinants of affinity and selectivity in the binding of inhibitors to histone deacetylase 6, Bioorg. Med. Chem. Lett. 30 (2020), 127023, https://doi.org/10.1016/j.bmcl.2020.127023.
[70] M. Lobera, K.P. Madauss, D.T. Pohlhaus, Q.G. Wright, M. Trocha, D.R. Schmidt, E. Baloglu, R.P. Trump, M.S. Head, G.A. Hofmann, M. Murray-Thompson, B. Schwartz, S. Chakravorty, Z. Wu, P.K. Mander, L. Kruidenier, R.A. Reid, W. Burkhart, B.J. Turunen, J.X. Rong, C. Wagner, M.B. Moyer, C. Wells, X. Hong, J. T. Moore, J.D. Williams, D. Soler, S. Ghosh, M.A. Nolan, Selective class IIa histone deacetylase inhibition via a nonchelating zinc-binding group, Nat. Chem. Biol. 9 (2013) 319–325, https://doi.org/10.1038/nchembio.1223.
[71] D.A. Stolfa, M. Marek, J. Lancelot, A.-T. Hauser, A. Walter, E. Leproult, J. Melesina, T. Rumpf, J.-M. Wurtz, J. Cavarelli, W. Sippl, R.J. Pierce, C. Romier, M. Jung, Molecular basis for the antiparasitic activity of a mercaptoacetamide derivative that inhibits histone deacetylase 8 (HDAC8) from the human pathogen schistosoma mansoni, J. Mol. Biol. 426 (2014) 3442–3453, https://doi.org/10.1016/j.jmb.2014.03.007.
[72] Schrödinger Release 2021-1, QikProp, Schrödinger, LLC, New York, NY, 2021.
[73] O.G. Scharovsky, L.E. Mainetti, V.R. Rozados, Metronomic chemotherapy: changing the paradigm that more is better, Curr. Oncol. 16 (2009) 7–15, https://doi.org/10.3747/co.v16i2.420.
[74] I. Hubatsch, E.G.E. Ragnarsson, P. Artursson, Determination of drug permeability and prediction of drug absorption in Caco-2 monolayers, Nat. Protoc. 2 (2007) 2111–2119, https://doi.org/10.1038/nprot.2007.303.
[75] C.M. Bowman, L.Z. Benet, Hepatic clearance predictions from in vitro-in vivo extrapolation and the biopharmaceutics drug disposition classification system, Drug Metab. Dispos. Biol. Fate Chem. 44 (2016) 1731–1735, https://doi.org/10.1124/dmd.116.071514.
[76] B. Davies, T. Morris, Physiological parameters in laboratory animals and humans, Pharm. Res. (N. Y.) 10 (1993) 1093–1095, https://doi.org/10.1023/a:1018943613122.
[77] G. Giannini, M. Marzi, R. Pezzi, T. Brunetti, G. Battistuzzi, M.D. Marzo, W. Cabri, L. Vesci, C. Pisano, N-Hydroxy-(4-oxime)-cinnamide: a versatile scaffold for the synthesis of novel histone deacetilase (HDAC) inhibitors, Bioorg. Med. Chem. Lett. 19 (2009) 2346–2349, https://doi.org/10.1016/j.bmcl.2009.02.029.
[78] P. Gediya, P.K. Parikh, V.K. Vyas, M.D. Ghate, Histone deacetylase 2: a potential therapeutic target for cancer and neurodegenerative disorders, Eur. J. Med. Chem. 216 (2021), 113332, https://doi.org/10.1016/j.ejmech.2021.113332.
[79] C. Micelli, G. Rastelli, Histone deacetylases: structural determinants of inhibitor selectivity, Drug Discov. Today 20 (2015) 718–735, https://doi.org/10.1016/j.drudis.2015.01.007.

[80] D. Mendez, A. Gaulton, A.P. Bento, J. Chambers, M. De Veij, E. Félix, M. P. Magariños, J.F. Mosquera, P. Mutowo, M. Nowotka, M. Gordillo-Marañón, F. Hunter, L. Junco, G. Mugumbate, M. Rodriguez-Lopez, F. Atkinson, N. Bosc, C. J. Radoux, A. Segura-Cabrera, A. Hersey, A.R. Leach, ChEMBL: towards direct deposition of bioassay data, Nucleic Acids Res. 47 (2019) D930–D940, https://doi.org/10.1093/nar/gky1075.

[81] J. Ai, Y. Lu, Q. Wei, H. Li, Comparative proteomics uncovers correlated signaling network and potential biomarkers for progression of prostate cancer, Cell. Physiol. Biochem. 41 (2017) 1–9, https://doi.org/10.1159/000447813.

[82] G.M. Sastry, M. Adzhigirey, T. Day, R. Annabhimoju, W. Sherman, Protein and ligand preparation: parameters, protocols, and influence on virtual screening enrichments, J. Comput. Aided Mol. Des. 27 (2013) 221–234, https://doi.org/10.1007/s10822-013-9644-8.

[83] C.J. Millard, P.J. Watson, I. Celardo, Y. Gordiyenko, S.M. Cowley, C.V. Robinson, L. Fairall, J.W.R. Schwabe, Class I HDACs share a common mechanism of regulation by inositol phosphates, Mol. Cell 51 (2013) 57–67, https://doi.org/10.1016/j.molcel.2013.05.020.

[84] M.J. Bottomley, P. Lo Surdo, P. Di Giovine, A. Cirillo, R. Scarpelli, F. Ferrigno, P. Jones, P. Neddermann, R. De Francesco, C. Steinkühler, P. Gallinari, A. Carfí, Structural and functional analysis of the human HDAC4 catalytic domain reveals a regulatory structural zinc-binding domain, J. Biol. Chem. 283 (2008) 26694–26704, https://doi.org/10.1074/jbc.M803514200.

[85] R.A. Friesner, R.B. Murphy, M.P. Repasky, L.L. Frye, J.R. Greenwood, T.A. Halgren, P.C. Sanschagrin, D.T. Mainz, Extra precision glide: docking and scoring incorporating a model of hydrophobic enclosure for protein-ligand complexes, J. Med. Chem. 49 (2006) 6177–6196, https://doi.org/10.1021/jm051256o.

[86] D.A. Case, H.M. Aktulga, K. Belfon, I.Y. Ben-Shalom, S.R. Brozell, D.S. Cerutti, T. E. Cheatham III, G.A. Cisneros, V.W.D. Cruzeiro, T.A. Darden, R.E. Duke, G. Giambasu, M.K. Gilson, H. Gohlke, A.W. Goetz, R. Harris, S. Izadi, S.A. Izmailov, C. Jin, K. Kasavajhala, M.C. Kaymak, E. King, A. Kovalenko, T. Kurtzman, T.S. Lee, S. LeGrand, P. Li, C. Lin, J. Liu, T. Luchko, R. Luo, M. Machado, V. Man, M. Manathunga, K.M. Merz, Y. Miao, O. Mikhailovskii, G. Monard, H. Nguyen, K. A. O'Hearn, A. Onufriev, F. Pan, S. Pantano, R. Qi, A. Rahnamoun, D.R. Roe, A. Roitberg, C. Sagui, S. Schott-Verdugo, J. Shen, C.L. Simmerling, N. R. Skrynnikov, J. Smith, J. Swails, R.C. Walker, J. Wang, H. Wei, R.M. Wolf, X. Wu, Y. Xue, D.M. York, S. Zhao, P.A. Kollman, Amber 2021, University of California, San Francisco, 2021 (n.d.).

[87] P. Li, K.M. Merz, MCPB.py: a Python based metal center parameter builder, J. Chem. Inf. Model. 56 (2016) 599–604, https://doi.org/10.1021/acs.jcim.5b00674.

[88] G.M.J. Barca, C. Bertoni, L. Carrington, D. Datta, N. De Silva, J.E. Deustua, D. G. Fedorov, J.R. Gour, A.O. Gunina, E. Guidez, T. Harville, S. Irle, J. Ivanic, K. Kowalski, S.S. Leang, H. Li, W. Li, J.J. Lutz, I. Magoulas, J. Mato, V. Mironov, H. Nakata, B.Q. Pham, P. Piecuch, D. Poole, S.R. Pruitt, A.P. Rendell, L.B. Roskop, K. Ruedenberg, T. Sattasathuchana, M.W. Schmidt, J. Shen, L. Slipchenko, M. Sosonkina, V. Sundriyal, A. Tiwari, J.L. Galvez Vallejo, B. Westheimer, M. Włoch, P. Xu, F. Zahariev, M.S. Gordon, Recent developments in the general atomic and molecular electronic structure system, J. Chem. Phys. 152 (2020), 154102, https://doi.org/10.1063/5.0005188.

[89] M.T. Panteva, G.M. Giambaşu, D.M. York, Comparison of structural, thermodynamic, kinetic and mass transport properties of Mg(2+) ion models commonly used in biomolecular simulations, J. Comput. Chem. 36 (2015) 970–982, https://doi.org/10.1002/jcc.23881.

[90] M.T. Panteva, G.M. Giambaşu, D.M. York, Force field for Mg^{2+}, Mn^{2+}, Zn^{2+}, and Cd^{2+} ions that have balanced interactions with nucleic acids, J. Phys. Chem. B 119 (2015) 15460–15470, https://doi.org/10.1021/acs.jpcb.5b10423.

[91] J. Wang, R.M. Wolf, J.W. Caldwell, P.A. Kollman, D.A. Case, Development and testing of a general amber force field, J. Comput. Chem. 25 (2004) 1157–1174, https://doi.org/10.1002/jcc.20035.

[92] F.-Y. Dupradeau, A. Pigache, T. Zaffran, C. Savineau, R. Lelong, N. Grivel, D. Lelong, W. Rosanski, P. Cieplak, The R.E.D. tools: advances in RESP and ESP charge derivation and force field library building, Phys. Chem. Chem. Phys. PCCP. 12 (2010) 7821–7839, https://doi.org/10.1039/c0cp00111b.

[93] U. Essmann, L. Perera, M.L. Berkowitz, T. Darden, H. Lee, L.G. Pedersen, A smooth particle mesh Ewald method, J. Chem. Phys. 103 (1995) 8577–8593, https://doi.org/10.1063/1.470117.

[94] S. Belluti, V. Semeghini, G. Rigillo, M. Ronzio, D. Benati, F. Torricelli, L. Reggiani Bonetti, G. Carnevale, G. Grisendi, A. Ciarrocchi, M. Dominici, A. Recchia, D. Dolfini, C. Imbriano, Alternative splicing of NF-YA promotes prostate cancer aggressiveness and represents a new molecular marker for clinical stratification of patients, J. Exp. Clin. Cancer Res. 40 (2021) 362, https://doi.org/10.1186/s13046-021-02166-4.

[95] P. Benatti, V. Basile, D. Dolfini, S. Belluti, M. Tomei, C. Imbriano, NF-Y loss triggers p53 stabilization and apoptosis in HPV18-positive cells by affecting E6 transcription, Oncotarget 7 (2016) 45901–45915, https://doi.org/10.18632/oncotarget.9974.

[96] Z. Tang, B. Kang, C. Li, T. Chen, Z. Zhang, GEPIA2: an enhanced web server for large-scale expression profiling and interactive analysis, Nucleic Acids Res. 47 (2019), https://doi.org/10.1093/nar/gkz430. W556–W560.

[97] D.S. Chandrashekar, B. Bashel, S.A.H. Balasubramanya, C.J. Creighton, I. Ponce-Rodriguez, B.V.S.K. Chakravarthi, S. Varambally, UALCAN: a portal for facilitating tumor subgroup gene expression and survival analyses, Neoplasia N. Y. N. 19 (2017) 649–658, https://doi.org/10.1016/j.neo.2017.05.002.